672975

ABSTRACT

TEMPERATURE DEPENDENCE OF THE NQR FREQUENCIES
OF PERIODATES AND PERRHENATES AND CALCULATION
OF ELECTRIC FIELD GRADIENTS FROM
X-RAY DIFFRACTION DATA

Ву

Richard Allen Johnson

The temperature dependence of the nuclear quadrupole resonance (NQR) frequencies in NaIO₄ and MReO₄ (M = Na, K, Ag) have been experimentally studied from liquid helium to room temperature. Theoretical curves were constructed based on the Kushida, Benedek, and Bloembergen theory and compared with experiment in order to determine the importance of lattice changes with temperature on the field gradient, which is often neglected in such treatments.

Frequencies, symmetries, and temperature variations of the external lattice vibrational modes were obtained from a detailed laser-Raman study of all the Scheelite-type per-rhenates. Mode assignments were made from depolarization ratio measurements on NaReO₄ single crystals and spectra of polycrystalline ND₄ReO₄ and ND₄IO₄.

Ammonium perrhenate exhibits an anomalous NQR temperature dependence with a loss of signal upon cooling at $245^{\circ}K$. A model for the motion of the ammonium group in the crystal has been constructed which is consistent with the NQR, Raman, and infrared results. The ammonium group in NH₄ReO₄ is apparently undergoing torsional motion at $77^{\circ}K$ and freely rotating at room temperature.

The possibility of calculating electric field gradients using electron densities obtained from accurate X-ray diffraction data was also investigated. Electron density maps were calculated from observed structure factors for several compounds, with actual field gradient calculations carried out only for β -ICl. The reliability of the results in terms of the assumptions made in the calculations is discussed in detail.

TEMPERATURE DEPENDENCE OF THE NQR FREQUENCIES OF PERIODATES AND PERRHENATES AND CALCULATION OF ELECTRIC FIELD GRADIENTS FROM X-RAY DIFFRACTION DATA

Ву

Richard Allen Johnson

A THESIS

Submitted to
Michigan State University
in partial fulfillment of the requirements
for the degree of

DOCTOR OF PHILOSOPHY

Department of Chemistry Program in Chemical Physics

ACKNOWLEDGMENTS

The author would like to express his indebtedness to Professor M. T. Rogers for his guidance, encouragement and patience during the course of this study, which ranged rather far afield from magnetic resonance at times.

Special thanks are also due to Professor G. E. Leroi for his help in certain aspects of the laser Raman study. The author would also like to thank Professors E. Carlson and A. Tulinsky, D. A. Hatzenbuhler, Dinesh, K. V. S. Rama Roo and the X-ray crystallography group for helpful discussions in various aspects of this work.

The support of my wife Kathy, both mentally and financially, in all aspects of this work is deeply appreciated.

Finally, the financial support of the Gulf Oil Corporation, the Atomic Energy Commission, and the Chemistry Department during various parts of this study are gratefully acknowledged.

TABLE OF CONTENTS

																		Page
	INT	RODU	CTIC	N		•	• •	•	•		•	•	•	•	•	•	•	1
ı.	THE	ORY	•					•	•		•	•.	. · • .	•	•	•	•	4
	Α.	Gene	eral	l Ba	ckç	rou	ınd	of	NQI	R S	pec	tr	os	C O	ру		•	4
		1.	Qua	adru	po l	ar	Ham	ito	nia	an	•	۰	•	•	•		۰	4
		2.	Ene	ergy	L€	vel	. Ex	pre	ssi	ion	s f	or	I	=	5/	2	•	10
	В.	Cal	cula	atio	n c	fE	lec	tri	c I	?ie	ld	Gr	ad	ie	nt	s	•	11
		1.	Nor	n-ov	er]	app	oing	Ch	arç	ge 1	Mod	le 1	•	•	•	•	•	12
		2.	Tov	vnes	-Da	ile	y M	eth	od	•	•	•	•	•	•	•	•	18
	c.	Temp	pera	atur	e I	epe	nde	nce	o t	E N	QR	Fr	eq	ue	nc	ie	s	21
ıı.	EXP	ERIM	ENT	\L		•		•	•		•	•	•	•	•	•	•	32
	Α.	Syn	thes	sis	and	Cr	yst	al	Gro	wi	ng	•	•				•	32
		1.	Syr	the	sis			•			•	•	•		•	•		32
		2.	Cry	sta	1 G	row	/th	•	•			•	•	•		•		33
	В.	Inf	care	ed a	nd	Ran	nan	Spe	cti	os	cop	у			•	•		37
		1.	Far	: In	fra	red	l .				•	•	•		•	•		37
		2.	Las	ser	Ran	an		•							•	•	•	39
	c.	NQR	Ten	nper	atu	re	Stu	die	s .							•		40
		1.	Cor	ısta	nt	Ten	per	atu	re	Ba	ths	3						40
		2.	Dev	var	Met	hod	ls .	•	•			•						42
		3.	Ten	nper	atu	re	Mea	sur	eme	ent								48
		4.	NQF	Os	cil	lat	or	Mod	lifi	ca	tic	ns	a	nd				
			Ope	erat	ion			•	•			•			o	•		53

TABLE OF CONTENTS (Cont.)

				Page
III.	RES	ULTS	AND DISCUSSION	57
	Α.	Far	IR and Raman Spectra	57
		1.	Factor Group Analysis	57
		2.	Frequencies and Symmetry Assignment	s 60
	В.	Temp	perature Dependence	96
		1.	Normal Behavior: $NaIO_4$ and $MReO_4$ (M = Na, K, Ag)	96
		2.	Anomalous Behavior: NH ₄ ReO ₄	121
	c.	Elec	ctric Field Gradient Calculations.	133
		1.	Method of Calculation	133
		2.	Results and Problems Encountered.	137
	I.TS'	т Оғ	REFERENCES	144

LIST OF TABLES

FABLE		Page
1.	Site and factor group splittings of Scheelite- type perrhenates	59
2.	Activity of polarizability derivative tensor components under C _{4h} point group symmetry.	60
3.	Infrared and Raman active ReO_4^- fundamentals at 294^0K	72
4.	Lattice modes in Scheelite-type perrhenates at 2940K	73
5.	Raman-active lattice modes in Scheelite-type perrhenates near 77^0K	73
6.	Experimental versus theoretical depolarization ratios in NaReO4	77
7.	$\mathrm{NH_4}^+$ and $\mathrm{ND_4}^+$ Raman-active fundamentals in the periodates and perrhenates	91
8.	Isotopic ratios for NH ₄ ⁺ fundamentals compared to valence force model predictions	93
9.	Raman-active lattice modes in NH_4^+ and ND_4^+ perrhenates and periodates near liquid nitrogent temperatures	n 93
10.	Lattice modes in $\mathrm{NH_4}^+$ and $\mathrm{ND_4}^+$ perrhenates and periodates at $298^0\mathrm{K}^-$	94
11.	Temperature dependences of periodate and perrhenate lattice modes	100
12.	Experimental frequencies and temperatures for the $(\pm 3/2 \iff \pm 1/2)$ ¹⁸⁷ Re pure quadrupole resonance transition in NaReO ₄	50 - 102
13.	Experimental frequencies and temperatures for the $(\pm 3/2 \iff \pm 1/2)$ ¹⁸⁷ Re pure quadrupole resonance transition in KReO ₄	103

LIST OF TABLES (Cont.)

TABLE	I	Page
14.	Experimental frequencies and temperatures for the $(\pm 3/2 \iff \pm 1/2)^{-187}$ Re pure quadrupole resonance transition in AgReO ₄	104
15.	Experimental frequencies and temperatures for the $(\pm 5/2 - \pm 3/2)^{-127}$ I pure quadrupole resonance transition in NaIO ₄	104
16.	Final parameters obtained in applying the adjusted Bayer theory	120
17.	Experimental frequencies observed at various temperatures for the $(\pm 5/2 \iff \pm 3/2)$ transition of the ¹⁸⁷ Re pure quadrupole resonance spectrum	1 124
18.	Positive temperature coefficients of NQR frequencies observed in NH ₄ ReO ₄ and several other compounds	132
19.	Calculated electric field gradient in β -ICl .	139

LIST OF FIGURES

Figur	е	Page
1.	Variable temperature water bath for single crystal growth	35
2.	Liquid helium Dewar with a 4" Pyrex pipe fitting for NQR and Q-Band ESR studies	43
3.	Cartesian manostat for pressure regulation .	45
4.	Cross-section of Swenson-type variable- temperature bomb used with the liquid helium Dewar	47
5.	Correction voltage between measured and tabulated emf's for the copper-constantan thermocouple used in this work	50
6.	Raman spectrum of polycrystalline NaReO ₄ using 5145A Ar(II) laser excitation	62
7.	Raman spectrum of the lattice region in polycrystalline KReO ₄ using 5145A Ar(II) laser excitation	64
8.	Raman spectrum of the lattice region in polycrystalline RbReO ₄ using 5145A Ar(II) laser excitation	66
9.	Raman spectrum of the lattice region in polycrystalline AgReO ₄ using 5145A Ar(II) laser excitation	68
10.	Infrared spectrum of polycrystalline NaReO $_4$ in Nujol mull at $298^{0}\mathrm{K}$ in the $400500~\mathrm{cm}^{-1}$ range	70
11.	Raman spectra of single crystal NaReO ₄ in the four unique orientations	74
12.	Raman spectra of the lattice region in poly- crystalline NH ₄ ReO ₄ using 5145A Ar(II) laser excitation	79

LIST OF FIGURES (Cont.)

Figur	e	Page
13.	Raman spectra of the lattice region in polycrystalline ND ₄ ReO ₄ using 5145A Ar(II) laser excitation	81
14.	Raman spectra of the lattice region in polycrystalline ND ₄ IO ₄ using 4880A Ar(II) laser excitation	83
15.	Raman spectra of ammonium fundamentals in NH_4R using 5145A Ar(II) laser excitation	e0 ₄ 85
16.	Raman spectra of deuteroammonium fundamentals in ND_4ReO_4 using 5145A Ar(II) laser excitation	n 87
17.	Raman spectra of deuteroammonium fundamentals in ND_4IO_4 using 4880A and 5145A Ar(II) laser excitation	89
18.	NQR spectrum of the $(\pm 3/2 \iff \pm 1/2)^{-187}$ Re pure quadrupole resonance transition in polycrystalline KReO ₄ at 30^{0} K	106
19.	Experimental and calculated temperature dependence of the 127I quadrupole resonance in NaIO4	109
20.	Experimental and calculated temperature dependence of the ¹⁸⁷ Re quadrupole resonance in NaReO ₄	111
21.	Experimental and calculated temperature dependence of the ¹⁸⁷ Re quadrupole resonance in KReO ₄	113
22.	Experimental and calculated temperature dependence of the ¹⁸⁷ Re quadrupole resonance in AgReO ₄	115
23.	Experimental temperature dependence of the $(\pm 5/2 \iff \pm 3/2)$ ¹⁸⁷ Re transition in NH ₄ ReO ₄	125

INTRODUCTION

Although the first quadrupole resonance experiment was performed over twenty years ago, the field has yet to undergo the rapid growth and wide application experienced by the analogous magnetic resonance spectroscopic techniques of NMR and ESR. Some of the reasons for the slow growth of NQR spectroscopy are more readily apparent by comparing the resonance equations relating the energy level splitting to the applied frequency v for the various types of magnetic resonance spectroscopy,

$$hv = g\beta H$$
 (NMR or ESR)

$$hv = \frac{e^2}{2} Qq$$
 (NQR)

where β, the Bohr magneton, and Q, the nuclear quadrupole moment, are nuclear properties. In the NMR-ESR case resonance may be achieved by varying the frequency V or the external magnetic field H, while in the case of NQR only the frequency may be varied since the electric field gradient q is fixed by the electronic environment of the quadrupolar nucleus. The difficulties associated with building high-sensitivity radio-frequency oscillators capable of scanning large frequency ranges and the inability of current theories relating experimental frequencies to molecular structure are

the principal reasons for the slow growth of NQR.

The approaches presently used to calculate electric field gradients have some serious deficiencies as a result of the approximations necessary in their application to solid state calculations. One of the projects in this work involved investigating an alternate, semi-empirical procedure for field gradient calculation based on using electron densities in crystals obtained from X-ray structure determinations. The ability to predict approximate values for quadrupole coupling constants for nuclei not previously studied by NQR would be of great advantage in locating new resonances experimentally.

In addition to the information concerning molecular structure obtainable from quadrupole coupling constants, studies of the quadrupole frequency shifts with temperature can provide detailed information about intermolecular interactions and motional changes in the crystal. The second project investigated in this work was the temperature dependence of the NQR frequencies in several perrhenates and periodates. According to conventional theories, in order to obtain agreement between theory and experiment an independent experiment, the pressure dependence of the NQR frequency, must be performed. Since the pressure experiment is difficult to perform, several approximations are made in order to account for the lack of pressure data. One of the assumptions involved, the neglect of the effect of lattice contraction or expansion on the field gradient, was tested in this work for the series of perrhenates and periodates studied.

Experimentally, this involved a detailed infrared and Raman study of the lattice region and the experimental temperature versus NQR frequency from liquid helium to room temperature. During the course of the work a liquid helium dewar system was constructed for both NQR and Q-Band EPR studies.

One of the perrhenates, NH₄ReO₄, showed an anomalous temperature dependence with loss of resonance upon cooling near 245°K. Use of the X-ray structure determination results, the vibrational spectra, and the quadrupole resonance results allow a model for the ammonium ion motion in the lattice to be constructed. The mechanism proposed to account for the anomalous behavior in ammonium perrhenate is different from previous hypotheses explaining anomalous NQR temperature dependences, which do not appear to be applicable to ammonium perrhenate.

I. THEORY

A. General Background of NQR Spectroscopy

1. Quadrupolar Hamiltonian

The quadrupole term H_Q in the total Hamiltonian can be looked upon as describing the effect of an interaction between a non-spherical nucleus and its environment. The quantum mechanical treatment of the quadrupolar Hamiltonian was first given by Casimir (1). More accessible treatments of the derivation are given by Ramsey (2), Kopfermann (3) and Cohen and Reif (4). An excellent discussion of the application of the Wigner-Eckart theorem to the matrix elements of H_Q is given by Slichter (5).

The total energy of a system of α -nuclei and i electrons can be written classically in the Hamiltonian formulism as

$$H_{TOT} = \sum_{\alpha} \frac{1}{2M_{\alpha}} P_{\alpha}^{2} + \sum_{i} \frac{1}{2m} P_{i}^{2} + V_{ee} + V_{nn} + V_{ne} ,$$

where P_{α} and P_{i} denote the momenta of the α^{th} nucleon and ith electron, respectively, V_{ee} the electron-electron potential, and V_{nn} the nucleon interaction potential. The potential energy term V_{ne} for nuclei and electrons is

given by the electrostatic interaction between point charges according to Coulomb's law

$$V_{ne} = -\sum_{\alpha} \sum_{i} \frac{z_{\alpha}e}{r_{i\alpha}}$$
 (1)

with $r_{i\alpha}$ the separation between the α nucleon and the i^{th} electron. As one would expect, however, the nucleus has a finite volume and the effect of this charge distribution within the nuclear volume V must be included in the expression for V_{ne} . If a continuous charge distribution $\rho(\underline{r}')$ is substituted for the point charge Z_{α} , the potential energy expression becomes

$$V_{ne} = H_{ne} = \int_{V'} \rho(\bar{r}') V(\bar{r} - \bar{r}') d^3 \bar{r}'$$
 (2)

where the electron is at a point \bar{r} , $|\bar{r}| >> |\bar{r}'|$, and the primed coordinates denote points inside the nuclear volume V'. Writing $V(\bar{r} - \bar{r}')$ explicitly and regrouping terms gives

$$H_{\text{ne}} = e \int_{V'}^{\cdot} \left| \frac{\rho(\bar{r}')}{\bar{r} - \bar{r}'} \right| d^3 \bar{r}' \qquad (3)$$

Since $\rho(\bar{r}')$ is the nuclear charge distribution, contained in a radius a $\ll |\bar{r}|$, the expression enclosed in the dotted lines may be considered as an electrostatic potential due to an unknown charge distribution. Therefore, carrying out a multipole expansion (6) of this potential we have

$$\left| \vec{r} - \vec{r}' \right|^{-1} = \frac{1}{r} \left\{ 1 - \frac{1}{2} \left[-\frac{2 \vec{r} \cdot \vec{r}'}{r^2} + \frac{\vec{r}'^2}{r^2} \right] + \frac{3}{8} \left[\right]^2 + \cdots \right\}$$
 (4)

which gives

$$H_{ne} = e \int_{V'} \left\{ \frac{1}{r} + \frac{\vec{r} \cdot \vec{r}'}{r^3} + \frac{1}{2} \left[\frac{3(\vec{r} \cdot \vec{r}')^2}{r^5} - \frac{r'^2}{r^3} \right] + \cdots \right\} \rho(\vec{r}') d^3\vec{r}'. (5)$$

Rewriting this expression in terms of potential energies and their derivatives leads to the expression for H_{ne} given by Cohen and Reif (4):

$$H_{\text{ne}} = \int_{V} d^{3}\bar{x} \rho(\bar{x}) \{ v_{0} + \sum_{j=1}^{3} (\frac{\partial V}{\partial x_{j}})_{\bar{x}=0}^{2} x_{j} + \frac{1}{2} \int_{j,k=1}^{3} (\frac{\partial^{2} V}{\partial x_{j}} \partial x_{k})_{\bar{x}=0}^{2} x_{j} x_{k} + \cdots \}$$
(6)

and the origin is now the nuclear center of mass, since its motion is unaffected by nuclear reorientation. If the terms independent of \bar{X} , the electron position vector, are taken from under the integral, it gives (from either Equation (5) or (6))

$$H_{ne} = Z_e V_o + \sum_{j} P_j V_j + \frac{1}{2} \sum_{j,k} Q_{jk} V_{jk} + \cdots, \qquad (7)$$

with

$$\int d^3 \bar{x} \rho \left(\bar{x} \right) = Z_e, \quad \text{the nuclear charge}$$

$$\int d^3 \bar{x} \rho \left(\bar{x} \right) X_j = P_j, \quad \text{nuclear electric dipole moment}$$

$$\int d^3 \bar{x} \rho \left(\bar{x} \right) X_j X_k = Q_j^i k, \quad \text{nuclear electric quadrupole}$$
 moment. (8)

The first term is simply the charge of a point nucleus and therefore has already been included in the Hamiltonian. In the quantum mechanical transformation, the charge distribution $\rho(\overline{X})$ is replaced by the operator $\hat{\rho}(\overline{X})$, which depends on the position vectors of the A nucleons in the nucleus. However, the energy separation between the ground and excited nuclear states is very large compared to the quadrupole splittings and to a very good approximation the matrix elements of \hat{H} can be considered diagonal in all quantum numbers characterizing the nuclear ground state, except the nuclear spin projection m. If all unspecified quantum numbers are denoted by η , the matrix elements will have the form $\langle \eta \text{Im} | \hat{H} | \eta \text{Im}^{\dagger} \rangle$.

Examination of the specific form of the matrix elements shows the second term in \hat{H}_{ne} gives integrals of the form

$$\sum_{j=1}^{3} \int \Psi (\eta Im) \hat{\rho}_{op} \Psi (\eta Im') X_{j} d^{3}\bar{r}_{1} \cdots d^{3}\bar{r}_{A} . \qquad (9)$$

If the nuclear ground state is non-degenerate in I and assuming all electrical effects arise from electrical charges, then the $\Psi(\eta Im)$'s have definite parities and the above integral must vanish. Furthermore, any term in the expansion containing an odd power of X_j will also lead to integrals of odd symmetry which vanish. Therefore, the Hamiltonian reduces to

$$\hat{H}_{ne} = \hat{H}_{Q} = \frac{1}{2} \sum_{j,k} \sum_{k=1}^{N} Q_{jk}^{i} \left(\frac{\partial^{2} V}{\partial x_{j} \partial x_{k}} \right)_{0} + \text{hexadecapole term} + \cdots$$
(10)

The hexadecapole term is of the order of $\left(\frac{r_n}{r_e}\right)^2$ or about

10⁻⁸ of the quadrupole term and non-vanishing on symmetry

grounds (7) only for $I \geq 2$, so it will be neglected.

It is convenient to express the symmetric tensor $\widetilde{\mathbb{Q}}^{i}$ in terms of the symmetric tensor $\widetilde{\mathbb{Q}}$, which is also traceless:

$$Q_{jk} = 3Q'_{jk} - \delta_{jk} \sum_{\ell=1}^{3} Q'_{\ell\ell} . \qquad (11)$$

Substitution of Q_{jk} into \hat{H}_Q will then result in two terms, the second involving only traces of second-rank tensors which are independent of nuclear orientation, and can be neglected here. Thus,

$$\hat{\mathbf{f}}_{Q} = \frac{1}{6} \sum_{j k} \sum_{k} Q_{jk} V_{jk} , \qquad (12)$$

with $V_{jk} = (\partial^2 V/\partial X_j \partial X_k)_0$. Recalling the properties of \tilde{Q} and the matrix elements of \hat{H}_Q , the Wigner-Eckart theorem, which proves that the corresponding matrix elements of all traceless second-rank symmetric tensors are proportional, is used to relate the elements of \tilde{Q} to those of a more familiar tensor (5) (Equation (16) below). The matrix elements of this tensor have the form

$$\langle \text{Im'} | Q_{jk} | \text{Im} \rangle = C \langle \text{Im'} | \frac{3}{2} (I_j I_k + I_k I_j) - \delta_{jk} \overline{I}^2 | \text{Im} \rangle$$
, (13)

where C is a proportionality constant independent of m or m' and $\overline{I}^2 = I_1^2 + I_2^2 + I_3^2$. The constant C is related to the nuclear electric quadrupole moment, Q , defined conventionally as

$$eQ = \langle II | Q_{33} | II \rangle . \qquad (14)$$

Then, (see Equation (13))

eQ =
$$C\langle II | 3I_z^2 - \overline{I}^2 | II \rangle = C\{3I^2 - I(I + 1)\}$$

and

$$C = \frac{eQ}{I(2I-1)}$$
 (15)

By incorporation of the above definitions into $\,\, \hat{H}_{\mbox{\scriptsize Q}} \,$, the quadrupolar Hamiltonian can be written as

$$\hat{H}_{Q} = \frac{eQ}{6I(2I-1)} \sum_{j,k} \left\{ \frac{3}{2} (I_{j}I_{k} - I_{k}I_{j}) - \delta_{jk} \bar{I}^{2} \right\} V_{jk} . (16)$$

The field gradient tensor, $\overset{\approx}{V}$, is also symmetric by its definition, resulting in six independent components rather than nine. By choosing the coordinate system to coincide with the principal axis system of $\overset{\approx}{V}$, only three components of $\overset{\approx}{V}$ need to be specified in addition to their direction cosines. In the principal axis system the Hamiltonian becomes

$$\hat{H}_{Q} = \frac{2Q}{4I(2I-1)} \{ v_{ZZ}(3I_{Z}^{2} - \overline{I}^{2}) + (v_{XX} - v_{YY})(I_{X}^{2} - I_{Y}^{2}) \}.(17)$$

Finally, since only spherically symmetric s state electrons have non-zero probability of being at the nuclear center of mass, Laplace's equation gives us the additional relationship $V_{XX} + V_{YY} + V_{ZZ} = 0$. The two independent components needed to characterize \widetilde{V} are conventionally defined as

eq
$$\equiv V_{ZZ}$$
, the field gradient,

and

$$\eta = \frac{V_{\mbox{\footnotesize{XX}}} - V_{\mbox{\footnotesize{YY}}}}{V_{\mbox{\footnotesize{ZZ}}}}$$
 , the asymmetry parameter.

Since the range of values of I is small, the resulting secular equations have been solved to give energy level expressions and transtion frequencies for most nuclei which it is feasible to study. References to such tables of eigenvalues and energy level expressions are given in Das and Hahn (8). Because of their applicability to nuclei studied here, the expressions for $I = \frac{5}{2}$ are developed in the following section.

2. Energy Levels and Frequencies for $I = \frac{5}{2}$

The nuclei studied in this work are all of nuclear spin $I=\frac{5}{2}; \ ^{127}I, \ ^{185}\text{Re}, \ ^{187}\text{Re} \ \text{and the energy level and transition frequencies for this case are developed below. Referring to the expression for \hat{H}_Q given above (see Equation 17))}$

$$\hat{H}_{Q} = \frac{e^{2}qQ}{4I(2I-1)} \{ (3I_{Z}^{2} - \bar{I}^{2}) + \frac{\eta}{2} (I_{+}^{2} + I_{-}^{2}) \} . \tag{19}$$

Of the possible matrix elements of \hat{H}_{Q} only two non-zero types remain,

$$\langle m | \hat{H}_{Q} | m \rangle = \frac{e^2 qQ}{4I(2I-1)} [3m^2 - I(I+1)]$$

and (20)

$$\langle m\pm 2 \mid H_{Q} \mid m \rangle = \frac{e^{2}qQ}{4I(2I-1)} \frac{\eta}{2} \{I(I+1)-m(m\pm 1)\}^{1/2} \{I(I+1)-(m\pm 1)(m\pm 2)\}^{1/2}.$$

The secular equation which results for spin $\frac{5}{2}$ cannot be solved exactly, but Bersohn (9) has derived a general expression convergent for $\eta \leq 0.25$. The energy levels to second order in η , sufficient if $\eta \leq 0.1$, are

$$E_{\pm 5/_{2}} = \frac{e^{2}qQ}{40} (10 + \frac{5}{9} \eta^{2} + \cdots)$$

$$E_{\pm 3/_{2}} = \frac{e^{2}qQ}{40} (-2 + 3\eta^{2} + \cdots)$$

$$E_{\pm 1/_{2}} = \frac{e^{2}qQ}{40} (-8 - \frac{32}{9} \eta^{2} + \cdots) .$$
(21)

A complete tabulation applicable to any value of η is given by Livingston and Zeldes (10), who give tables of eigenvalues for $I=\frac{5}{2}$ and η values from 0 to 1 at intervals of 0.001. Considering only allowed transitions two lines should be observable with frequencies

$$\omega_{Q} \left(\pm \frac{5}{2} - \pm \frac{3}{2} \right) = \frac{3e^{2}qQ}{10\hbar} \left(1 - \frac{11}{54} \eta^{2} \right),$$

$$\omega_{Q} \left(\pm \frac{3}{2} - \pm \frac{1}{2} \right) = \frac{3e^{2}qQ}{20\hbar} \left(1 + \frac{5}{54} \eta^{2} \right).$$
(22)

For the compounds considered in this study it has been found (11) that within experimental error $\eta=0$, resulting in the $(\pm \frac{5}{2} \iff \pm \frac{3}{2})$ line being twice the frequency of the $(\pm \frac{3}{2} \iff \pm \frac{1}{2})$ line.

B. Calculation of Electric Field Gradients

As shown in the preceding section, the observed quadrupole frequencies permit the determination of two quantities, e^2qQ and η . Since values of Q can in most cases be obtained from molecular or atomic beam measurements or gas phase coupling constants, the calculation of quadrupole frequencies reduces to calculating q and q, the electric field gradient (EFG) tensor components. Since pure quadrupole resonance is observable only in solids, the discussion

here will be limited to solid state calculations of EFG's.

The non-overlapping charge or ionic method will be discussed first, followed by a brief discussion of the Townes
Dailey theory as background for references to the theory

in discussing the anomalous temperature effects in Section C.

1. Non-overlapping Charge Model

The general problem is to calculate the electrostatic potential at the center of mass of the quadrupolar nucleus due to an external charge distribution $\rho(\bar{r})$. The potential is given by

$$V(0) = \int \frac{d^3\vec{r} \rho(\vec{r})}{\vec{r}} , \qquad (23)$$

with the integration extending over the range of $\rho\left(\overline{r}\right)$. Correspondingly, the field gradient tensor components are given by

$$V_{KK}(0) = \int \rho(\overline{r}) \frac{3K^2 - r^2}{r^5} d^3\overline{r}$$
and
$$V_{KV}(0) = \int \rho(\overline{r}) \frac{KV}{r^5} d^3\overline{r}$$
(24)

where κ , ν denote Cartesian components of \bar{r} and again the integration is over the range of $\rho(\bar{r})$. In cases where accurate wave functions are available, such as isolated simple molecules, this involves the evaluation of one-, two- and three-center integrals. In most cases this results in fairly close agreement between theory and experiment. For solids, however, existing wave functions are

not of sufficient quality for such calculations and approximations must be made. Presently the most widely used approximation is the non-overlapping charge model, in which the charge distribution in the solid is assumed to be centered on the nuclei such that the charge clouds do not overlap. This clearly implies complete ionic bonding and is not expected to give completely realistic results for a crystal with any appreciable amount of covalent bonding. The second, and more restrictive, assumption usually made is that these non-overlapping charge distributions are spherical. As electrostatic theory states that such a distribution behaves as if the charge were concentrated at the center of the sphere, this assumption is referred to as the point-charge model. In this model the field gradient components can be calculated by evaluating two types of sums,

$$v_{\kappa\kappa} = \sum_{j} \epsilon_{j} \frac{3\kappa_{j}^{2} - r_{j}^{2}}{r_{j}^{5}}$$
(25)

and

$$V_{\kappa\nu} = \sum_{j} \epsilon_{j} \frac{\kappa_{j} v_{j}}{r_{j}^{5}} ,$$

where ϵ_j is the ionic charge of the jth atom, κ_j and ν_j are components of the position vector of the jth atom, and the sum extends over the atoms of an infinite crystal. Contrary to the feeling that the $\frac{1}{r_3}$ dependence should lead to rapid convergence of these conditionally convergent sums, the number of terms needed to achieve reliable results is

quite large and is strongly dependent upon the method of summation employed. Direct summation requires summing in spheres of increasing radius, first carried out by Bersohn (12), but convergence is slow and spheres as large as 100% diameter are often needed to get satisfactory convergence. Several rapidly converging methods involving cumbersome neutral units such as the crystallographic unit cell have been developed (13,14), but one of the most elegant and rapidly convergent methods is that given by DeWette and Schacher (15,16) based on transforming the slowly converging series into one which is rapidly convergent.

The method is derived from a procedure (17) for calculating internal fields in dipole lattices, an important problem in dielectric constant theory. The sums in Equation (25) are broken up into summations over sublattices of identically charged ions and then summed over the total number of unit cells. For a crystal containing Σ_j different ions the tensor components are

$$v_{\kappa\kappa}(0) = \sum_{\lambda j} \left\{ \frac{3\kappa^{2}(\lambda,j)}{r_{\lambda,j}^{5}} - \frac{1}{r_{\lambda,j}^{3}} \right\}$$
and
(26)

$$v_{k,\nu}(0) = \sum_{\lambda j} \sum_{i} \epsilon_{j} \left(\frac{3 \kappa_{\lambda,j}^{\nu} \lambda_{i,j}}{r_{\lambda,j}^{5}} \right)$$

where Σ_{λ} is the sum over the unit cells. The number of terms in Σ_{λ} is large, but should converge rather rapidly otherwise the calculated field gradient would depend upon

the external crystal shape. Instead of summing Equation (26), the order of the λ and j summation is interchanged and the conditionally convergent sums evaluated planewise rather than spherically. The first sum is over λ_1 , λ_2 with $\lambda_3 = 0$, then over λ_1 , λ_2 with $\lambda_3 = \pm 1$, etc. The advantage of such an ordering is that instead of summing the slowly convergent λ_1 , λ_2 series directly, its Fourier transform is evaluated in the reciprocal lattice. The resulting sum is absolutely convergent with rapid convergence in most cases, leading to consistent results after combining the sums from each of the sublattices. Although this method removes uncertainties in the results due to convergence errors, agreement of the calculated field gradients with those obtained from experiment is still extremely poor, indicating that several important effects have not been considered.

One of the assumptions up to now is that the electron shell around the quadrupolar nucleus itself contributes nothing to the field gradient, since it is in an 1S state. In reality, however, this electron cloud is distorted due to polarization by the external field gradient or alternatively by the aspherical quadrupolar nucleus, giving rise to a significant, and in some cases exteremely large, contribution to the lattice field gradient (18). Regardless of the point of view, the calculated field gradient is altered from \widetilde{V}_{lat} , the calculated external field gradient. The new tensor \widetilde{V} is given by

$$\tilde{\mathbf{v}} = (\mathbf{1} - \gamma_{\mathbf{c}}) \tilde{\mathbf{v}}_{lat}$$
 (27)

where γ_{∞} is the Sternheimer shielding factor. This correction to $\stackrel{\approx}{V}_{lat}$ is often very large, since γ_{∞} is usually negative and ranges up to 100 or more. The Sternheimer factors are not measureable experimentally and the uncertainties in calculating values for larger ions makes comparison between theory and experiment difficult. In many cases, however, unusually large γ_{∞} 's are needed to give agreement with experiment, indicating that the point charge assumption is invalid and some distortion from sphericity in the other ionic charge distributions must be included.

Since the site symmetry of nuclei in lattices in which quadrupole resonance can be observed is necessarily less than cubic, it might be expected that easily polarizable ions such as 0²⁻ would undergo some distortion. To take this distortion into account the charge distribution is replaced by a multipole expansion, with the resulting potential

$$\mathbf{v} = \sum_{\lambda} \frac{\mathbf{e}}{\mathbf{R}_{\lambda}} + \sum_{\alpha, \lambda} \mathbf{p}_{\alpha} \left[\frac{\partial}{\partial \mathbf{x}_{\alpha}} (\frac{1}{\mathbf{r}}) \right]_{\mathbf{R}_{\alpha}} + \frac{1}{2} \sum_{\alpha, \beta, \lambda} \mathbf{q}_{\alpha\beta} \left[\frac{\partial^{2}}{\partial \mathbf{x}_{\alpha} \partial \mathbf{x}_{\beta}} (\frac{1}{\mathbf{r}}) \right]_{\mathbf{R}_{\alpha}} + \cdots$$

where Σ_{λ} denotes summation over all lattice points, p_{α} is the α component of the dipole moment, $q_{\alpha\beta}$ is the $\alpha\beta$ component of the quadrupole moment, the cubic term is assumed negligible and the expansion is truncated. The induced moments can be written as

$$\mathbf{p}_{\alpha} = \alpha \mathbf{v}_{\alpha}$$
 , $\mathbf{q}_{\alpha\beta} = \beta \mathbf{v}_{\alpha\beta}$ (29)

where α,β are the dipolar and quadrupolar polarizabilities, respectively, for each ion, although the smaller cation polarizabilities are usually neglected. Several problems arise in applying this correction to the calculated field gradient, which makes the significant improvement in agreement with experiment questionable. Since alternate independent experiments don't exist to give α and β for these ions they are often treated as adjustable parameters. Values obtained from this procedure usually don't agree with polarizabilities calculated from ab initio wave functions, but the calculated values are strongly dependent upon the wave functions used. Even more discouraging, however, the dipolar and quadrupolar terms are of comparable, or even larger magnitude, to the point-charge term, contrary to the assumption made in truncating the series in Equation (28).

As a result of such uncertainties in γ_{∞} and in the induced polarizabilities, agreement between theory and experiment does not necessarily imply validity of the ionic model. The need for such modification is a result of attempting to modify the non-overlapping charge model to accommodate some degree of covalent bonding, certainly present even in "ionic" crystals. When the degree of covalency is high enough to consider the quadrupolar nucleus as forming part of a molecular unit an alternate procedure

is used. In this procedure the EFG contribution from the lattice is calculated as outlined above and added to the covalent contribution calculated from the Townes-Dailey theory discussed in the next section. Unfortunately, the empirical nature of the Townes-Dailey theory usually results in agreement with experiment, obscuring the deficiencies in this type of approximation.

2. Townes-Dailey Method

This discussion is only a brief outline of the complete theory which has been presented elsewhere (8,19,20), with an outline of the main assumptions and resulting equations relating the coupling constant, e^2qQ , to the bonding parameters for the molecule containing the quadrupolar nucleus.

If the Sternheimer polarization factor is neglected, the value of ${\bf q}$ in isolated atoms arises only from the electrons outside the closed shells. The magnitude of this atomic field gradient is known from atomic fine or hyperfine structure studies or can be calculated from atomic wave functions. The central assumption which Townes and Dailey make is that the quadrupolar nucleus retains its outer electrons in hybridized atomic orbitals that take part in forming molecular orbitals, and that the resulting coupling constant is proportional to ${\bf q}_{\rm at}$, the field gradient for the isolated atom. Therefore, Townes and Dailey express

$$q_{mol} = f q_{at}$$
 (30)

where the quantity f depends on the electronic structure calculated according to the prescription given by the Townes-Dailey theory.

For simplicity consider the case of one valence electron in a molecular orbital ϕ_i constructed from a basis set of atomic orbitals χ_r ,

$$\phi_{i} = \sum_{r} C_{ri} \chi_{r} , \qquad (31)$$

the contribution to the field gradient from this electron can be written

$$(eq)_{e1} = e \int (\sum_{r} c_{ri}^* \chi_r^*) \left(\frac{3\cos^2 \theta_{iA}^{-1}}{r_{iA}^3} \right) (\sum_{s} c_{si} \chi_s) d\tau$$
 (32)

for the field gradient at nucleus A. Rearranging,

$$(eq)_{e1} = e\sum_{r} \sum_{s} [c_{ri}^* c_{si}] \int \chi_r^* (\frac{3\cos^2\theta_{iA}^{-1}}{r_{iA}^3}) \chi_s d\tau$$

$$= e\sum_{r} \sum_{s} R_{rs} q_{rs}$$
(33)

where the C_{ri} 's are the expansion coefficients from Equation (31), θ_{iA} and r_{iA} components of the position vector in polar coordinates, and R_{rs} denotes the term in brackets and q_{rs} the integral involving the atomic basis functions χ . For hydrogen-like atomic orbitals contributions to the field gradient from orbitals with $\ell > 1$ are

relatively unimportant, since

$$(eq)_{n,\ell,m=0} = \frac{4eZ^3}{n^3a_0^3(2\ell-1)(2\ell+1)(2\ell+3)}$$
 and (34)

$$(eq)_{n, \ell, m = \pm \ell} = \frac{-2\ell-1}{\ell+1} (eq)_{n, \ell, m=0}$$
.

This inverse third power dependence of q_{at} upon ℓ is the basis for the assumption that contributions from orbitals with $\ell > 1$ are negligible, with the result that only valence electrons in p orbitals need to be considered, since the spherically symmetric s electrons don't contribute to $(eq)_{at}$.

Following Scrocco (21), consider as an example the field gradient at nucleus A in a diatomic molecule AB. The expression for $(eq)_{mol}$ following the notation given above is

$$(eq)_{mol} = (eq)_{el} + (eq)_{nuc} = (2e\sum \sum R_{rs}q_{rs})_{atom A}$$

$$+ (2e\sum \sum R_{rs}q_{rs})_{atom B} + (2e\sum \sum R_{rs}q_{rs})_{overlap AB}$$

$$- \frac{2eZ_B}{R_{AB}^3}.$$
(35)

Two primary assumptions are now made (19) to simplify this expression;

1) Due to the $1/r_{1A}^3$ term in q_{rs} (see Equation (33)) the second and third terms are rather small and are assumed to be cancelled by the last term, leaving only the first

term contributing to (eq)_{mol}.

2) Assuming contributions from inner shell polarization is negligible compared to the field gradient from the valence p electrons we arrive at the simple result

$$(eq)_{mol} = (eq)_{atom A}^{el} = (n_x(eq)_{p_x} + n_y(eq)_{p_y} + n_z(eq)_{p_z})_{atom A}^{(36)}$$

Assuming the field gradient is equal to the corresponding free atom quantities reduces the relationship to the form given in Equation (30),

$$e^{2}Qq_{mol} = eQ\{[n_{z} - \frac{1}{2}(n_{x} + n_{y})] (eq)_{p_{z}}\}_{atom A}$$
 (37)

In treating specific examples the occupation numbers n_{χ} , n_{χ} of the p_{χ} and p_{χ} orbitals are often related to π molecular orbital occupation numbers and n_{χ} to the fraction of sp hybridization in the σ bonds. For transition metal nuclei a corresponding expression involving and valence orbitals is used, since the (n+1)p orbitals are too high in energy to contribute to the bonding.

C. Temperature Dependence of NQR Frequencies

Since the electric field gradient and hence the frequency of absorption are dependent upon the positions of other ions in the crystal lattice, the observed temperature dependence of NQR frequencies is reasonable. In practice two general types of behavior are observed: (a) the NQR frequency increases with decreasing temperature, termed the

normal temperature dependence, and (b) the frequency decreases with decreasing temperature, termed the anomalous temperature dependence. Other types of behavior include changes in the number of absorption lines and the disappearance of a line due to phase transitions or the creation of slightly inequivalent sites as the crystal contracts. This discussion will deal primarily with normal temperature variation, but a short discussion of possible origins of the anomalous temperature effect will be given, since NH4ReO4 exhibits this behavior.

In the case of normal temperature dependence, the NOR frequencies increase as the temperature is lowered. Since the quadrupole moment, Q, is a nuclear ground state property it should experience no change over normal temperature ranges, therefore changes in the field gradient tensor must be responsible for the shifts of frequency with temperature. A mechanism was first advanced by Bayer, who attributed (22) the observed behavior to low-frequency vibrations of the atoms or molecules in the crystal. In many cases, however, the Bayer theory gives poor agreement with experiment, since it neglects lattice expansion. The theory was extended (23) by Kushida, Benedek and Bloembergen in a phenomenalogical theory including the Bayer theory as one of several terms. An outline of this theory is given below along with a discussion of the model of the crystal vibrations used in calculating the Bayer term. The following discussion is derived mainly from references 8, 22 and 23 with a number of missing steps supplied.

As discussed in Section A and above, the quadrupole interaction is completely characterized by two parameters, e^2qQ and η . Before examining the microscopic model relating crystal vibrations to these parameters, consider the quadrupole frequency ν to be a function of volume, temperature and the low frequency vibrations, with the frequency of the ℓ^{th} vibrational mode denoted by ν_{ℓ} . The total differential of ν , with $\nu = \nu(\nu_{\ell}, \nu, \tau)$ is

$$dv = \sum_{\ell} \left(\frac{\partial v}{\partial v_{\ell}}\right) v_{\ell} + \left(\frac{\partial v}{\partial v}\right) v_{\ell} + \left(\frac{\partial v}{\partial v}\right) v_{\ell} dv + \left(\frac{\partial v}{\partial v}\right) v_{\ell} dv$$
(38)

where the sum is over all possible modes of vibration, both internal modes and external lattice modes. Partial differentiation with respect to T at constant P,N gives

$$(\frac{\partial v}{\partial \mathbf{T}})_{\mathbf{P},\mathbf{N}} = \sum_{\ell} (\frac{\partial v}{\partial \mathbf{v}}_{\ell})_{\mathbf{V},\mathbf{T}} (\frac{\partial v}{\partial \mathbf{T}})_{\mathbf{P},\mathbf{N}} + (\frac{\partial v}{\partial \mathbf{V}})_{\mathbf{V}_{\ell},\mathbf{T}} (\frac{\partial v}{\partial \mathbf{T}})_{\mathbf{P},\mathbf{N}} + (\frac{\partial v}{\partial \mathbf{T}})_{\mathbf{V},\mathbf{v}_{\ell}}$$
Similarly, (39)

$$\left(\frac{\partial \mathbf{P}}{\partial \mathbf{v}}\right)^{\mathbf{T'N}} = \sum_{\mathbf{V}} \left(\frac{\partial \mathbf{v}}{\partial \mathbf{v}}\right)^{\mathbf{V'T}} \left(\frac{\partial \mathbf{P}}{\partial \mathbf{v}}\right)^{\mathbf{T'N}} + \left(\frac{\partial \mathbf{V}}{\partial \mathbf{v}}\right)^{\mathbf{V'T}} \left(\frac{\partial \mathbf{P}}{\partial \mathbf{v}}\right)^{\mathbf{T'N}}.$$

Assuming that the lattice vibrations depend only on volume, <u>i.e.</u>, that the crystal vibrates isotropically then $v_{\ell} = v_{\ell}(v)$ and

$$(\frac{\partial v_{\ell}}{\partial T})_{P,N} = \frac{dv_{\ell}}{dV}(\frac{\partial V}{\partial T})_{P,N}$$
and
$$(\frac{\partial v_{\ell}}{\partial P})_{T,N} = \frac{dv_{\ell}}{dV}(\frac{\partial V}{\partial P})_{T,N}.$$
(40)

Substitution of these relations into Equation (39), gives the necessary final relationships:

$$(\frac{\partial v}{\partial \mathbf{T}})_{\mathbf{P},\mathbf{N}} = \{ \sum_{\ell} (\frac{\partial v}{\partial \mathbf{v}_{\ell}})_{\mathbf{V},\mathbf{T}} \frac{d\mathbf{v}_{\ell}}{d\mathbf{V}} + (\frac{\partial v}{\partial \mathbf{V}})_{\mathbf{V}_{\ell},\mathbf{T}} \} (\frac{\partial v}{\partial \mathbf{T}})_{\mathbf{P},\mathbf{N}} + (\frac{\partial v}{\partial \mathbf{T}})_{\mathbf{V},\mathbf{v}_{\ell}}$$

$$(\frac{\partial v}{\partial \mathbf{P}})_{\mathbf{T},\mathbf{N}} = \{ \sum_{\ell} (\frac{\partial v}{\partial \mathbf{v}_{\ell}})_{\mathbf{V},\mathbf{T}} \frac{d\mathbf{v}_{\ell}}{d\mathbf{V}} + (\frac{\partial v}{\partial \mathbf{V}})_{\mathbf{V}_{\ell},\mathbf{T}} \} (\frac{\partial v}{\partial \mathbf{P}})_{\mathbf{T},\mathbf{N}} .$$

$$(41)$$

Note that the bracketed terms are identical in the above equations, although they are multiplied by different partial differentials. These differentials are related to two experimentally observable quantities

$$\alpha \equiv \frac{1}{V}(\frac{\partial V}{\partial T})_{P,N}, \text{ Coefficient of thermal expansion}$$
 and
$$K_T \equiv -\frac{1}{V}(\frac{\partial V}{\partial P})_{T,N}, \text{ Isothermal compressibility.}$$

In principle, therefore, it should be possible to remove the effects of lattice expansion by performing an additional experiment, the measurement of pressure dependence of the NQR frequency and either measuring, or obtaining from the literature, values of α and K_T over the range of temperatures covered. Then the bracketed term could be calculated from the pressure-dependence data leaving only the desired Bayer term, $(\partial v/\partial T)_{V,V_\ell}$; to be calculated from an appropriate microscopic model and compared to experiment. Unfortunately, compressibility data below room temperature

are rare, and since K_T is a function of temperature an equation of state is needed from which K_T can be calculated at any desired temperature. Before discussing the method used by Kushida, et al. a short discussion of the harmonic potential model for a crystal is given.

The method of treating vibrations in solids (24) is the harmonic approximation in which the displacements of atoms from their equilibrium positions are assumed small and as a result the potential $V(\bar{R}_j)$ can be written as $V(\bar{R}_j^0 + \bar{\mu}_j)$ where the \bar{R}_j^0 's are equilibrium coordinates and the $\bar{\mu}_j$'s displacement coordinates. Expanding $V(\bar{R}_j)$ in a Taylor series and truncating the series after the term second order in μ_j gives the well-known result for the vibrational Hamilitonian,

$$H_{vib} = \sum_{i=1}^{3N} \frac{P_{i}^{2}}{2m} + \frac{1}{2} \sum_{i=1}^{3N} \sum_{j=1}^{3N} A_{ij}^{\mu}_{i}^{\mu}_{j} . \qquad (43)$$

The displacement coordinates which diagonalize this Hamilitonian are called normal coordinates, the resulting Hamilitonian being identical to that for the harmonic oscillator with the eigenvalues termed normal modes. In a three-dimensional crystal the number of normal modes is very large, on the order of 3nN for a crystal with an n-atom basis (n-atoms per lattice point). These quantized vibrations are known as phonons and are conventionally labelled by k vectors, which are the position vectors in reciprocal lattice space. Additional details concerning phonons, the harmonic approximation and the Brillouin zone representation

can be found elsewhere (24,25).

. If the phonon states are labelled by \underline{k} -vectors, the molecular partition function becomes

$$\mathbf{z}_{\mathbf{k}} = \sum_{\mathbf{k}} \mathbf{e}^{-\beta \epsilon_{\mathbf{k}}} = \sum_{\mathbf{n}_{\mathbf{k}}} \mathbf{e}^{-\beta \tilde{\mathbf{n}} \omega_{\mathbf{k}} (\mathbf{n}_{\mathbf{k}}^{+1/2})} = \frac{\mathbf{e}^{-\beta \tilde{\mathbf{n}} \omega_{\mathbf{k}}}}{2} \cdot (44)$$

The total partition function, $z = \pi_k z_k$, becomes

$$z = \pi_{k} \frac{1}{2 \sinh(\frac{\beta \hbar \omega_{k}}{2})}$$
 (45)

and, remembering that $A = -kT \ln Z$, one obtains

$$A = U_{cohesive}(V) - kT \sum_{k=1}^{3N} ln(2 sinh(\frac{\hbar \omega_k}{2kT})), \qquad (46)$$

where the $U_{cohesive}(V)$ term arises from a redefinition of the zero of potential energy. Since

$$P = -\left(\frac{\partial A}{\partial V}\right)_{T,N}, \text{ then } \frac{1}{K_T} = V\left(\frac{\partial^2 A}{\partial V^2}\right)_{T,N}$$
 (47)

and the compressibility may be obtained from A at any temperature by differentiating twice with respect to volume.

By the above procedure the only remaining unknown is the Bayer term, $(\partial V/\partial T)_{V,V}$. Bayer assumed that the field gradient would be averaged in the crystal by librational, or torsional, motions which modify the field gradient tensor by mixing field gradient components. Following Das and Hahn (8), the general case of a molecule undergoing

torsional motion about all three principal tensor axes, in a system without axial symmetry, will be considered. Small rotations $\theta_{\mathbf{x}}$, $\theta_{\mathbf{y}}$, $\theta_{\mathbf{z}}$ about the molecule-fixed axes \mathbf{x} , \mathbf{y} , \mathbf{z} can be related to the space-fixed system $\mathbf{x'}$, $\mathbf{y'}$, $\mathbf{z'}$ by a unitary transformation. To find the transformation consider first a rotation $\theta_{\mathbf{x}}$ about the \mathbf{x} axis, then successive rotations about the \mathbf{y} and \mathbf{z} axes of our coordinate system. Combining these will give the desired transformation matrix. The rotation $\theta_{\mathbf{y}}$ gives

$$x' = x$$

 $y' = y\cos \theta_{x} - z\sin \theta_{x}$ (48)
 $z' = z\cos \theta_{x} + y\sin \theta_{x}$.

Similarly for θ_y and θ_z

$$x'' = x'\cos \theta_{y} + z'\sin \theta_{y} \qquad x''' = x''\cos \theta_{z} - y''\sin \theta_{z}$$

$$y'' = y' \qquad \qquad y''' = y''\cos \theta_{z} + x''\sin \theta_{z}$$

$$z'' = z'\cos \theta_{y} - x'\sin \theta_{y} \qquad z''' = z'' \qquad (49)$$

where the axis system to the left in each set corresponds to the rotated system. Substitution and combination of terms gives the relationship between the space-fixed x, y, z axes and the moving x', y', z' axes

$$\mathbf{x'} = (\cos\theta_{\mathbf{y}}\cos\theta_{\mathbf{z}})\mathbf{x} + (\cos\theta_{\mathbf{y}}\sin\theta_{\mathbf{z}})\mathbf{y} - (\sin\theta_{\mathbf{y}})\mathbf{z}$$
(50)

$$\mathbf{y'} = (\sin\theta_{\mathbf{x}}\sin\theta_{\mathbf{y}}\cos\theta_{\mathbf{z}} - \cos\theta_{\mathbf{x}}\sin\theta_{\mathbf{z}})\mathbf{x} + (\cos\theta_{\mathbf{x}}\cos\theta_{\mathbf{z}})\mathbf{y}$$

$$+ (\sin\theta_{\mathbf{x}}\cos\theta_{\mathbf{y}})\mathbf{z}$$

$$\mathbf{z'} = (\sin\theta_{\mathbf{x}}\sin\theta_{\mathbf{z}} + \cos\theta_{\mathbf{x}}\sin\theta_{\mathbf{y}}\cos\theta_{\mathbf{z}})\mathbf{x} + (\cos\theta_{\mathbf{x}}\sin\theta_{\mathbf{y}}\sin\theta_{\mathbf{z}})\mathbf{x}$$

 $z' = (\sin\theta_x \sin\theta_z + \cos\theta_x \sin\theta_y \cos\theta_z)x + (\cos\theta_x \sin\theta_y \sin\theta_z)$ $-\sin\theta_x \cos\theta_z)y + (\cos\theta_x \cos\theta_y)z.$

Use of this transformation and expansion of the sines and cosines in a MacLaurin series, since the rotations θ_{x} , θ_{y} , θ_{z} are assumed small, gives

$$v_{X'X'} = (1 - \theta_{Y}^{2} - \theta_{Z}^{2}) v_{XX} + \theta_{Z}^{2} v_{YY} + \theta_{Y}^{2} v_{ZZ}$$

$$v_{Y'Y'} = \theta_{Z}^{2} v_{XX} + (1 - \theta_{X}^{2} - \theta_{Z}^{2}) v_{YY} + \theta_{X}^{2} v_{ZZ}$$

$$v_{Z'Z'} = \theta_{Y}^{2} v_{XX} + \theta_{X}^{2} v_{YY} + (1 - \theta_{X}^{2} - \theta_{Y}^{2}) v_{ZZ}$$

$$v_{X'Y'} = (\theta_{X} \theta_{Y} - \theta_{Z}) v_{XX} + \theta_{Z} v_{YY} - \theta_{X} \theta_{Y} v_{ZZ}$$

$$v_{Y'Z'} = -\theta_{Y} \theta_{Z} v_{XX} + (\theta_{Y} \theta_{Z} - \theta_{X}) v_{YY} + \theta_{X} v_{ZZ}$$

$$v_{Y'Z'} = (\theta_{Y} \theta_{Z} + \theta_{Y}) v_{YY} - \theta_{Y} \theta_{Z} v_{YY} - \theta_{Y} v_{ZZ} .$$

Only displacements up to second order have been retained in the above products. Thus, the instantaneous field gradient tensor is both time dependent and non-diagonal as a result of these librational motions. If the time-averaged effect on q and η is considered, and it is remembered that

$$\langle \theta_{\mathbf{X}} \rangle = \langle \theta_{\mathbf{Y}} \rangle = \langle \theta_{\mathbf{Z}} \rangle = 0$$
 (52)

we have

$$\mathbf{q'} = \mathbf{q} \left[\mathbf{1} - \frac{3}{2} \left(\left\langle \theta_{\mathbf{X}}^{2} \right\rangle + \left\langle \theta_{\mathbf{Y}}^{2} \right\rangle \right) - \frac{\eta}{2} \left(\left\langle \theta_{\mathbf{X}}^{2} \right\rangle - \left\langle \theta_{\mathbf{Y}}^{2} \right\rangle \right) + \frac{1}{2} \left(\mathbf{3} - \eta \right) \left\langle \theta_{\mathbf{X}}^{2} \right\rangle \left\langle \theta_{\mathbf{Y}}^{2} \right\rangle \right]$$

$$(53)$$

and

$$\eta' = \frac{\mathbf{q}}{\mathbf{q}'} \left[\eta - \frac{3}{2} (\langle \theta_{\mathbf{X}}^2 \rangle - \langle \theta_{\mathbf{Y}}^2 \rangle) - \frac{1}{2} \eta (\langle \theta_{\mathbf{X}}^2 \rangle + \langle \theta_{\mathbf{Y}}^2 \rangle) \right]$$

$$\frac{1}{2} (3 - \eta) \langle \theta_{\mathbf{X}}^2 \rangle \langle \theta_{\mathbf{Y}}^2 \rangle \right].$$

For all compounds considered here η has been found to be zero experimentally and, therefore, the effect of η on q' and η' will not be considered further. The $\langle \theta_i^2 \rangle$ terms can be related to measured vibrational frequencies by use of the harmonic approximation and the quantum mechanical analysis for a harmonic oscillation, leading to

$$m\omega^2\langle x^2\rangle = \langle E\rangle = (\langle \eta \rangle + \frac{1}{2}) \hbar\omega$$
 (54)

Recalling that phonons obey Bose-Einstein statistics, and by use of rotational counterparts of m and x, the expression becomes

$$\mathbf{A}_{\ell}\omega_{\ell}^{2}\langle\theta_{\ell}^{2}\rangle = \hbar\omega_{\ell} \left(\frac{1}{2} + \frac{1}{\exp(\hbar\omega_{\ell}/k\mathbf{T})-1}\right) \tag{55}$$

for the ℓ^{th} vibrational mode. Substitution of Equation (53) into the expression for q', the final expression relating the time dependent quadrupole frequency ν to ν_0 , the quadrupole frequency of the rigid lattice, becomes

$$v(\mathbf{T}) = v_0 \left(1 - \sum_{\substack{\text{normal} \\ \text{modes}}} \frac{3\hbar}{2A_{\ell}^{\omega} \ell} \left\{ \frac{1}{2} + \frac{1}{\exp(\hbar \omega_{\ell}/kT) - 1} \right\} \right). (56)$$

The summation term is written in a general way including other motions besides librations, although the derivation of Equation (55) assumed that only librations along the principal tensor axis modified the EFG. A discussion of

this point in this work and its treatment in the literature will be given in Chapter III.

As mentioned above, in a few cases an anomalous temperature effect is seen in which the quadrupole frequency increases with increasing temperature. In almost all such cases the compounds contain transition metal ions in oxidation states in which the t_{2g} orbitals which take part in $d\pi$ -p π metal-ligand bonding are partially filled. The anomalous behavior has been attributed (26,27) to the effects of fundamental vibrations of the transition metal complex on the degree of π -bonding.

In Section B the f factor in the Townes-Dailey theory for interpreting quadrupole coupling constants was shown to be

$$f = N_z - [(N_x + N_y)/2],$$
 (57)

where the N_i are ligand p_i orbital occupation numbers. In the cases involving chlorine ligands, Haas and Marram (26) assumed that the p_x , p_y orbitals were involved in π -bonding with the central metal ion, giving

$$f = N_{\tau} - N_{\tau} . \qquad (58)$$

Since the vibrational fundamentals are primarily stretching and bending motions the effects of each will be considered. The effect of the stretching motions was shown by Haas and Marram to be zero if a harmonic potential for the stretching vibrations was

chosen, since second-order terms in the expansion were then cancelled by deviations from harmonicity. In contrast, they postulated that the bending vibrations perturbed the bonding wave functions such that N_{π} increased linearly with $\langle \theta^2 \rangle$, the time average of the square of the bending angle. Since $N_{\pi} > N_{\sigma}$ for the halogens, the result was an increase in |f| with increasing $\langle \theta^2 \rangle$; $\langle \theta^2 \rangle$ is proportional to temperature hence they obtained an increase in the coupling constant with increase in temperature which overcame the negative temperature dependence of the Bayer term. Recently this explanation has been disputed (28) by Brown, who contends that it is the stretching, rather than the bending, motions which give rise to the observed effects. An excellent treatment of the two competing effects has been discussed in a series of papers (29) by Armstrong and coworkers.

The above mechanism which give rise to an anomalous NQR temperature dependence are not applicable to NH₄ReO₄, where the anomalous behavior is believed to result from the freezing out of the rotation of the ammonium ion. The specific mechanism will be discussed in detail in Chapter III.

	,
	à.
	Ş
	:
	ž
	:
	Ċ
	2
	ņ
	•
	:

II. EXPERIMENTAL

A. Synthesis and Crystal Growing

1. Synthesis

Most of the compounds used in this study had been prepared and purified previously (11) and were used without further purification. However, the ammonium and deutero-ammonium salts were prepared for this work and purification continued until impurity bands observed in the Raman spectra disappeared. The method of preparation for each compound is summarized below.

NH₄IO₄ and ND₄IO₄

These salts were prepared by neutralization of ammonium hydroxide or deuteroammonium hydroxide with periodic acid. The ammonium salt was prepared by dissolving periodic acid $(H_5IO_6, G. F. Smith Chemical Co.)$ in distilled water and adding ammonium hydroxide solution $(\sim 6N)$ dropwise to phad. The deuteroammonium salt was made in a similar manner, except the H_5IO_6 was dissolved in a large amount of D_2O to reduce the probability of isotopic mixing and the acid solution neutralized with a 26% solution of ND_4OD in D_2O

(Diaprep, Inc.). In both cases, if the neutralization was carried out by adding acid to a basic solution strong impurity peaks, apparently due to ${\rm IO_3}^-$, were found in the Raman spectra. No evidence of these impurity peaks was obtained in the samples used.

NH4ReO4 and ND4ReO4

Rhenium heptoxide, Re_2O_7 , was dissolved in water to form perrhenic acid which was then neutralized by the corresponding base. For the deuteroammonium salt the Re_2O_7 (Pressure Chemical Co.) was dissolved in D_2O forming $DReO_4$ which was then neutralized (pH ~ 5) by the ND_4OD solution. Because of its hygroscopic nature, the rhenium heptoxide was handled in an inert atmosphere until just prior to addition of the H_2O or D_2O .

RbIO4

This compound was prepared by neutralizing a solution of H_5IO_6 with a solution of rubidium hydroxide (Alfa Inorganics, Inc.).

2. Crystal Growth

Large, good quality crystals of both NaIO₄ and NaReO₄ were needed for Raman polarization studies. A suitable crystal of NaReO₄ was obtained by evaporation of an aqueous solution of the salt at room temperature, but several methods were tried before good crystals of sodium periodate

were obtained. Neither crystal could be grown from the melt since decomposition occurs before melting.

The first attempt to grow the NaIO₄ crystals was by slow evaporation of a saturated aqueous solution in a partially covered beaker at room temperature. The seed crystals were either laid on the bottom of the beaker or suspended by thin string. In both cases the resulting crystals were encrusted with small crystallites which formed at the evaporating surface and dropped onto the seeds. The latter problem was taken care of by covering the seed crystals with an inverted beaker perforated to allow free circulation of solution. The resulting crystals were relatively free of attached crystallites but the larger ones became cloudy. In order to prevent the formation of spurious seeds an alternate method (31) employing a completely closed system was used but crystallites still formed on the seed crystals.

The procedure finally adopted was based on a method (32) used in growing crystals for X-ray studies. If crystallization is carried out by this method in a slightly acidic ($\rm H_2SO_4$) solution between 40^0 and 45^0 C the resulting crystals do not have any cloudiness, even when grown rapidly. Also, the number of spurious crystallites formed is smaller and they do not seem to adhere to the seed crystal as much. The crystals were grown in sealed vials immersed in a large water bath (Figure 1) at a temperature of about 50^0 which was cooled at a rate of $1^0/{\rm day}$ for 10-14 days. Heat was supplied by a 125 watt blade heater connected to a

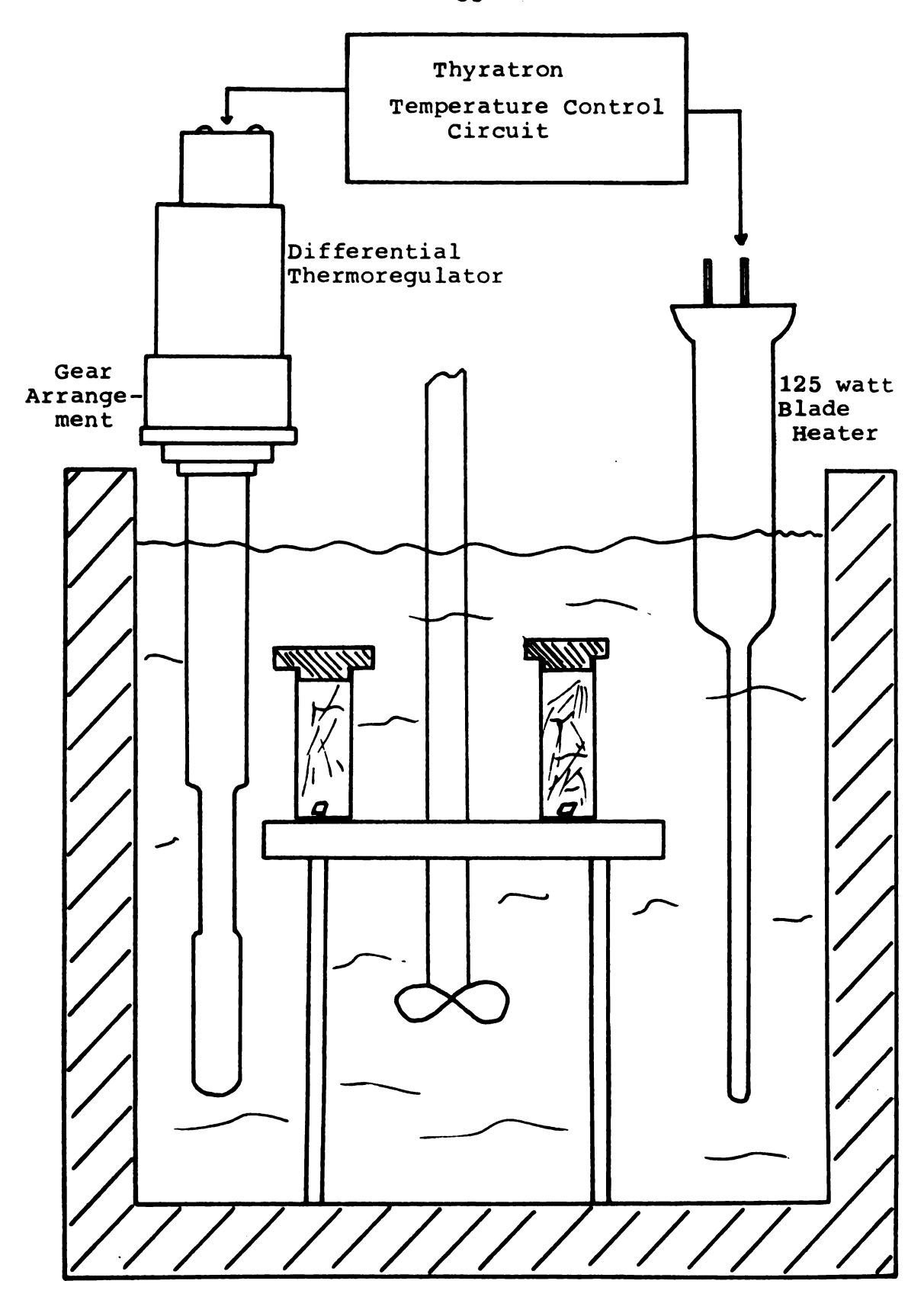


Figure 1. Variable temperature water bath for single crystal growth.

thermoregulator circuit containing a Precision Scientific Differential-Range Thermoregulator. The temperature was lowered by slowly moving the contact pointer of the thermoregulator by means of a gear system connected to a one RPM motor. Some problems were encountered in achieving saturation of the initial solutions in the sealed vials so the seed crystals would not be dissolved. The best procedure was to prepare a saturated solution by filling a vial with excess solid, leaving the vial in the 500 bath for several days, then decanting (rather than filtering) the saturated solution into a separate vial containing the seed crystal; this vial was then quickly capped and returned to the warm bath before crystallization could occur. The seed crystals were usually placed on the bottom of the vials although attempts were made to glue the seeds to the vial walls. However, none of the adhesives tried would hold the seeds for the full time required.

The external faces exhibited by crystals with the Scheelite structure are given by Tutton (33). For both NaIO₄ and NaReO₄ the face lying on the beaker bottom is the (111) first-order bipyramid with (110) faces as the other primary set. A small segment of the third-order (311) set is also present. Measurement of the angles between the crystal faces using an optical goniometer was unsuccessful due to the large size of the faces. The crystals were also examined under polarized light in a polarizing microscope to check the quality of the crystal and to locate the

unique (S_4) axis. All the crystals used showed no evidence of twinning or enclosed crystallites when examined under polarized light. However, the S_4 axis lies along the elongated physical axis of the crystal and it was not possible to mount the crystal so the characteristic extinction (34) could be observed. Attempts to cleave or grind crystals to provide faces perpendicular to the S_4 axis were unsuccessful. Rough measurements made with a makeshift contact goniometer, plus the Raman depolarization results, substaniate the assignment of (110) and (111) faces as the major external growth faces.

B. <u>Infrared and Raman Spectroscopy</u>

1. Far Infrared

All of the far-IR spectra reported here were run on a Fourier-transform instrument, a Digilab Inc. Model FTS-16 Far-Infrared Spectrometer with Mylar film beamsplitters. The interferograms were digitized and transformed to conventional frequency plots on a Data General Nova computer interfaced with the FTS-16. The computer has a 16-bit word length, 12K of core and a 15-bit A/D converter. The spectrometer records in either a single beam or pseudodouble-beam mode or can store a reference spectrum to be combined internally to give a double-beam result. A single scan takes about 1 second and in normal operation a large number of scans, ranging from 500 to 2000, are

en e
5
:
:
:
:

accumulated to improve the single-to-noise ratio before transforming.

The samples were run as polycrystalline powders in Nujol mulls between polystyrene plates. To remove water vapor the spectrometer can be either purged with nitrogen or evacuated. In most cases the spectra were run with the spectrometer evacuated which greatly reduced the amount of time required to eliminate water vapor before scanning.

In order to characterize the instrument spectra of several periodates were run for comparison with previous results (35). The agreement was excellent, frequencies usually agreeing within 3 cm⁻¹, despite the broad lines. Two methods were used in obtaining the double-beam spectra. The normal method employed in the FTS-16 is to take 20 scans of the sample cell, then 20 scans of the reference cell, etc. Although not a true double-beam technique the procedure minimizes errors due to long term fluctuations such as light source warmup or water vapor purging. For some of the compounds the above technique could not be used as a result of an instrument malfunction and an alternate procedure was used. A single-beam reference spectrum was taken, stored, and compared to a sample spectrum to give a doublebeam result. New reference spectra were run at frequent intervals to check for instrumental drifts but no noticeable changes occurred.

2. Laser-Raman

The general layout and design of the laser Raman spectrometer used in this work has been described elsewhere (36). The light source was a Coherent Radiation Model 52A Ar(II) ion laser. The scattered light was collected at 90° to the incident beam, passed through a Spex Double Monochromator and detected with an TIT FW-130 Photomultiplier tube cooled to -30°. The signal was do amplified and recorded. Two lines of the Ar(II) ion laser were used, the 4880Å and 5145Å lines, each with about 1.5 watt output power. In most cases it was necessary to attenuate the incident beam to avoid sample decomposition. This was a definite problem with the ammonium perrhenates, which exploded violently after a short time in the unattenuated beam.

Polycrystalline samples were run using ordinary capillary melting point tubes as sample cells. The single crystals were mounted in a piece of modeling clay attached to a glass rod. The crystals were of sufficient size so that no portion of the laser beam was incident on the clay or sample supports. For low temperature work samples were mounted inside an unsilvered Dewar cell (37) through which cold nitrogen gas was passed. Temperature variation was accomplished either by changing the nitrogen gas flow or the liquid nitrogen level in the Dewar used to precool the gas flow. Temperature in the Dewar cell was measured by use of a copper-constantan thermocouple placed near the

sample. No special precautions were taken to calibrate the thermocouple and all temperatures are accurate to $\pm 5^{\circ}K$ except at $77^{\circ}K$, where an appreciable amount of liquid nitrogen collected as a result of Joule-Thompson cooling of the gas entering the cell.

Single crystal depolarization spectra were obtained by orienting the single crystals in the plane-polarized laser beam and placing a polarizer in front of the monochromator to admit only the desired component of the scattered light. Rough alignment of the crystal was done by eye then final adjustements made by monitoring the photomultiplier tube current at the V1 fundamental frequency while moving the crystal. Since the crystal had only (110) and (111) external faces the incident beam was never perpendicular to a crystal face and both internal and external scattering occurred. The internal reflection destroyed the original polarization and resulted in scattered light contributions that led to deviations from theoretically predicted depolarization ratios. This problem could have been prevented by using crystals large enough to grind into cubic shape along the crystallographic axes.

C. NOR Temperature Studies

1. Constant Temperature Baths

In obtaining the temperature variation of the NQR frequencies a variety of techniques were employed for achieving and maintaining low temperatures. The different techniques

will be discussed in chronological order. Constant temperature baths were used first because of availability and ease of preparation; finally, a liquid helium Dewar system, which required a considerable amount of work in design and implementation, was employed.

In the constant temperature baths the liquid and solid phases of a pure substance were placed in equilibrium. The available baths ranged from 273°K (ice-water) to 113°K (isopentane) selected from an extremely useful compendium (38) of such mixtures. A large number of possible liquids could not be used since the oscillator would not oscillate with the sample coil immersed in liquids of high dielectric constant. For suitable liquids a slush was prepared by adding small amounts of liquid nitrogen to a Dewar containing the liquid until a thick viscous mixture of liquid and solid phases formed.

The sample and coil were allowed to equilibrate in the bath for about one-half hour and the spectrum recorded.

During this time the temperature was held constant by adding small amounts of liquid nitrogen to the mixture. The temperature was monitored with a copper-constantan thermocouple and remained constant during the time required to record the spectra. Although this procedure was accurate it was used only with NaIO₄ since it was extremely time consuming to make measurements at a series of temperatures. Both of the other methods used Dewar containers and liquid nitrogen or liquid helium as coolants.

2. Dewar Methods

The first Dewar container used was the variable temperature Dewar system for the ENDOR (Varian Associates Model E-700) spectrometer in conjunction with a Varian ESR Variable Temperature Controller, Model V-4540. The samples were placed in glass tubes and inserted into the unsilvered Dewar with the oscillator sample coil wrapped around the outside of the Dewar. This arrangement severely reduced the signal-to-noise ratio due to the low rf power density at the sample but was suitable for NaIO₄ and KReO₄, where large amounts of sample were available.

Cooling was achieved by blowing cold nitrogen gas past the sample and out the top of the Dewar. The gas temperature could be set on the Varian Temperature Controller and sample temperatures were measured by a theromocouple inside the sample with leads extending out the top of the Dewar to a potentiometer. The lowest temperature reached was -180°, with marginal temperature stability at the lower portion of the range. These problems clearly indicated the need for a Dewar especially designed for variable temperature NQR measurements.

The liquid helium dewar, shown in Figure 2, was designed to be used for both NQR measurements and Q-Band ESR measurements and was constructed by H. S. Martin Co., Evanston, Illinois. This double Dewar was constructed as a single unit with a Pyrex pipe fitting which greatly simplified mounting and dismounting of the Dewar from its

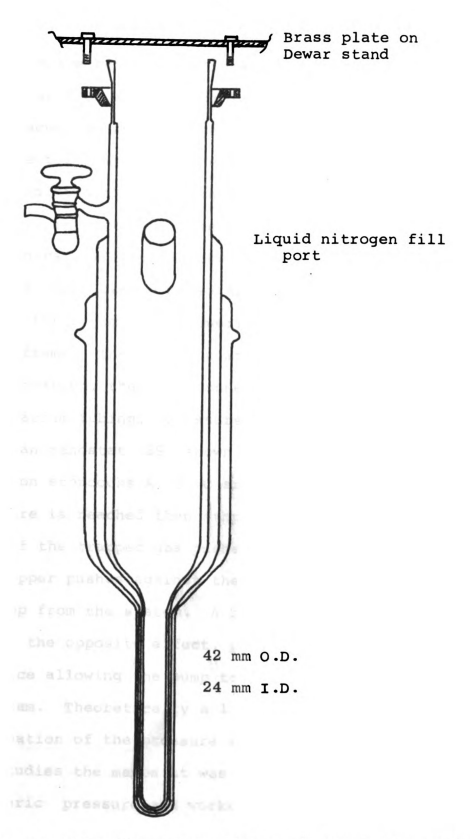
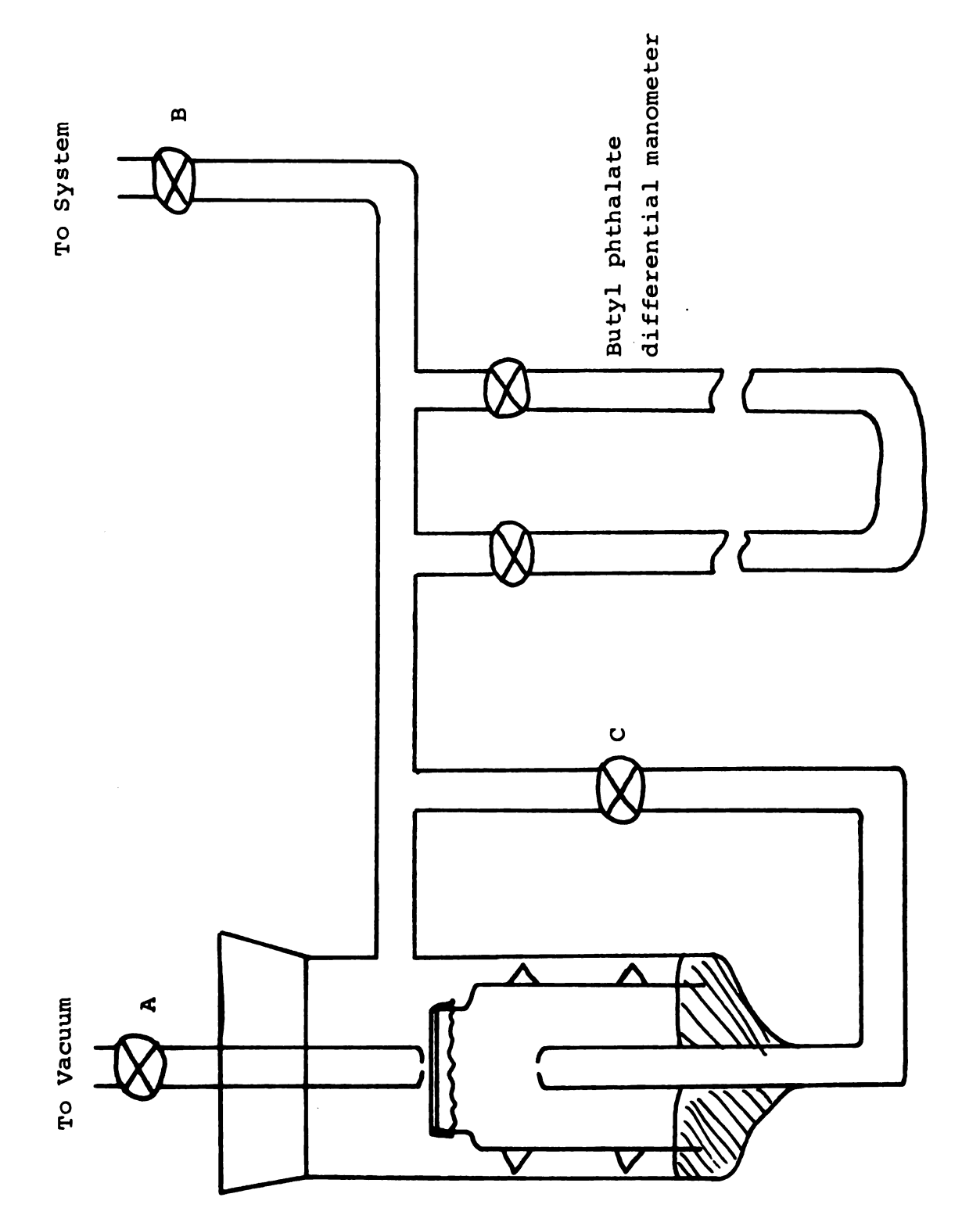


Figure 2. Liquid helium Dewar with a 4" Pyrex pipe fitting for NQR and Q-Band ESR studies.

stand. In designing the Dewar stand several objectives were taken into account. A good vacuum line was needed for pumping the vacuum space between the inner helium section and outer nitrogen section and for pumping down the transfer tube vacuum space. To reach temperatures below 4.20K provision was made for pumping on the liquid, monitoring the pressure, and holding the pressure constant at some reduced value. Flexible metal vacuum hose was used for the connection between vacuum line and Dewar.

The entire stand can be moved about on wheels or raised off the ground for rigidity by lowering four heavy bolts welded to the frame. The vacuum pump is mounted separately to minimize vibration, the only connection to the system being rubber vacuum tubing. Pressure control is obtained with a Cartesian manostat (39) shown in detail in Figure 3. During operation stopcocks A, B, C are opened until the desired pressure is reached then stopcock C is closed. The pressure of the trapped gas pushes the float up until the rubber stopper pushes against the orifice, isolating the vacuum pump from the system. A build-up of pressure in the system has the opposite effect, pushing the float away from the orifice allowing the pump to again begin evacuating the system. Theoretically a 1 mm orifice gives a 5% maximum fluctuation of the pressure at any given pressure. For the NQR studies the manostat was operated slightly below atmospheric pressure and worked well. Butyl Phthalate was used in the differential manometer for greater sensitivity.



Cartesian manostat for pressure regulation. Figure 3.

Since a range of temperatures was needed for the NOR measurements direct sample immersion in the cryogenic liquid was not employed, but rather a variable-temperature bomb similar to that of Swenson (40). The sample is placed in a coil inside a $1 \frac{1}{2}$ OD copper cylinder with about 20 feet of 3/16" OD copper tubing coiled in three layers around the outside and silver-soldered in place. The bomb is attached to either of two Dewar tops, each with a different length of stainless steel connecting tubing, as shown in Figure 4, and placed inside the helium Dewar. A pressure differential at the top of the apparatus pulls liquid into a 1/8" stainless steel tube which extends into the liquid reservoir, up through the 30 coils of copper tubing acting as a heat exchanger and finally past the sample. For the longer Dewar top the apparatus was too efficient and heat had to be supplied. Therefore, a onewatt 100Ω resistor was mounted in the base of the bomb to supply a variable heat influx to balance the cooling. Normally about one-half to one watt of power gave acceptable heat influx with the combination of variable heat input and adjustable gas flow giving a wide range of heating or cooling rates. For the shortest Dewar top used the heat exchanger coils were above the outer nitrogen section and the heat influx was great enough so that no external heating was necessary. The maximum warming rate was about 0.50K/min with no appreciable broadening of the NQR resonance from temperature inhomogeneities.

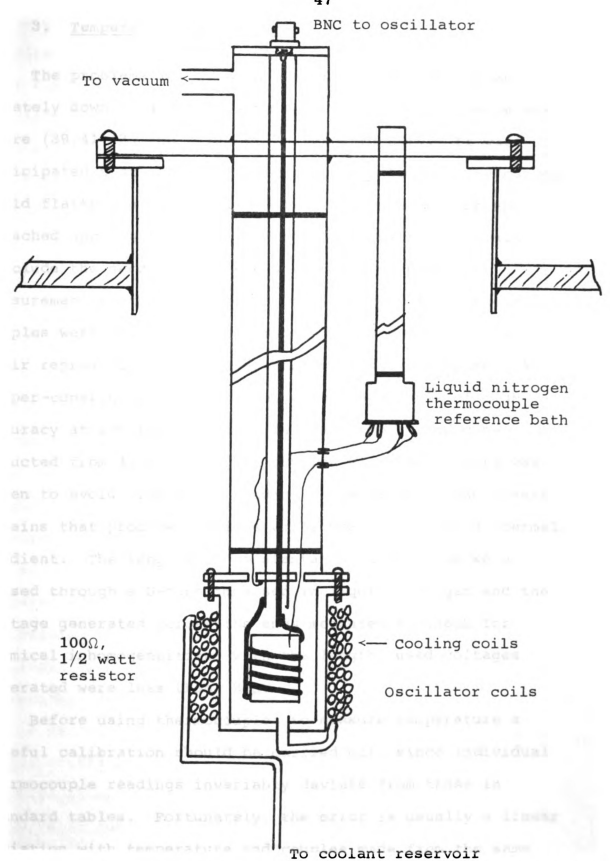


Figure 4. Cross-section of Swenson-type variable-temperature bomb used with the liquid helium Dewar.

3. Temperature Measurement

The problems involved in measuring temperatures accurately down to 4.20K have been thoroughly discussed elsewhere (39,41-43) and will not be repeated here. It was anticipated that the NQR frequency versus temperature curves would flatten out as liquid helium temperatures were approached such that errors in frequency measurement would preclude the need for extremely accurate temperature measurement at these low temperatures. Therefore, thermocouples were chosen for temperature measurement because of their reproducibility, convenience, and quick response. A copper-constantan thermocouple, which is capable of high accuracy at low temperatures (44), was chosen and constructed from 40 A.W.G. nylon covered wire (45). Care was taken to avoid flexing or bending the wire which can create strains that produce spurious emf's when placed in a thermal gradient. The lengths of constantan wire employed were passed through a U-tube immersed in liquid nitrogen and the voltage generated across the ends measured to check for chemical inhomogeneities; with the lengths used voltages generated were less than 2 uV.

Before using thermocouples to measure temperature a careful calibration should be carried out, since individual thermocouple readings invariably deviate from those in standard tables. Fortunately, the error is usually a linear deviation with temperature and couples made from the same

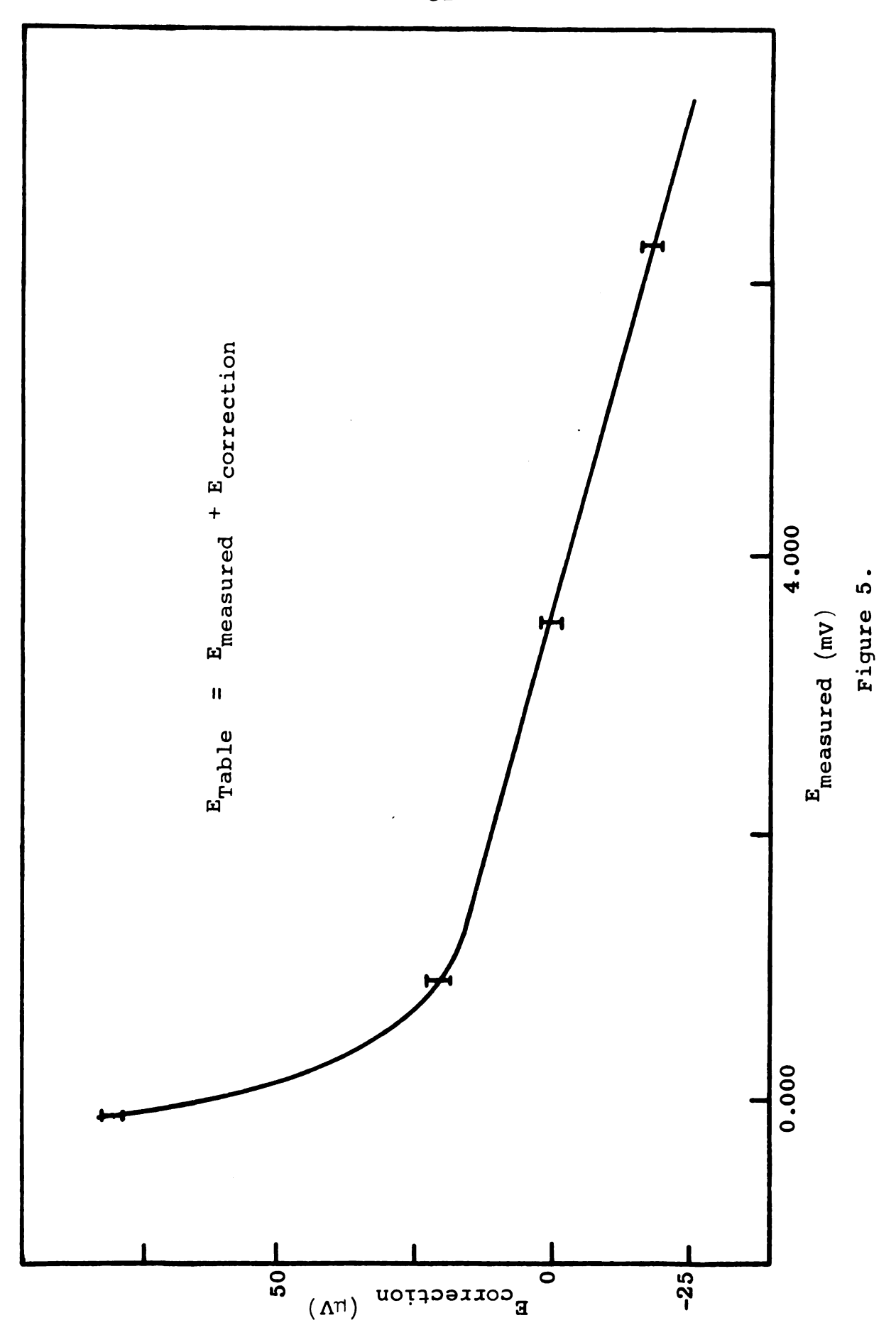
spool of wire can use the same calibration chart. The couples used here were calibrated by measuring emf's at four fixed points and constructing such an error curve by comparing true and tabulated temperatures. The four fixed points used were (1) an ice-water mixture, (2) the boiling point of liquid oxygen, (3) the boiling point of liquid helium, and (4) the sublimation point of CO₂.

Liquid oxygen was produced by passing oxygen gas into a cold trap immersed in liquid nitrogen; oxygen gas was also bubbled through constantly during measurements to avoid superheating. Crushed CO₂ was allowed to stand overnight to equilibrate before use. The boiling and sublimation points were corrected to actual atmospheric pressure. All measurements, including the later measurements, were made using the same Leeds and Northrup Model 2745 Potentiometer to eliminate errors in absolute emf measurements.

Measured emf's were compared with values in a comprehensive collection of various thermocouple tables by Powell and coworkers (46) covering the range O⁰K to 300°K. The resulting calibration curve for the copper-constantan couple, Figure 5, is linear within experimental error down to around 70°K with appreciable deviations appearing below that temperature.

A serious problem with using thermocouples, especially copper-constantan, at low temperatures is the low thermoelectric power. The copper-constantan couple goes from 41 $\mu\text{V}/^0\text{K}$ at 300°K to 1.2 $\mu\text{V}/^0\text{K}$ at 4°K. Obviously, measurement errors and spurious emf's can lead to large temperature

Correction voltages between measured and tabulated emf's for the copper-constantan thermocouples used in this work (Reference junction at liquid nitrogen boiling point). Figure 5.



errors near 40K and several precautions must be taken to minimize these. A reference junction at either liquid nitrogen or liquid helium temperatures is a necessity in order to keep measurement errors a minimum. For example, with copper-constantan a reference junction at 770K and cold junction at 40K gives an emf of -0.724 mV contrasted with an emf of -7.327 mV for a 3000K reference junction and the same cold junction. For the same absolute error the second measurement must be made with a factor of ten better accuracy. In addition to measurement errors, leading constantan wires out to room temperature from 4.20K can generate appreciable induced thermal emf's. Therefore, the reference junction used here consisted of a reservoir containing liquid nitrogen extending into the helium Dewar (Figure 4). Thermocouple wires ran from the sample to the reference bath through the cooling gas stream such that the warmest temperature they were exposed to was 770K. Care was taken that the liquid nitrogen used contained no dissolved oxygen and the boiling point was calculated from a table in the book by White (41).

To take the precautions discussed above is extremely important in obtaining accurate temperature measurements near liquid helium temperatures. During these experiments the lowest measured atmospheric pressure was 732 torr, resulting in a 6 μV correction in the reference emf. Neglecting this correction would give a $5^0 K$ error at $4^0 K$. The need for a calibration curve is even more important,

as is evident in the magnitude of the 20 μV correction at $10^{0}K$. The following example clearly illustrates the magnitude of the errors from thermal gradients which were present in experiments attempting to get a liquid helium calibration point for the thermocouple. With helium in the Dewar a thermocouple was lowered into the liquid with the $77^{0}K$ reference bath for the thermocouple outside the Dewar. The measured emf was $-3~\mu V$, indicating an error of only $6~\mu V$ from the tabulated valve (+ $3~\mu V$). However, with the thermocouple mounted completely inside the Dewar using the internal nitrogen reference bath the measured voltage was $-77~\mu V$, corresponding to an $80~\mu V$ error. Apparently this large discrepancy was due to the spurious voltage induced by bringing the wire out to room temperature.

4. NOR Oscillator Modifications and Operation

All the resonances measured in this work were observed using a Dean-type superregenerative oscillator constructed by Ryan (47), who gives a detailed discussion of its circuit and operation. The superregenerative oscillator is distinctive in that in the normal mode of operation the oscillation is periodically damped or quenched. As a result of this quenching action the oscillator output contains a number of frequencies—the center frequency, v_0 , and a series of sidebands on either side at $v_0 \pm v_Q$, $v_0 \pm 2v_Q$, ..., where the quench frequency v_Q ranges from 20 to 40 kHz. The NQR spectrum will show an absorption for each

of these discrete frequencies, resulting in a complex pattern. In theory, the center frequency should be the most intense but in practice the oscillator is difficult to adjust for this condition and at least one of the sidebands is usually of equal intensity. This leads to problems in frequency measurement as will be discussed below. Despite these disadvantages the superregenerative oscillator is widely used in NQR because of its greater sensitivity than the marginal oscillator commonly used in NMR circuits.

The normal physical arrangement of the oscillator described by Ryan was employed with the oscillator coil immersed in a slush bath or in the ESR ENDOR Dewar to provide controlled temperatures. The normal frequency range covered by the oscillator is from 10 to 60 MHz; this is achieved by changing the sample coils. For use with the liquid helium Dewar, as shown in Figure 4, the sample coil was located in the variable-temperature bomb between 25 and 50 cm from the oscillator. The connection was made by a coaxial line constructed from 1/2" stainless steel tubing and #24 B. & S. gauge coated copper wire. Correct spacing of the central copper wire was maintained using small styrofoam separators. The extra length added to the sample coil due to this coaxial lead-in added a large impedance to that of the normal configuration, thus giving a much lower frequency and range of operation. For example, the longest bomb assembly resulted in a maximum obtainable frequency of only 33 MHz with the minimum one-turn sample coil.

In order to look at the higher frequency NaReO₄ and AgReO₄ resonances a lead-in tube of very short length was used giving a maximum frequency of 48 MHz. However, this placed the heat exchanger portion of the bomb assembly above the outer nitrogen shield of the helium Dewar resulting in poor temperature stability. For both configurations the effective tuning range of the sample coils was reduced by a factor of three to about 3 MHz. Operation of the oscillator at low temperature was the same as at room temperature except that mounting the oscillator flat rather than on one edge substantially reduced sensitivity to vibration and markedly more stable operation was achieved. Modulation was usually 39 Hz, although frequencies as high as 200 Hz were tried with no appreciable gain in signal-to-noise ratio.

Frequency measurements were made by beating the output of a Hewlett Packard Model 608A Signal Generator against the oscillator frequency and monitoring the oscillator output on an oscilloscope. The signal generator output was then measured by use of an electronic counter. The tuning capacitor position was monitored by a large dial which turned as the capacitor turned but rotated three times as fast. During each scan the chart paper was marked at frequent intervals with the corresponding dial position so that the center absorption line could be specified in relation to the dial position. Immediately after each scan the capacitor was swept manually and the oscillator frequency

at various dial positions measured to calibrate the chart paper. From the calibration so obtained the absorption frequency could be calculated directly assuming a linear variation of frequency with capacitor position; this is a good assumption over the small frequency ranges between calibration points.

The main source of error in measuring NOR absorption frequencies from superregenerative patterns is the possibility of erroneously choosing a sideband rather than the center line as the main absorption. The oscillator used here gave a characteristic absorption pattern, with the higher frequency sidebands stronger and more resolved than those on the low frequency side. For each compound studied the room temperature lines were well characterized before studying the temperature variation of the frequencies. The center line was located by changing the quench frequency and observing which line moved least. For all succeeding measurements the pattern was similar enough so that the same line could always be distinguished. The absolute error could therefore be ±30 kHz if a sideband, rather than the center line, was chosen. However, assuming correct choice of the center line there would be a relative error of only ± 1 kHz for a series of measurements on a particular compound. In view of the care taken in the determination of the temperature dependence of the frequencies the relative error of ±1 kHz is believed to be appropriate and will be used as the quoted measurement error in this work.

III. RESULTS

A. Far-IR and Raman Spectra

1. Factor Group Analysis

As discussed in Chapter I, in order to apply the Kusida et al. theory to predicting the observed NQR temperature dependence, information about the low frequency librational modes is needed. The frequencies of these modes obtained from infrared and Raman spectroscopy are those at the center of the Brillioun zone and may be used in Equation (54) to calculate the NQR temperature dependence if the modes are assumed to show negligible dispersion for other k values in the zone. This assumption may be invalid in certain cases but unless independent information on the phonon density of states and dispersion curves is available no other approach is possible. For the periodates some previous work has been done (48) in addition to a more detailed study carried out as a joint project by Doug Hatzenbuhler and myself (37,49). Only that portion of the study not previously reported by Hatzenbuhler (37) is included here. In the perrhenate case the fundamentals and some lattice frequencies have been reported (50-52), with most of the earlier results summarized by Ulbricht and Kriegemann (52).

Further study was needed to assign symmetries and observe the remaining lattice modes. To aid in the symmetry assignments, depolarization ratios were measured for a single crystal of NaReO₄. For the ammonium salts the ND₄ analogs were prepared in order to separate the ammonium librations from the other lattice modes.

The symmetry and number of $\underline{k}=0$ modes to be expected in the crystalline IR and Raman spectra can be predicted if the space group and site symmetry are known. All the perrhenates and periodates studied here have the Scheelite (CaWO₄) structure, space group C_{4h}^6 , with both the anions and cations occupying S_4 sites in the crystal. From this data a factor group analysis (53-56) was carried out. Only the results are given here, since the treatment is identical to the periodate case given elsewhere (37). A very clear discussion of the method, including many illustrative examples, has recently been published (57).

The isolated ReO_4 group is tetrahedral with 3(5)-6 = 9 fundamental vibrations. These may be classified under the T_d group in four irreducible representations, A_1 + $E + 2T_2$ (58). These four fundamentals are split in the crystal, first by the S_4 site symmetry and then by the coupling of the two inequivalent sites in the primitive unit cell, termed the factor group coupling. In a similar manner the external vibrations of the ReO_4 and the cation are also split. The resulting symmetries and number of vibrational modes are shown in Table 1. Since the ammonium

Table 1. Site and factor group splittings of Scheelitetype perrhenates.

Isolated Molecule	Site	Symmetry	Factor Group Symmetry	Spectral Activity
^T d		S ₄	c _{4h}	
ν ₁ Α ₁		Α	A _g	R
			B _u	inactive
ν ₂ Ε		В	Bg	R
			\longrightarrow A _u	IR
ν ₃ , ν ₄ Τ ₂		E	E g	R
			E _u	IR
External Modes	_		A _g	R
(R _x ,R _y ,R _z) _{anic}	on T ₁	A	B _u	inactive
			E _g	R
(T _x ,T _y ,T _z) _{anic}		E	E _u	IR^a
(T _x ,T _y ,T _z) _{cati}	on T ₂		В _д	R
	·	В	A _u	IR^a

^aIncluding three accoustic modes not observable at $\underline{k} = 0$.

group is also located on an S_4 site the predicted splittings for the ammonium fundamentals are analogous to the ReO_4 group.

In order to make symmetry assignments in the observed polycrystalline spectra single crystal spectra of $NaReO_4$ were run at various orientations. Since the laser light is plane polarized, a single crystal may be oriented so that only certain polarizability derivative tensor components contribute to the transition integral (59). The derived polarizability components, grouped according to symmetry for the C_{Ab} point group, are given in Table 2.

Table 2. Activity of polarizability derivative tensor components under C_{4h} point group symmetry.

$$Ag : \begin{pmatrix} C_1 & O & O \\ O & C_1 & O \\ O & O & C_2 \end{pmatrix} \qquad Bg : \begin{pmatrix} C_3 & C_4 & O \\ C_4 & -C_3 & O \\ O & O & O \end{pmatrix}$$

$$Eg : \begin{pmatrix} O & O & C_5 \\ O & O & C_5 \\ C_5 & C_5 & O \end{pmatrix}$$

2. Frequencies and Symmetry Assignments

The samples were run as polycrystalline powders in addition to the NaReO₄ single crystal work. The spectra

were obtained at room temperature and near liquid N₂ temperature in order to resolve the lattice modes and get data concerning the frequency shifts with temperature. The observed Raman spectra for the Na, K, Rb, and Ag perrhenate salts are given in Figures 6-9, while the ammonium and deuteroammonium salts will be discussed separately below. Only the lattice region is shown in most cases, since the frequencies of the fundamentals (see Table 3) agreed fairly well with the previous work of Ulbricht and Kriegsmann (52). The far-IR spectra of the powdered samples were run as Nujol mulls at room temperature and are of poorer quality overall. A representative infared spectrum, of polycrystalline NaReO₄; is shown in Figure 10 for illustration.

The powder spectra for the series of salts were very similar in appearance so that assignments based on the NaReO₄ single crystal results, which are discussed below, were straightforward. The results are summarized in Table 3 for the fundamentals and Table 4 for the lattice modes at room temperature. Table 5 gives the Raman results obtained near 77°K, which allows several more lattice modes to be resolved. Apparently the highest frequency Bg mode was observable only in KReO₄; it was unobservable in all the Scheelite-type periodates also.

The single crystal results for NaReO₄ are shown in Figure 11, with both the lattice region and the fundamentals included. As can be seen from Table 2, there are only four unique orientations among the possible combinations of

Figure 6. Raman spectrum of polycrystalline NaReO₄ using 5145Å Ar(II) laser excitation.

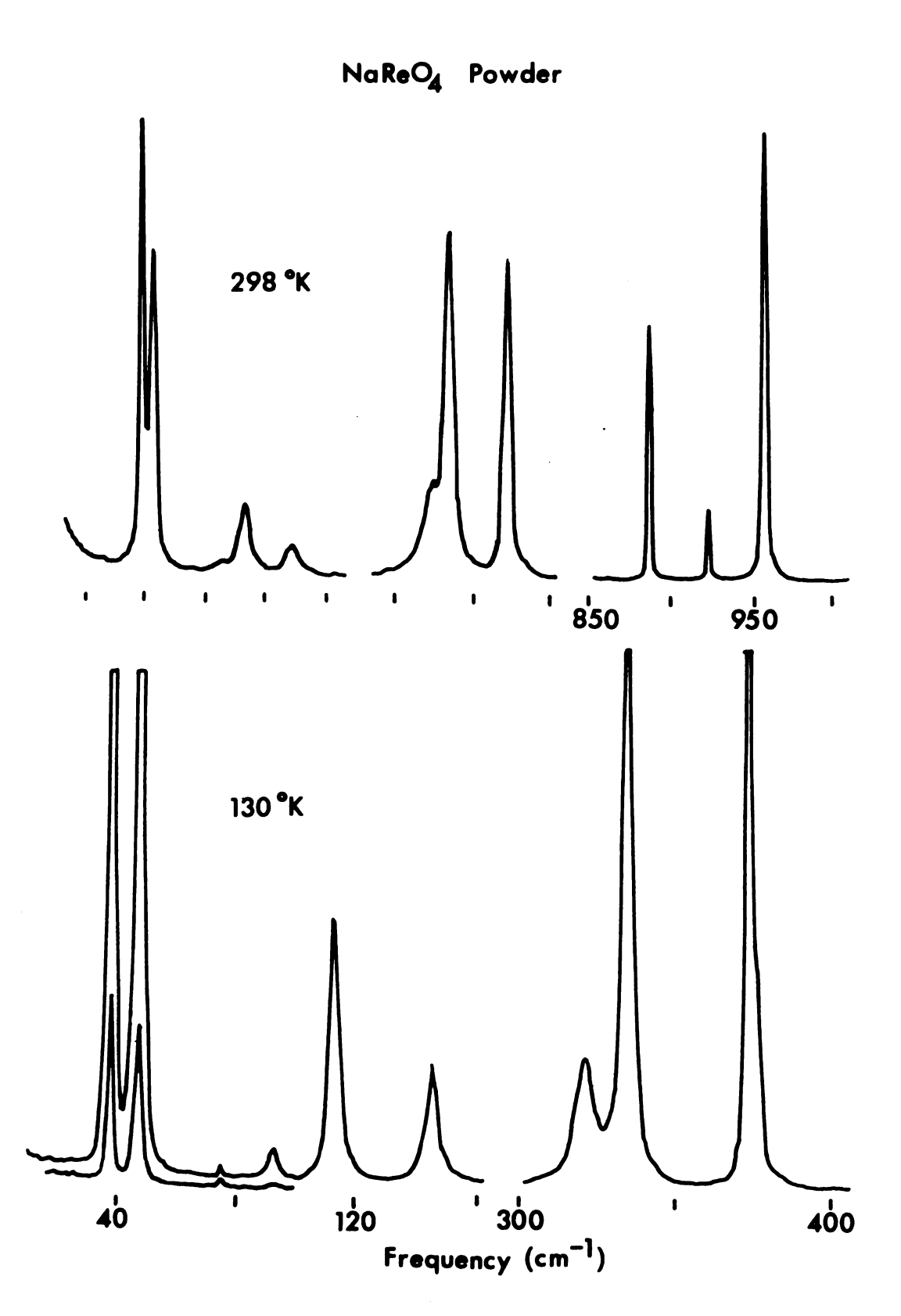


Figure 6.

Figure 7. Raman spectrum of the lattice region in polycrystalline KReO₄ using 5145A Ar(II) laser excitation.

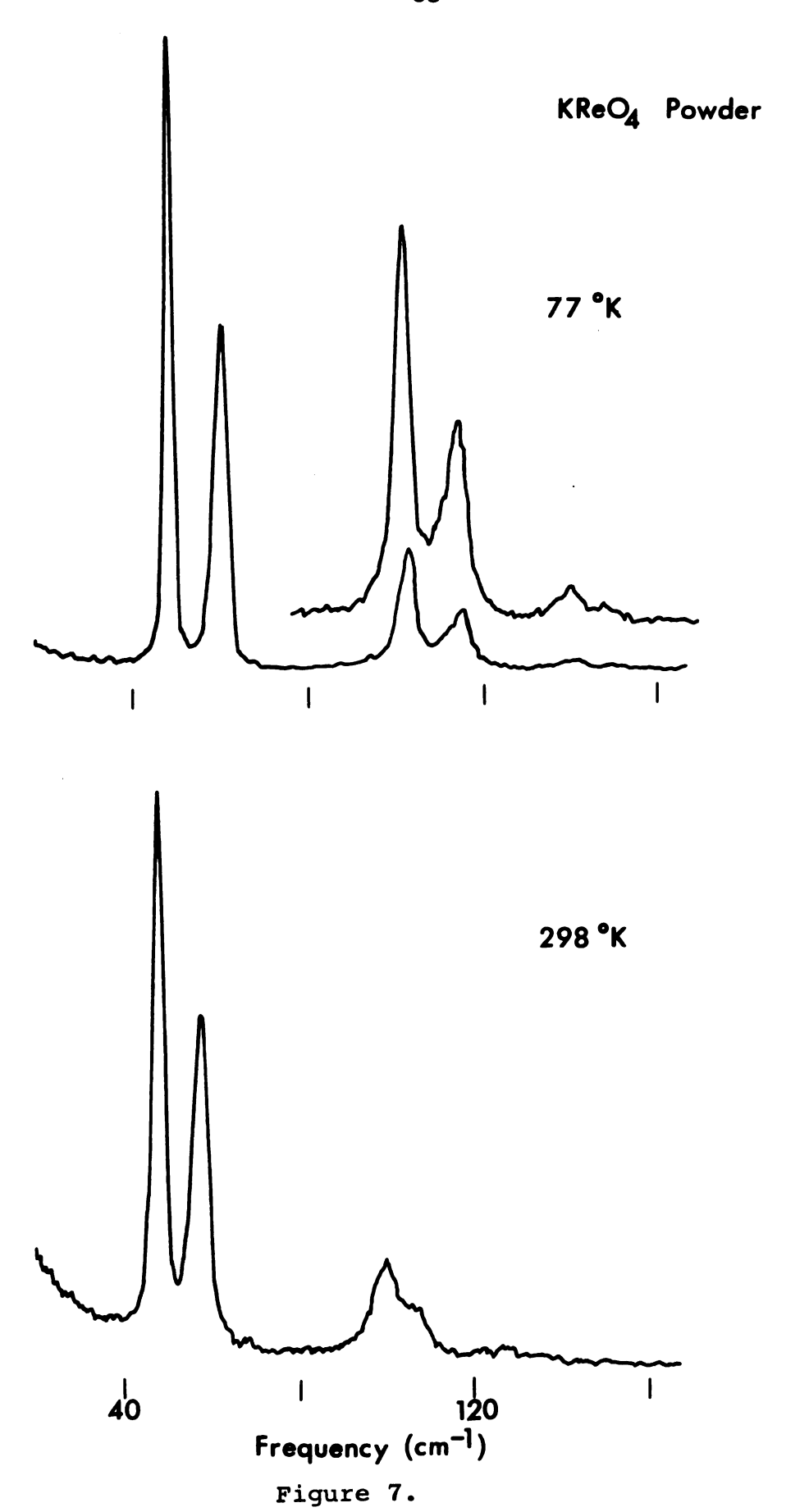


Figure 8. Raman spectrum of the lattice region in polycrys-talline RbReO₄ using 5145Å Ar(II) laser excitation.

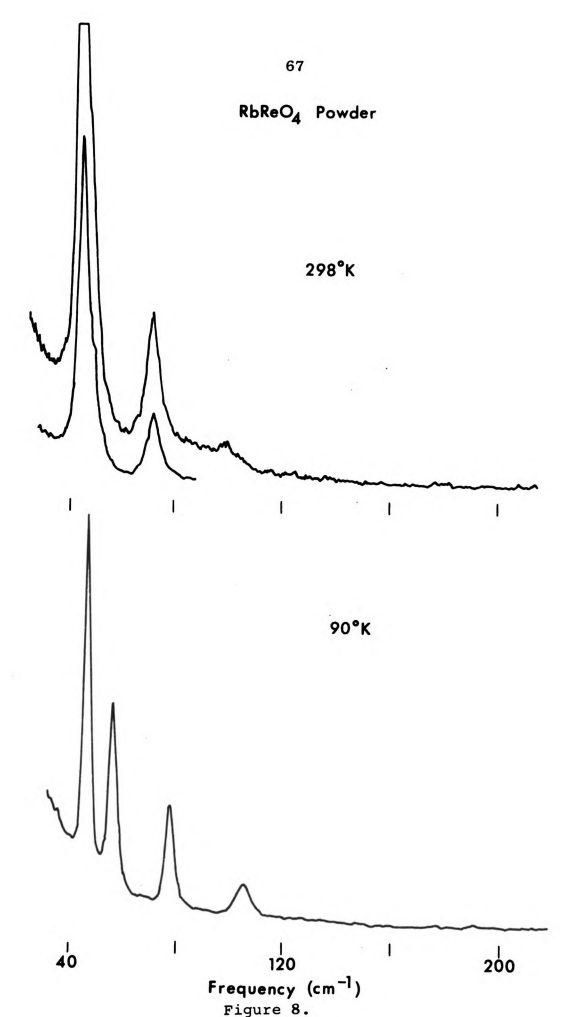
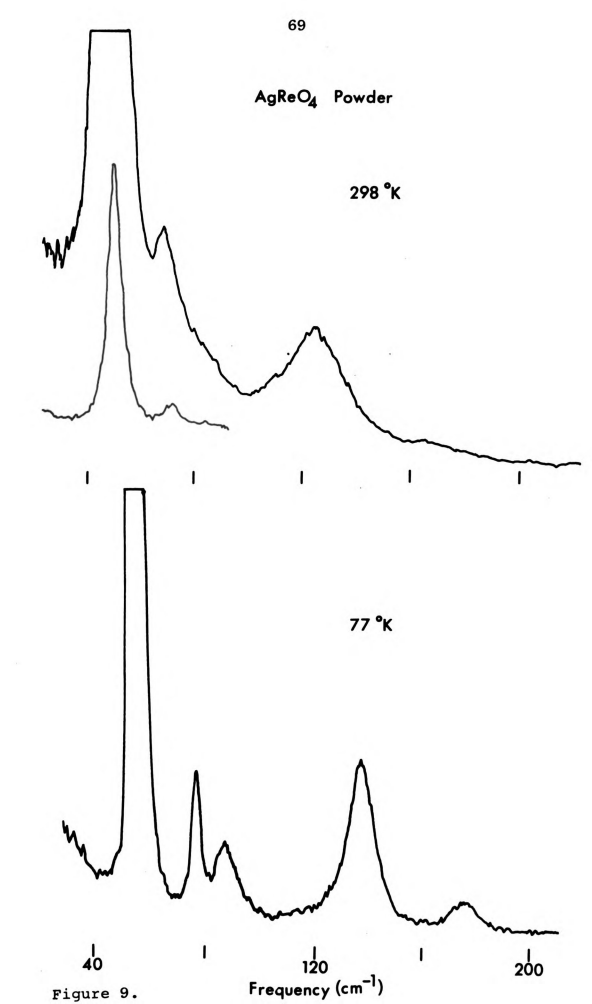
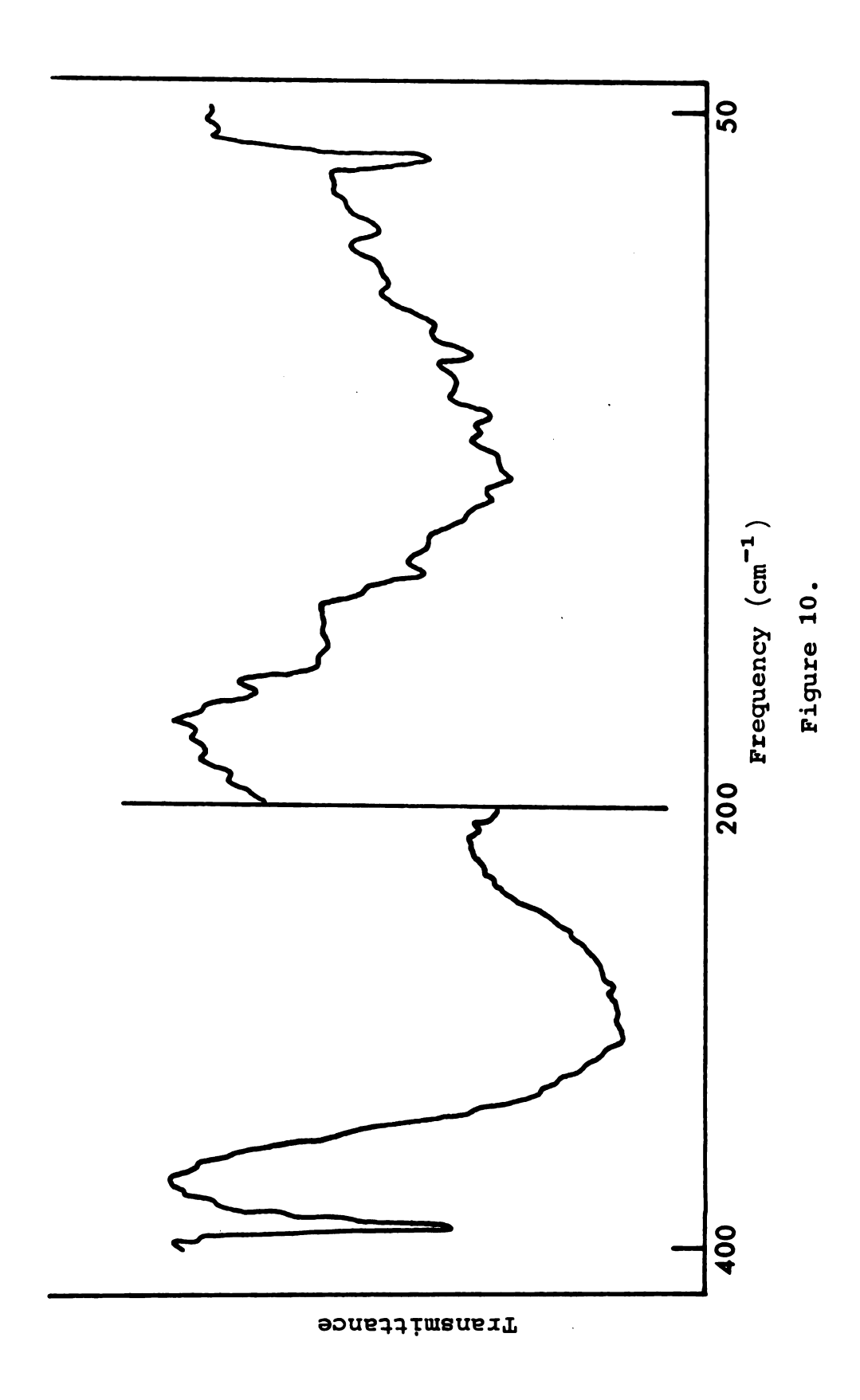


Figure 9. Raman spectrum of the lattice region in polycrys-talline AgReO₄ using 5145A Ar(II) laser excitation.



Infrared spectrum of polycrystalline NaReO $_4$ in Nujol mull at $298^0 K$ in 400-500 cm⁻¹ range. Figure 10.



Infrared and Raman active ReO4 fundamentals at 2940K (cm-1). Table 3.

		4	Na	**		Rb+	+,	Agt		NH	 	ND.	+
			Pre-3		Pre-		Pre-	`	Pre-		Pre-		Pre-
Symmetry		This viou	vious Th	This		This	vious	This	vious	This		This	vious
		WOLK	WOFK	WOLK	WOrk	WOrk	WOLK	WOrk	Work	WOLK	Work	Work	Work
v ₁ (970) ^a	Ag	958	926	964	965	196	896	942	942	Q	996	996	•
	В	325	324 ^C	330	330°	331	331°	318	315 ^c	Ą	330°	328	•
v ₂ (332) ^a	A	335	333°	337	336 ^c	335	336 ^c	329	$329^{\rm C}$	д	335 ^C	336	•
	A D	388	:	364	361	348	350	381	315	357	361	353	:
6,010	В	888	886	895	968	897	899	862	863	р	893	888	•
^{V3} (919)	្តិ	924	924	918	924	923	922	868	899	д	914	910	•
	A.	278	•	305	304	306	308	270	278	292	303	286	•
B (000)	ធ្ន	297	•	314	317	315	316	289	296	312	318	301	•
V4 (332)	B B	372	371	349	348	341	341	363	365	Q	342	342	•
v4 (single	ង	378.3	8										
$\mathtt{crystal})_{\mathtt{B}^{ec{g}}}$.) Bg	373.8	æ										

d Raman results aSolution frequency. bNot observed. CIncorrect assignment reversed. from Ref. 52, infrared results from Ref. 51.

Table 4. Lattice modes in Scheelite-type perrhenates at $294^{0}K$ (cm⁻¹)

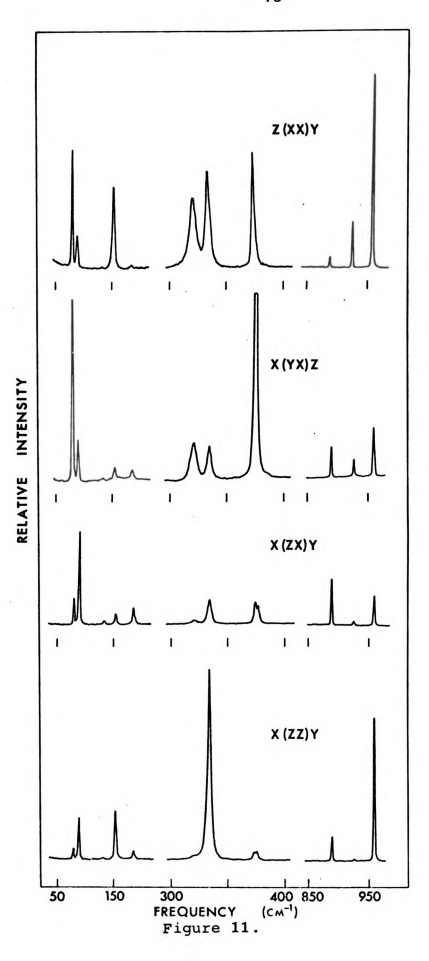
Symmetry	Na ⁺	K ⁺	Rb ⁺	Ag ⁺
Bg	77	55	45	59
Eg	84	65	48	76
Eg	131	107	72	
Ag	145	113	98	132
Eg	181		100	
Bg				
A _u	98		67	57
Eu	140	125	98	85
Eu	163	158	104	102

Table 5. Raman active lattice modes in Scheelite-type perrhenates near $77^{\circ}K$ (cm⁻¹).

Symmetry	Na ⁺ 130 ⁰ K	к ⁺ 77 ⁰ к	Rb ⁺ 1420K	Ag ⁺ 770 _K
Bg	79	55	46	63
Eg	88	70	56	85
Eg	132	110	77	95
Ag	153	122	102	148
Eg	185	147	104	185
Bg	a	155	a	a

a Not observed.

Figure 11. Raman spectra of single crystal $NaReO_4$ in the four unique orientations.



incident and reflected polarizations and the results obtained for these orientations are shown in Figure 11. The spectra are labelled following conventional notation (60) by a series of letters which describe propagation and polariztion directions in terms of the crystallographic axes. symbols inside the parentheses are, left to right, the polarization of the incident and scattered light, while the ones to the left and right of the parentheses are the propagation directions of the incident and scattered light respectively. The results of the polarization study are summarized in Table 6. The agreement between theoretical and experimental depolarization ratios are consistent in all but a few cases, although the ratios are not as large as theoretically predicted. As discussed previously, the crystal's external habit is such that the incident light was never perpendicular to a crystal face and internal reflection always occurred. In cases where experimental values are reported for theoretical ratios of 0/0, the line was extremely weak in both orientations. The single crystal study also resolved the small site splitting of v_4 , the asymmetric bending vibration. This band is incorrectly assigned by Ulbricht and Kriegsmann (52) to give $v_2 > v_4$, in agreement with the order found for the infrared active modes (see Table 3). The depolarization study, however, shows unambiguously that the order of the Raman active modes is $v_4 > v_2$.

Table 6. Experimental vs theoretical depolarization ratios in NaReO4.

	$\begin{vmatrix} 1 & z \\ 1 & z \end{vmatrix} = z$	(XX)Y (XZ)Y	= x(y)	Y)z XY)z	= x = x	(ZZ)Y (XZ)Y
Symmetry	Ratio Exp.	(/ <u> </u>) Tneo.	Ratio ($\frac{1}{1}$	Ratio Exp.	(\parallel/\perp)
Fundamenta	ls					
A_g (v_1)	6.2	∞	~ 4.2	ω	4.4	œ
$^{\mathbf{A}}$ g($\mathbf{v_2}$)	2.5	œ	2.4		14.5	ω
B _g	7.0	∞	1.7	$-\frac{C_3}{C_4}$ a	-	0/0
B _g (ν ₃)	5.7	∞	2.4	a'	-	0/0
Eg	.14	0	.42	0/0	.54	0
$^{\mathrm{B}}$ g (v_{4})	.70	œ	.12	a"	.21	0/0
E _g	.33	0		0,⁄0	.33	0
Lattice Mod						
Bg (77 cm ⁻¹	¹) .71	∞	.22	a'''	.41	0/0
E _g (84)	~ .10	0	~ .37	0/0	.44	0
E _g (131)	~0	0		0/0	~0	0
A _g (145)	11.3	Φ	7.9	co	5.0	00
E _g (181)	~ .02	0		0/0	.38	0

The ammonium salt will be discussed separately for several reasons. As mentioned earlier, the vibrational spectra should contain additional lines from the ammonium librational modes and absorptions of the ammonium group fundamentals. In addition, the NQR results show that the 187Re temperature dependence in NH4ReO4 is anomalous in

studied. This anomalous behavior probably arises from the presence of the ammonium group rather than a simple cation, particularly the possibility of a phase transition from libration to free rotation near 25°C, the temperature at which the quadrupole resonance signal disappears. Therefore a more detailed study of the ammonium salt was indicated, which included obtaining spectra for the ND₄⁺ salts of ammonium perrhenate and periodate.

The resulting spectra for both the lattice region and the fundamentals are shown in Figures 12-17; the analogous NH₄IO₄ spectra are given elsewhere (37). In several of the spectra Ar(II) fluorescence lines are also present and are marked by asterisks. Assignments for the ammonium fundamentals were made by comparison to the solution frequencies for ammonium ion (58). The experimentally observed frequencies for the ammonium ion fundamentals are given in Table 7 along with the NH4IO4 results. In addition to the fundamentals additional bands were observed in several of the spectra. In NH4ReO4 (Figure 15) there is a weak absorption at 3064 cm⁻¹ which can be assigned as a ammonium combination band " $v_2 + v_4$ " (k = 0 sum = 3095). In ND4IO4 (Figure 17) there is a fairly strong line present at 2306 cm $^{-1}$ which may be the "2 v_2 " overtone (\underline{k} = 0 sum = 2376) in Fermi resonance with v_1 or less likely the " $v_2 + v_4$ " combination (k = 0 sum = 2276) in Fermi resonance with v_3 , as in the NH_4ReO_4 case. These overtones

Figure 12. Raman spectra of the lattice region in polycrystalline NH₄ReO₄ using 5145A Ar(II) laser excitation.

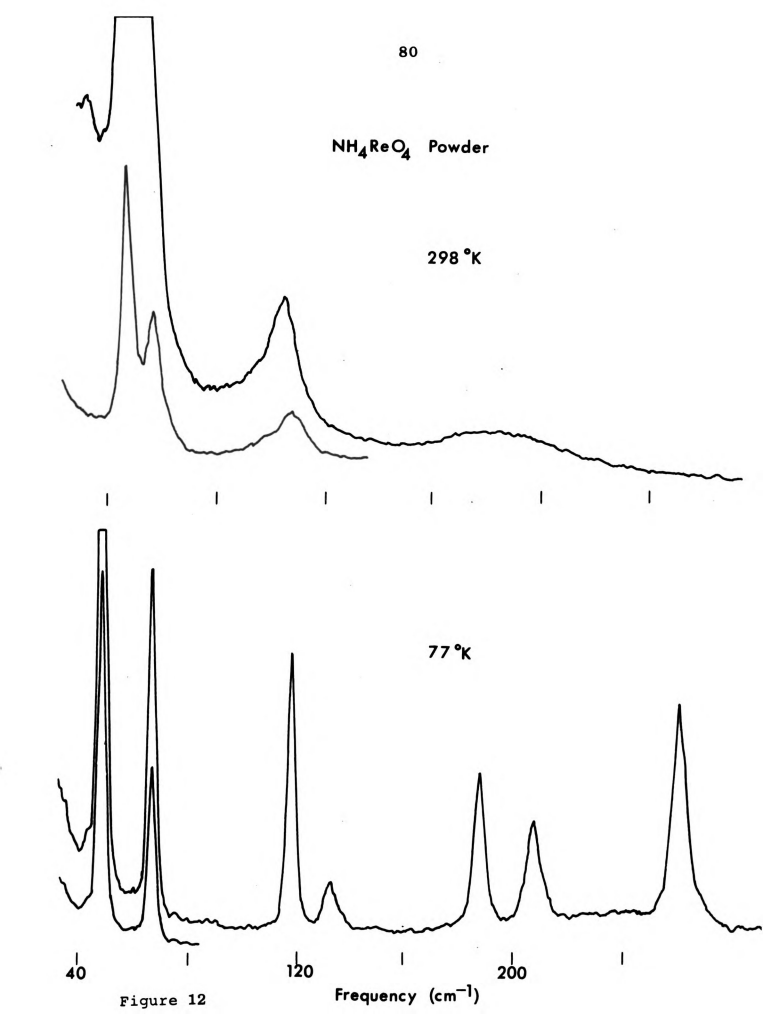


Figure 13. Raman spectra of the lattice region in polycrystalline ND₄ReO₄ using 5145A Ar(II) laser excitation.

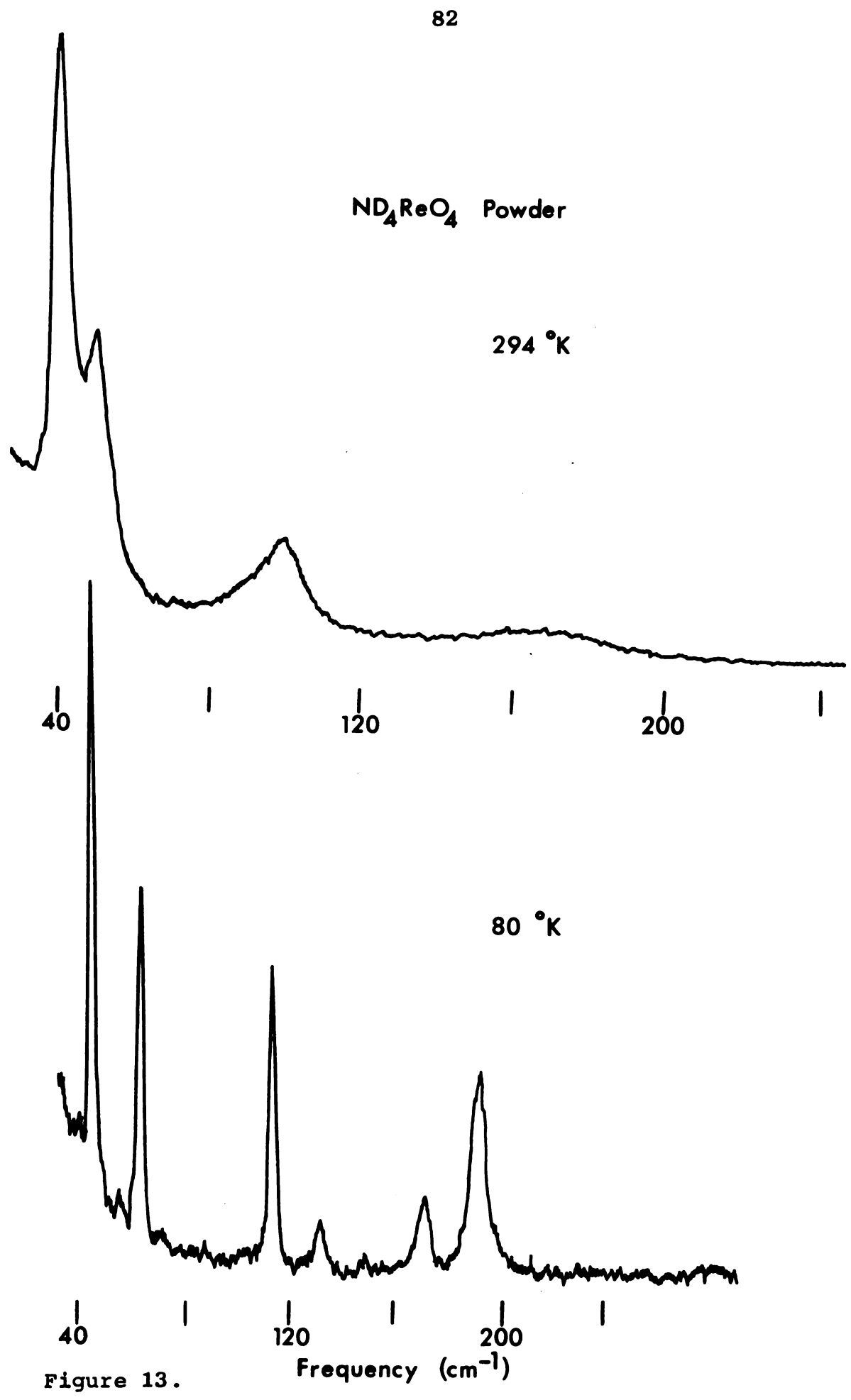
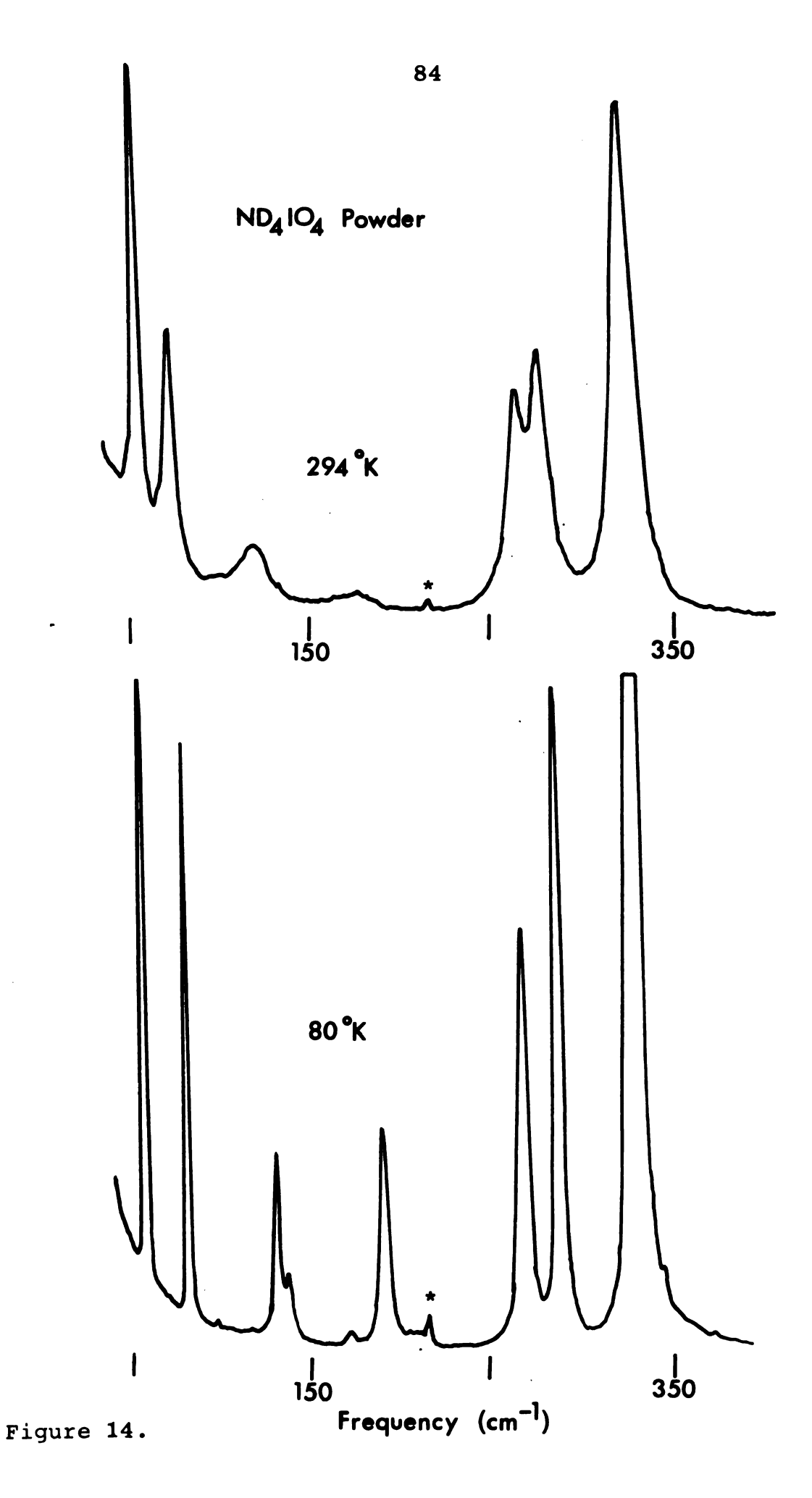
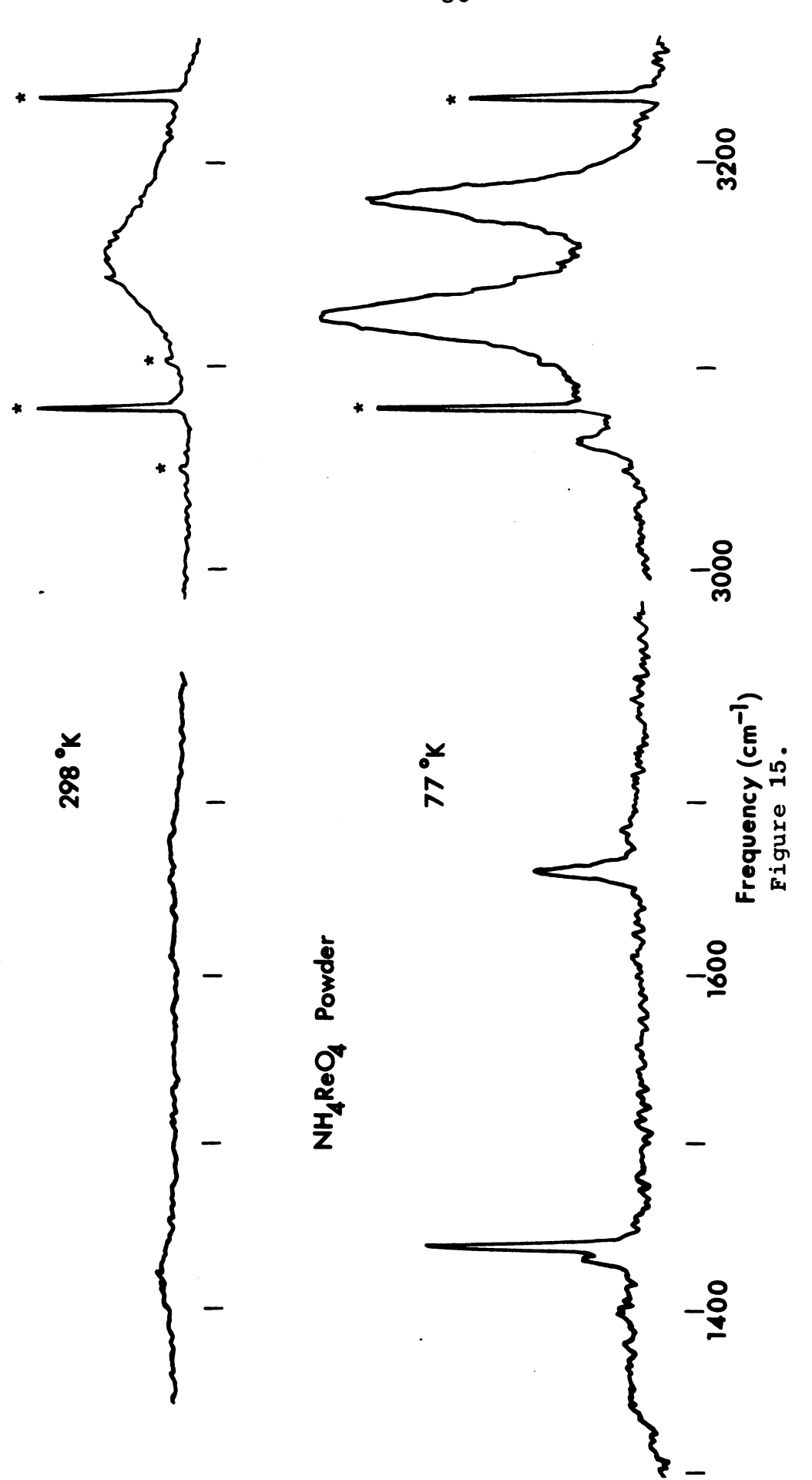


Figure 14. Raman spectra of the lattice region in polycrystalline ND₄IO₄ using 4880A Ar(II) laser excitation.

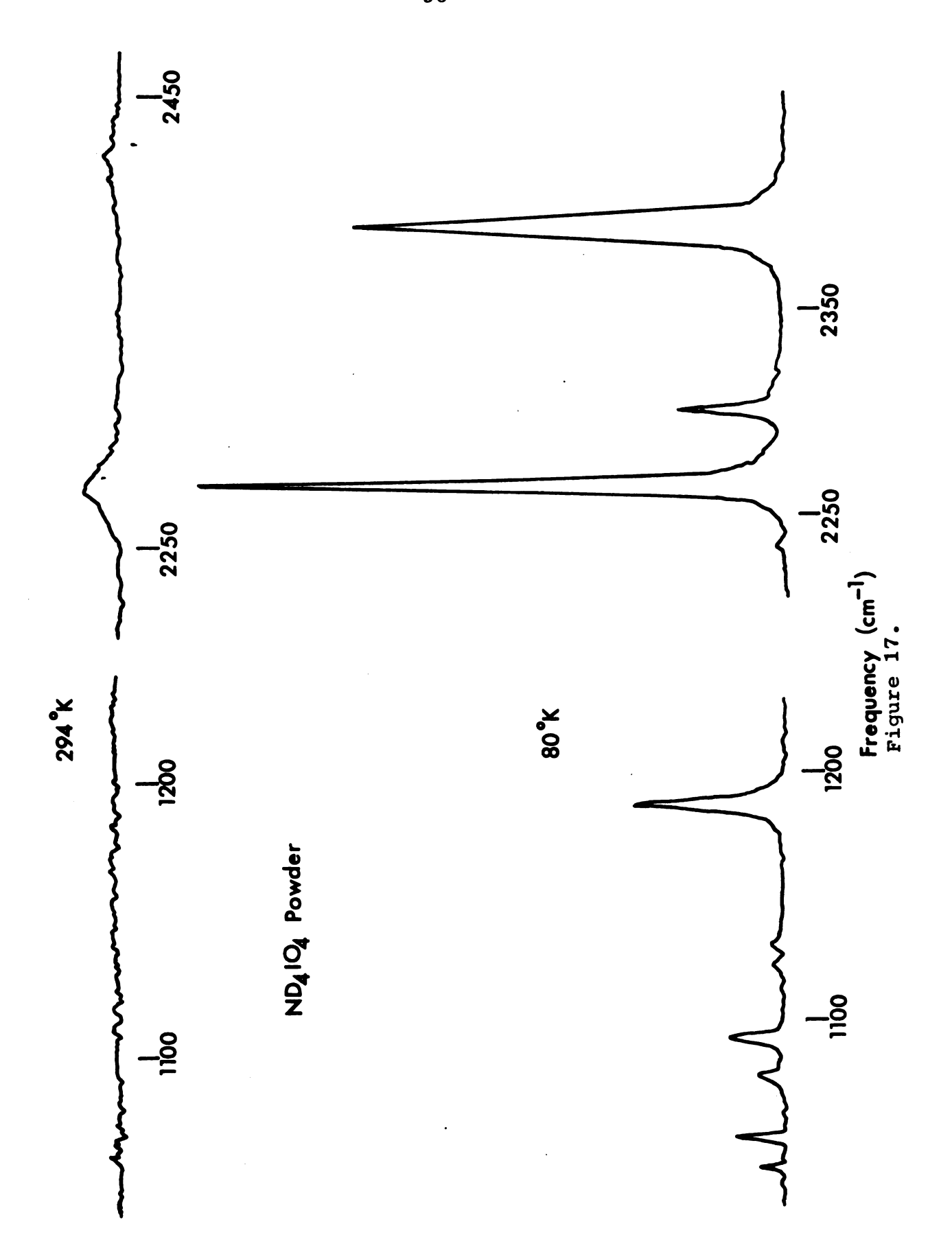


Raman spectra of ammonium fundamentals in ${\rm NH_4ReO_4}$ using $5145{\rm \AA}$ Ar(II) laser excitation Figure 15.



Raman spectra of deuteroammonium fundamentals in $\mathrm{ND_4ReO_4}$ using 5145\AA Ar(II) laser excitation. Figure 16.

Raman spectra of deuteroammonium fundamentals in ${\rm ND_4IO_4}$ using $4880{\rm \AA}$ and $5145{\rm \AA}$ Ar(II) laser excitation. Figure 17.



 $\mathtt{NH_4}^{f +}$ and $\mathtt{ND_4}^{f +}$ Raman-active fundamentals in the periodates and perrhenates. Table 7.

Symmetry	Solution Frequency	NH4ReO4 2980K 770K	e04 77°K	ND4ReO4 294°K 77°K	e04 77°K	NH4IO4 293°K 91°K	04 910K	ND ₄ IO ₄ 294 ⁰ K 80 ⁰ K	04 80 ⁰ K
v ₁ Ag	3033		3126	2275	2257	3171	3147	2280	2267
ь в В	1685	ŀ	1661	I	1192	1680	1649	1	1188
د* ه ه ه	3134	3156	3183	2409	2382	3237	3210	2426	2396
B V.≰ Bg	1397	ł	1431	;	1081	1429	1434	}	1080

^aFrom Reference (37).

and combinations are labelled conventionally by the $\underline{k}=0$ designations such as $2\nu_2$, although such labels are misleading since the phonon wave vector for these multiphonon transitions can range over the entire zone. The narrow half width of the two-phonon transitions and the small shift away from the predicted zero phonon frequency indicates that the internal ammonium modes show little dispersion with the maximum in the phonon density of states away from $\underline{k}=0$. These assignments agree with similar two-phonon bands in other ammonium salts (62,63,66-69). The isotopic ratios of the various fundamentals are compared to the valence force model predictions (58) in Table 8. The agreement is surprisingly good since we are not considering isolated NH₄ ions, but distorted tetrahedrons in the solid.

Symmetry assignments and motional character for the lattice modes are much more difficult since the isotopic ratios expected from a simple Born-von Karman model are not obeyed and correlation to the NaReO₄ single crystal results is rather uncertain. Also, the various modes with the same symmetry certainly undergo mixing, resulting in modes with mixed anion and cation character, giving an additional mechanism by which the isotopic ratios may be in error. The frequencies and assignments for the external modes are given in Tables 9 and 10 for the liquid nitrogen and room temperature results respectively. For the room temperature infrared modes no attempt is made to assign symmetries,

Table 8. Isotopic ratios for NH₄ fundamentals compared to valence force model predictions.

Symmetry	ReO ₄	104	Theoretical
$v_1 v_D^{\prime} / v_H^{\prime}$	0.734	0.721	0.707
$v_2 v_D^{\prime} v_H^{\prime}$	0.719	0.720	0.707
$\begin{array}{c} \begin{array}{c} \begin{array}{c} \begin{array}{c} \begin{array}{c} \begin{array}{c} \begin{array}{c} \begin{array}{c} $	0.564	0.564	0.560

Table 9. Raman active lattice modes in $\mathrm{NH_4}^+$ and $\mathrm{ND_4}^+$ per-rhenates and periodates near liquid nitrogen temperatures (cm⁻¹).

	ReC	4	I	04
Symmetry	NH ₄ (77°K)	ND ₄ (800K)	NH ⁴ (800K) _g	ND ₄ (80°K
Вg	49	50	65	64
Eg	68	69	90	86
Eg	120	117	141	135
A g	134	135	149	141
^B g	189	175	195	175
E g	209	(194)	216	(195)
Eg	-	-	241	213
A _g	264	194	260	195

a See Reference 37.

Table 10. Lattice modes in NH₄⁺ and ND₄⁺ perrhenates and periodates at 294°K (cm⁻¹).

	Re	e0 ₄	a IC	04
Symmetry	NH ₄	ND ₄	NH ₄ .	ND ₄
Bg	48	46	64	58
Eg	58	54	83	75
E _g	109	104	129	122
A _g	-	-	-	-
Ammonium Modes	183	167	202	179
$(A_u + 3E_u)$	108 134 170	106 ~ 140 169	88 ^b - 190 ^b	84 (126,16 188

asee Reference 37.

bSee Reference 48.

since the optical branch modes are a combination of anion and cation motion. The infrared spectrum should contain two modes primarily of torsional character, one perrhenate motion and the other mainly ammonium character. If the infared results correlate with the Raman results only three modes should therefore be observable at room temperature, since the ammonium libration is not observed in the Raman spectra.

The application of vibrational data to the determination of transition temperatures relating to ammonium rotation in solids is extremely active at present (References 62-70 are a few representative examples). The results can be compared to other methods (65,70) of obtaining the transition temperature, such as NMR line width studies, X-ray diffraction, or specific heat measurements. The best indication from IR and Raman studies of free or restricted rotation is the presence or absence of the ammonium torsional vibration (v_6) and combination bands such as $v_2 + v_6$ or $v_4 + v_6$.

In the ammonium ion salts studied here the presence of this librational mode at 77° K indicates that the ammonium group is not freely rotating near 77° K but apparently undergoes a transition between 77° K and 300° K, where no evidence of the ammonium ion libration is present. The second librational mode, of E_{g} symmetry, was not observed in the perrhenate but was present in the periodate salt. This may indicate that the ammonium ion in ammonium

perrhenate is undergoing rotation about the Z axis at 770K, while still librating about a perpendicular axis. When warmed from 770K the torsional mode in NH₄ReO₄ was observed to lose intensity rapidly and move toward lower frequencies; the spectra obtained at -500 and 250 are nearly identical with no evidence of the librational mode. Additional discussion of the molecular motion in these compounds will be given in the next section in connection with the NQR results in NH₄ReO₄.

B. Temperature Dependence

1. Normal Behavior: $NaIO_4$ and $MReO_4$ (M = Na, K, Ag)

Before discussing the experimental results and method of analysis used for the compounds studied here a brief survey of previous studies of the temperature dependence of NQR frequencies will be given since several of the conclusions to be drawn are better understood if earlier treatments are familiar. Only inorganic salts showing normal temperature dependence of the frequencies will be discussed. The origin and mechanism producing positive temperature coefficients is covered in the following section.

As shown earlier (Chapter I) a complete treatment of the NQR frequency shift with temperature also involves performing a separate pressure experiment to separate the volume effects. However, the required experiment is difficult to perform, requiring special pressure bombs and presses,

and a complete treatment has been carried out in only a few cases (71a-d). In most cases approximations to both terms of the bracketed expression in Equation (41) are used. The approximation to the first term,

$$\left(\frac{\partial \mathbf{v}}{\partial \mathbf{v}}\right)_{\mathbf{V},\mathbf{T}} = \frac{\mathbf{d}\mathbf{v}_{\ell}}{\mathbf{d}\mathbf{v}}$$

has been discussed by Brown (72). This term represents the change in vibrational frequency upon volume and the effect of this change on the quadrupole frequency. The variation in vibrational frequency with lattice size can usually be approximated by a linear function of temperature,

$$v = v_0 (1 - \alpha T),$$
 (59)

in which α is ordinarily an adjustable parameter but may be evaluated from IR-Raman data as discussed below, v_0 is the extrapolated frequency at $T=0^0K$ and v is the frequency at some temperature T. If the fixed frequency v_ℓ in Equation (56) is replaced by the expression given above, Equation (59) provides an approximation to $(\partial v/\partial T)_{P,N}$ given in Equation (41). The remaining volume dependence is given by the term $(\partial v/\partial V)_{V_\ell,T}$, which represents the effect of lattice expansion on the field gradient at the nucleus for which the temperature dependence is being calculated. In principle, this term could be calculated if data on the atomic positions as a function of temperature were available and, more importantly, if an accurate procedure for calculating field gradients in crystals was available.

Therefore, if a pressure versus frequency experiment is not carried out application of the two corrections given above should result in a better fit to experiment than using the Bayer term alone. In practice, calculation of the second term cannot be carried out due to a lack of the necessary X-ray data but some calculations have been made; Hewitt (73) performed a calculation for KNbO3 based on thermal expansion data for BaTiO3, while Gutowsky and Williams (74) calculated the volume dependence in NaClO3 using only the change of unit cell parameters with temperature. The results in both cases were uncertain, due more to the approximate nature of the structural data available than to the approximations used in calculating the field gradient. Because of the problems in attempting to calculate the volume dependence of the field gradient properly, the usual procedure is to neglect this term and only use the correction based on Equation (59). This involves varying both the vibrational frequency, v_0 , and its temperature variation, α , until a best fit to experiment is obtained. some cases the moment of inertia is included as an adjustable parameter also. Use of these parameters along with $\nu_{\boldsymbol{0}}\,\text{,}$ the rigid lattice NQR frequency, leads to an equation containing four adjustable parameters to be fit to a simple curve. This will be designated here as the adjusted Bayer theory and the resulting fit is usually quite good. It has, however, been applied in cases where some volume dependence of the field gradient is expected and therefore some

ment is expected. Some compounds where this type of treatment has been carried out include LiNbO₃ (75) and a large number of chlorate and bromate salts (76-79).

Since the periodates and perrhenates form ionic-type lattices the adjusted Bayer theory described above should not give close agreement to experiment over the whole temperature range studied. In order to reduce the number of the adustable parameters an infrared and Raman study was carried out to measure experimentally the vibrational frequencies and their temperature variations and the moments of inertia were calculated from the X-ray data, leaving only the rigid lattice quadrupole frequency v_0 as an adjustable parameter. The infrared and Raman results are summarized in the previous section except for the temperature variations of the lattice modes which are given in Table 11. Lattice translations do not average the field gradient tensor as the librational modes do and should not be included in the analysis. Recalling the discussion of the Raman results for the ammonium ion presented in the last section, the four lowest lattice modes are primarily the ReO_4 motions. The $A_{_{\mathrm{CI}}}$ mode is assigned as a libration and the B_{α} as a translation on the basis of symmetry requirements. The two $\mathbf{E}_{\mathbf{q}}$ modes, intermediate in frequency between the A_{α} and B_{α} modes, are probably of mixed librational-translational character due to symmetry mixing of the states. Despite the mixed character the lower

Temperature dependences of periodate and perrhenate lattice modes.^a Table 11.

Symmetry	NaReO ₄ $v_0 (cm^{-1})$ $\alpha \times 10^4 (^0K^{-1})$	$v_0 (cm^{-1})$ $\alpha x 10^4 (^0K^{-1})$	04 m ⁻¹) (0K ⁻¹)	ν ₀ (αx10	$v_0 (cm^{-1})$ $v_1 (cm^{-1})$	ν ₀ (αx10	KREO4 AGREO4 AGREO4 v_0 (cm ⁻¹) v_0 (cm ⁻¹) v_0 (cm ⁻¹) σ_0 (cm ⁻¹) σ_0 (cm ⁻¹) σ_0 (cm ⁻¹)	$V_0 (cm^{-1})$ $\propto 104 (^{0}K^{-1})$	$^{-1}_{ m 0}$	ν ₀ (αx10	$V_0 (cm^{-1}) V_0 (cm^{-1})$ $\alpha x 10^4 (^0K^{-1}) \alpha x 10^4 (^0K^{-1})$
Вд	80 (1.41)	54 (0.330)	49	54 (0.330) 49 (2.93) 64 (2.68)	64	(2.68)	99 (1	.05)	74	99 (1.05) 74 (1.81)
, р П	90 (2.18)	71 (:	71 (2.92)	61	61 (7.18) 88 (4.49)	88	(4.49)	113 (1.59)	.59)		96 (2.98)
) b	133 (0.492)	110 (1.14)	1.14)	82	82 (3.89)	95	!	155 (1.76) 125 (2.29)	.76)	125	(2.29)
, 4	159 (2.92)	125 (125 (3.33)	110	110 (3.68) 153 (4.53)	153	(4.53)	172 (1.81) 152 (4.24)	.81)	152	(4.24)
, ल	189 (1.45)	147	1	!	;	185	1	221 (1.62) 179	.62)	179	}

Assuming $v = v_0 (1 - \alpha T)$.

mode is more likely to be chiefly translational with the remaining mode having more librational character. Because of their higher frequencies relative to the lattice modes, the internal vibrations are assumed to have a negligible effect on the averaging of the field gradient and will not be included in the analysis. Before discussing the application of these results to the calculation of the temperature dependence of the NQR frequencies to be expected in these compounds, the experimental results will be presented.

The experimental 127 quadrupole frequencies in NaIO. and ¹⁸⁷Re quadrupole frequencies in NaReO₄, KReO₄, and AgReO₄ are listed in Tables 12-15, at the experimental temperatures from 120K to 3000K. In both NaIO, and in the perrhenates the asymmetry parameter remained zero over the temperature range and only the $(\pm 5/2 \iff \pm 3/2)$ or the $(\pm 3/2 \iff \pm 1/2)$ transitions were followed, but not both. For the rhenium resonances the isotopic ratio ¹⁸⁷Re/¹⁸⁵Re remained constant so only the more abundant 187Re isotope resonance was followed. For NaReO4 and AgReO4 the higher frequency required to observe the resonance made necessary the use of a Dewar arrangement such that stable low temperatures were very difficult to achieve and for these compounds fewer measurements are reported. It should be pointed out, however, that many more experimental measurements were made which could not be included because the rapidly changing temperature at the sample resulted in unacceptable errors in temperature measurement. The

Table 12. Experimental frequencies and temperatures for the $(\pm 3/2 \iff \pm 1/2)$ ¹⁸⁷Re pure quadrupole resonance transition in NaReO₄.

Temperature (⁰ K)	Frequency (MHz)	
30.4	46.3869	
56.1	46.1382	
59.3	46.0957	
71.1	45.8242	
93.4	45.6453	
96.5	45.6184	
203.1	44.0122	
205.3	43.9873	
206.7	43.9200	
208.3	43.8918	
208.6	43.9375	
209.1	43.8877	
209.5	43.9039	
216.1	43.7088	
226.8	43.7257	

Table 13. Experimental frequencies and temperatures for the $^{187}{\rm Re}~(\pm 3/2 \iff \pm 1/2)$ pure quadrupole resonance transition in KReO4.

Temperature (°K)	Frequency (MHz)	Temperature (°K)	Frequency (MHz)
16	27.9025	93.4	27.7920
18	27.8978	125.4	27.6247
23	27.9010	162.2	27.5056
30	27.8868	179.4	27.4554
36.6	27.8831	193.6	27.3650
38.6	27.8823	199.0	27.3465
42.8	27.8834	204.2	27.3111
46.3	27.8809	205.2	27.2777
49.0	27.8742	209.2	27.2508
52.0	27.8736	240.3	27.0104
5 4.3	27.8567	247.4	27.0870
59.0	27.8642	256.7	27.0269
63.5	27.8539	298.7	26.7750
66.4	27.8445		
Points obtain	ed with ENDOR Dew	ar. ^a	
121	27.8233	200	27.3897
141	27.7091	212	27.3104
150	27.5971	228	27.2768
162	27.5425	238	27.2005
172	27.5060	248	27.1274
183	27.4578	263	26.9926
191	27.3897	268	27.0039
		273	26.9500
		298	26.9095

^aObtained with an uncalibrated thermocouple.

Table 14. Experimental frequencies and temperatures for the $^{187}\text{Re}~(\pm 3/2\iff \pm 1/2)$ pure quadrupole resonance transition in AgReO4.

Temperature (OK)	Frequency (MHz)
46.6	39.3973
63.6	39.3851
76.2	39.3017
86.0	39.2579
95.0	39.0584
96.5	39.0710
98.5	39.0140
120.5	38.8742
131.5	38.7761
252.4	37.8706
275.4	37.7661
283.5	37.6475

Table 15. Experimental frequencies and temperatures for the ^{127}I $(\pm 5/2\iff \pm 3/2)$ pure quadrupole resonance transition in NaIO4.

Temperature (°K)	Frequency	Temperature (°K)	Frequency (MHz)
18	13.2850	200.7	13.0033
29	13.2852	201.2	13.0240
41.3	13.2790	194.4	13.0538
46.1	13.2804	212.3	12.9780
49.0	13.2796	223.0	12.9485
59.2	13.2671	233.1	12.9360
75.3	13.2598	250.4	12.8599
120.2	13.2288	251.5	12.8570
141.7	13.1579	273.0	12.8062
158.9	13.1125	273.2	12.7985
168.3	13.0975	300.2	12.7255
180.3	13.0586		

temperature variation in the case of KReO4 was very thoroughly studied and revealed anomalies, such as phase transitions to less symmetric phases or changes in slope of the temperature curve, so experimental points available for other simple perrhenate salts are not serious. The experimental errors, previously discussed in Chapter II, are ±10K below about 30° K, and $\pm 0.1^{\circ}$ K above 80° K; the frequency measurements have a relative accuracy of ±5 kHz. A representative NQR signal is shown in Figure 18, with the center line indicated by an arrow. Usually the shape of the resonance line remained relatively constant over the range of temperatures so that the selection of center line was consistent. No problems were encountered with saturation of the signals at helium temperatures, although the resonance line was not observable in NaReO₄ for about an hour after initial cool-down. This loss of signal was probably due to thermal strains induced by the rapid temperature changes. The room temperature resonance in KReO4 returned to full intensity quite slowly if the sample was abruptly warmed to room temperature; usually three to five days were required and in one instance, no signal was observable the first two days after warming. If the samples were left in the helium Dewar to warm up gradully no loss of signal was encountered.

Several different methods were used to calculate the temperature shifts to be compared with experiment. For applying the adjusted Bayer theory a computer program (TFIT)

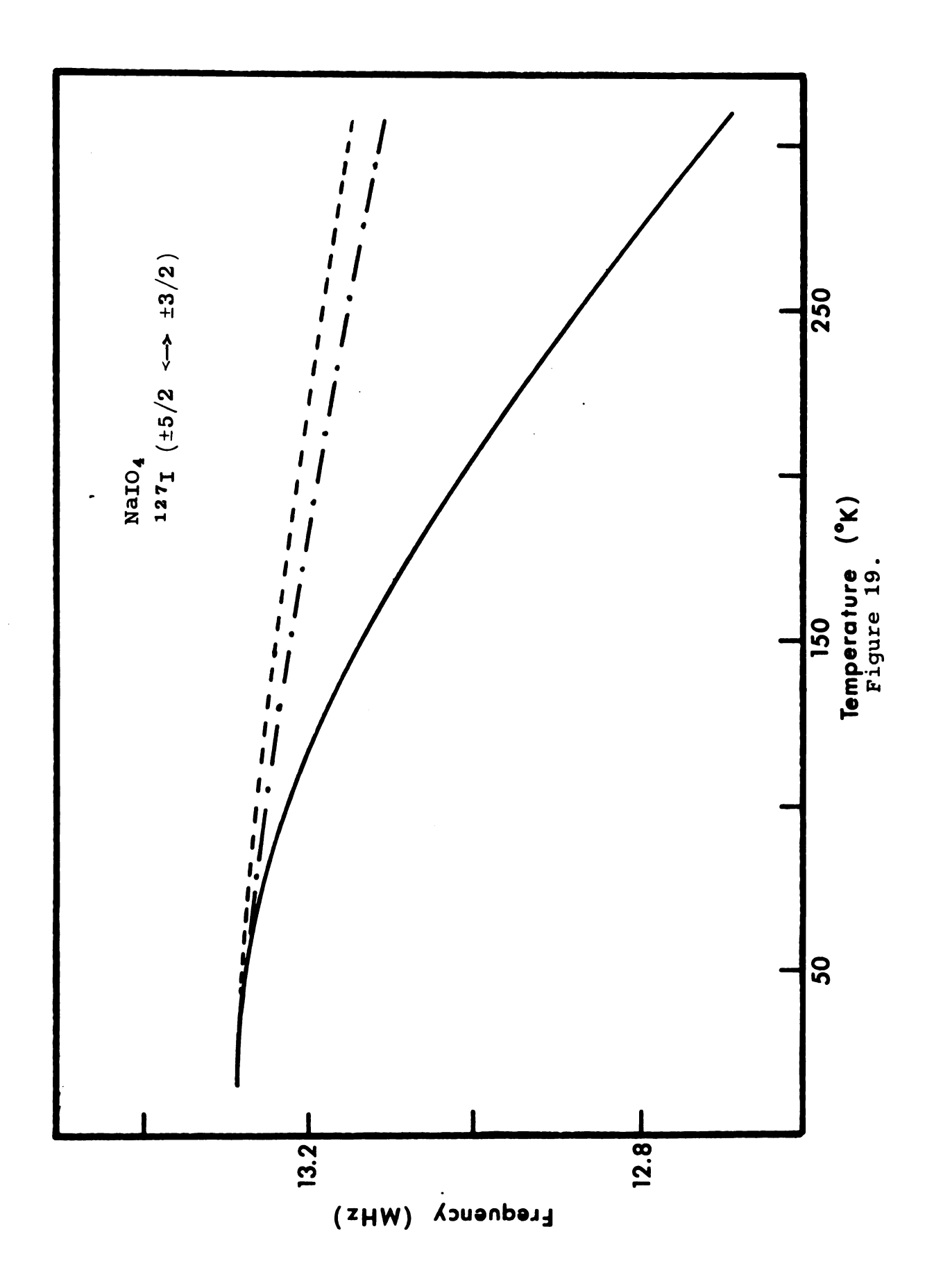
NQR spectrum of the $(\pm 3/2 \leftrightarrow \pm 1/2)$ ¹⁸⁷Re pure quadrupole resonance transition in polycrystalline KReO₄ at 30⁰K. Figure 18.

Figure 18.

was written to calculate the temperature variation for any input values of lattice frequency, vibrational frequency temperature coefficient, and moment of inertia for up to four different vibrational modes. In the calculations in this thesis two different curves were calculated. The first assumed that the highest frequency ReO4 or IO4 lattice mode of E_{cr} symmetry is 100% librational (no symmetry mixing) and this mode alone is used. Since there is an IR active E, component the mode degeneracy used was four instead of two as implied by the E_{α} symmetry. The $\mathbf{A}_{\mathbf{q}}$ mode is by symmetry the Z axis librational mode which has no effect on the EFG averaging and therefore is omitted. The second calculation assumes some degree of symmetry mixing between the E_{α} latice modes of the ReO_4 and IO_4 ion and a mixed contribution from the two modes to the temperature dependence is calculated. The experimental and calculated curves for NaIO4 and sodium, potassium, and silver perrhenate are shown in Figures 19-22. In each curve the solid line is drawn through the experimental points; the (----) curve is calculated assuming pure librational character for the highest frequency E_{α} mode; the (---) curve is calculated assuming partial librational character in both E modes. The interpretation of these results will be discussed after outlining the method of treating the data in which all the parameters of the adjusted Bayer theory are allowed to vary.

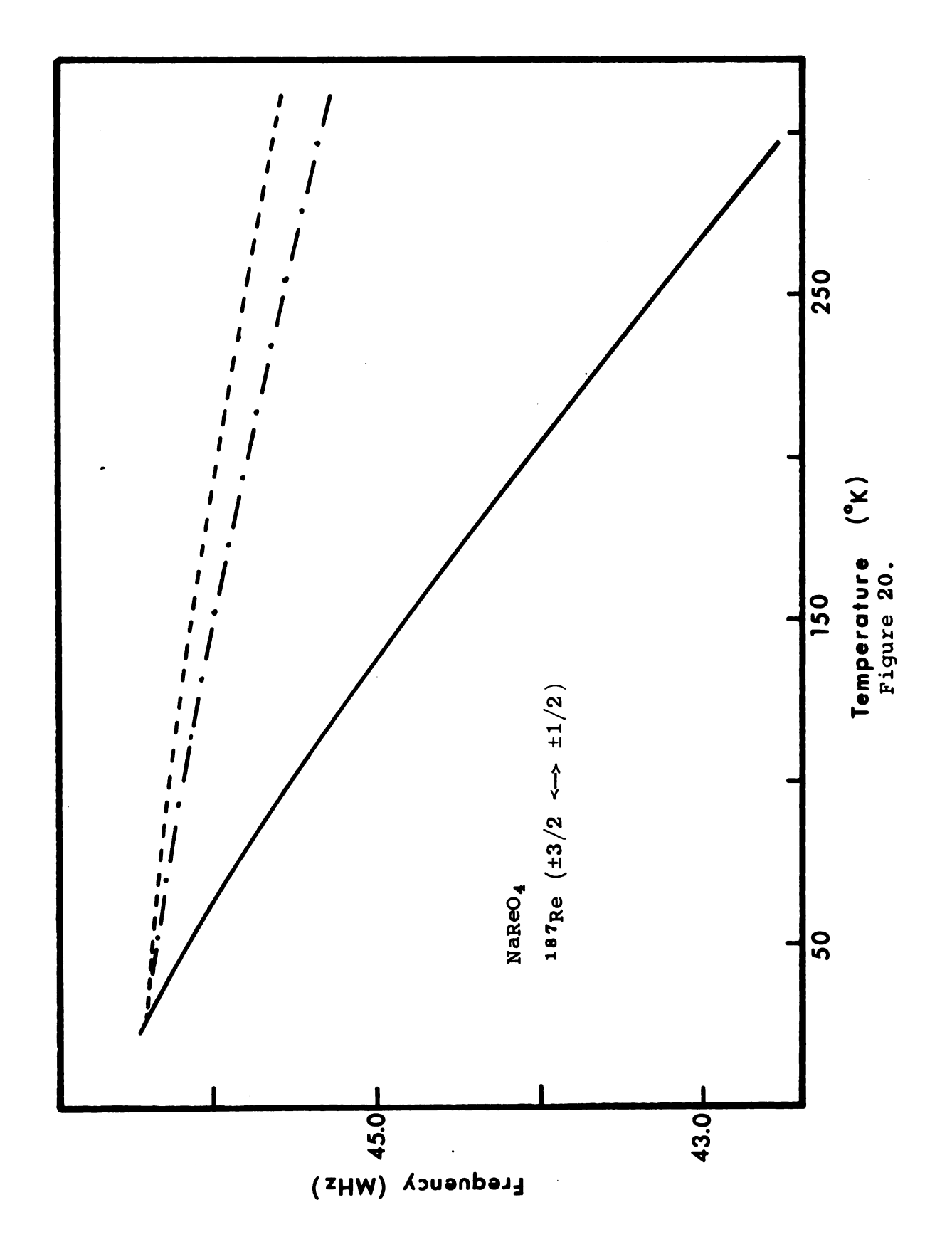
Experimental and calculated temperature dependence of the $^{127}\mathrm{I}$ quadrupole resonance in NaIO4. Figure 19.

The solid curve is experimental, the curve (———) assumes symmetry mixing of the two IO4 E modes with the highest frequency E mode 75% librational character and the lowest frequency mode 25% librational character for character, and the curve (----) assumes pure librational character for mode. the highest frequency E



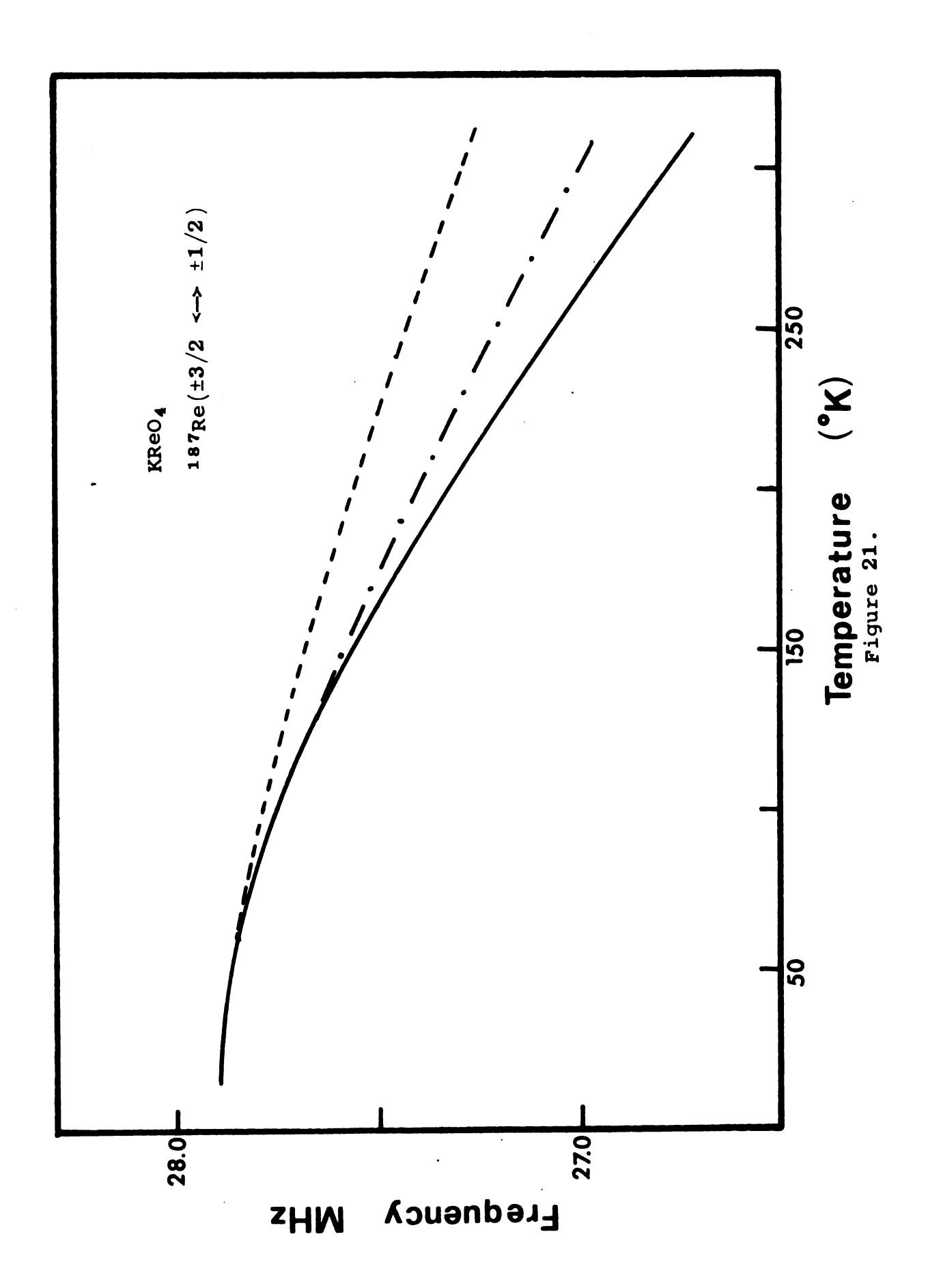
Experimental and calculated temperature dependence of the 187Re quadrupole resonance in NaReO4. Figure 20.

The solid curve is experimental, the curve (----) assumes symmetry mixing of the two ReO₄ E modes with the highest frequency E mode 75% librational character and the lowest frequency mode 25% librational character, and the curve (----) assumes pure librational character for the highest frequency E mode.



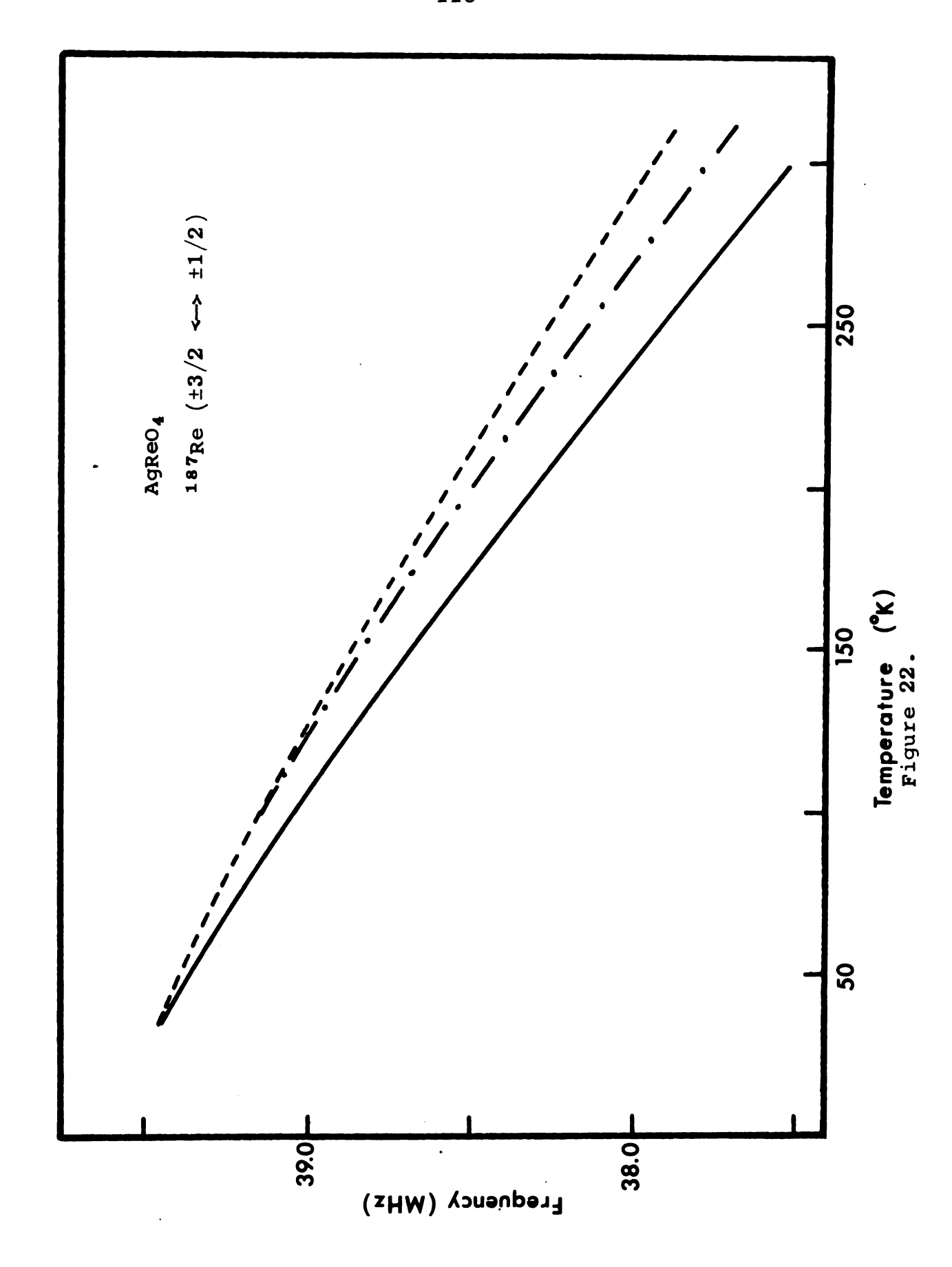
Experimental and calculated temperature dependence of the 187Re quadrupole resonance in KReO4. Figure 21.

mixing of the two ReO E modes with the highest frequency E mode 75% librational character and the lowest frequency mode 25% librational character for character, and the curve (----) assumes pure librational character for The solid curve is experimental, the curve (----) assumes symmetry mode. the highest frequency Eg



Experimental and calculated temperature dependence of the ¹⁸⁷Re quadrupole resonance in AgReO4. Figure 22.

The solid curve is experimental, the curve (----) assumes symmetry mixing of the two ReO₄ E modes with the highest frequency E mode 75% librational character and the lowest frequency mode 25% librational character, and the curve (----) assumes pure librational character for the highest frequency E mode.



As pointed out earlier one purpose of this study is to show that conventional treatments using the lattice frequencies and temperature variations as adjustable parameters can lead to a misleading agreement between theory and experiment. In order to illustrate this point a conventional treatment of the compounds studied here was carried out to compare the parameterized librational frequencies with those obtained directly by experiment. For fitting the data a general non-linear least squares program (80), KINET, was used. Before fitting the experimental data an artificial curve was constructed with simulated moments of inertia, vibrational frequencies, and temperature variations of the vibrational modes and the ability of a least-squares fit to reproduce the known simulated parameters was determined.

The results of the simulation illustrate several problems involved in fitting a curve with a function of the form used in the interpretation of experimental NQR frequency versus temperature curves (Equation 56). If both the moment of inertia A_{ℓ} and the vibrational frequency ω_{ℓ} in one of the summation terms in Equation (56) are allowed to vary, difficulties are encountered because they appear as a product and so are strongly correlated (105). The same problem with correlation is also present when the substitution of Equation (59) for the vibrational frequencies is made and both v_0 and α are allowed to vary. Fitting the constructed frequency versus temperature curve

using either of the above strongly correlated pairs gives excellent results; however, the final values of the parameters in most instances were physically meaningless and far away from the actual values used in constructing the problem. In most cases one member of the parameter product would go to very large values while the other would go to extremely small values, the resulting product remaining nearly constant.

The second simulation tested the ability of the computer program to fit a constructed experimental curve with two separate terms in the adjusted Bayer summation (Equations (56) and (57)). In this case the lower vibrational frequency was reproduced fairly well, but the second frequency was reproduced poorly, especially in cases where the second frequency was 30 to 50 cm⁻¹ higher. In this case only one parameter in each term of the sum was allowed to vary in order to avoid correlation problems as discussed above. In summary, therefore, attempting to fit experimental NQR frequency versus temperature plots using the adjusted Bayer theory must be carried out with care if the final parameter values are to correspond to physical reality.

In the Scheelite-type perrhenates and periodates studied here agreement between experiment and theory over the entire range of temperatures studied can be obtained by such a procedure allowing only one frequency to vary. Because of problems with strongly correlated parameters the moment of inertia for the lattice librational mode, which

averages the field gradient, was held constant; only the static lattice NQR frequency v_0 and the libration frequency v_ℓ were adjustable. The librational mode temperature coefficient α usually used was the experimentally determined value. Attempts to improve the fit by varying α gave final values for v_ℓ^0 and α which were not physically meaningful. The values of v_0 and v_ℓ which gave the best fit of Equation (56) to the experimental data are listed in Table 16. The experimentally determined quantities v_ℓ^0 , α , and I_n are also listed, along with the sum of the square of the residual frequency between calculated and experimental data points. In general this difference was less than 25 kHz.

Referring again to the results displayed in Figures 19-22 several significant results obtained with the use of only one adjustable parameter, ν_0 , in the adjusted Bayer theory are apparent. In the case of NaIO₄, NaReO₄, and KReO₄ the calculated curves begin to show deviations from the experimental curve below $100^0 \mathrm{K}$. This is precisely the effect expected from neglect of changes in the field gradient directly due to lattice expansion, since one expects the lattice to begin showing significant expansion in the range $10-100^0 \mathrm{K}$. The extremely bad fit in the case of NaReO₄ implies that volume effects on the field gradient are of greater importance in this salt. In contrast, the agreement in the case of AgReO₄ seems to indicate that neglect of the volume term may not be as serious here.

The extent to which the adjusted Bayer theory provides agreement with experiment might be expected to depend on the nature of the bonding in the crystal. However, the limited number of salts studied here has not provided any obvious correlation.

Table 16. Final parameters obtained in applying the adjusted Bayer theory.

	Adjustable Parameters		Experimental Constants		Residual ²
Compound	[∨] 0 (MHz)	(cm 1)	$\alpha \times 10^4$ $({}^0K^{-1})$	I	$\Sigma (X_{i \text{ (exp)}}^{-X}_{i \text{ (calc)}})^{2}$
NaReO ₄	47.136	63	0.492	18.55	3.28×10^{-2}
KReO ₄	28.150	85	1.14	22.80	5.48×10^{-2}
AgReO ₄	39.895	84	2.00	18.72	4.33×10^{-2}
$NaIO_4$	13.404	86	1.76	23.06	2.75×10^{-2}

An important deficiency in using the spectroscopically determined librational frequencies in the above method for fitting the experimental NQR frequency versus temperature curves is the neglect of phonon dispersion. The mechanism for averaging the field gradient involves phonons with wave vector ranging over the entire Brillioun zone and not restricted to the $\underline{\mathbf{k}} = 0$, spectroscopically-active phonons. Since the maximum in the phonon density of states usually doesn't occur at $\underline{\mathbf{k}} = 0$ the choice of librational frequency to use in fitting the experimental curve is difficult.

However, in the compounds presented here the differences between the experimental vibrational frequencies and the average vibrational frequencies listed in Table 16 are too large to be accounted for solely by dispersion effects.

In these compounds with ionic-type lattices neglecting field gradient changes due to lattice expansion or contraction is not valid.

2. Anomalous Behavior: NH₄ReO₄

In contrast to the perrhenates just discussed, ammonium perrhenate exhibits a large positive temperature coefficient of the NQR frequencies indicating that the temperature dependent mechanism modulating the field gradient is radically different in this case. Before discussing what appears to be the origin and nature of this mechanism the various proposals previously advanced to explain anomalous quadrupole temperature shifts will be discussed and their applicability to NH4ReO4 examined. A short but not comprehensive review of positive temperature coefficients in NQR is also given.

Positive temperature coefficients of nuclear quadrupole resonance signals have been observed in a relatively small number of compounds, mainly transition metal halides such as TiCl₄ and WCl₆ (81), TiBr₄(82), ThCl₄ (83), and hexahalometallate-type compounds which have been studied (28, 29,84). In all these compounds, measurements have been made only of the halogen NQR frequencies and not those of the

metal. Anomalous behavior in compounds not containing transition metals is much rarer, having been observed only in NH_4I_3 (85) to my knowledge. In the compounds containing transition metal complexes the transition metal invariably has d orbital vacancies, and the proposed mechanism causing the anomalous behavior is a destruction of the metal-halogen $d\pi$ -p π bonds from the increased amplitude of the metal complex internal vibrations with increasing temperature as discussed in Chapter I. Haas and Marram (26) attribute π -bond destruction through rehybridization to the bending fundamentals while Brown and Kent (28) attribute this to the bond stretching vibrations, showing that only the latter can be effective. Regardless of the type of fundamental causing the rehybridizations the mechanism predicts that all the isostructural compounds differing only in the cation should exhibit the same type of behavior. Since this is not the case for the perrhenate series this mechanism does not account for the present observations.

A second mechanism, competing with the π -bonding mechanism just described, which also predicts positive NQR temperature coefficients, has been proposed by O'Leary (86). If the frequency of the torsional mode (ω_{ℓ}) which, according to the conventional theories (Equation 56), averages the field gradient increases in frequency with increasing temperature at a fast enough rate, then the magnitude of the exponential term in Equation (56) will increase with increasing temperatures giving rise to a positive value for

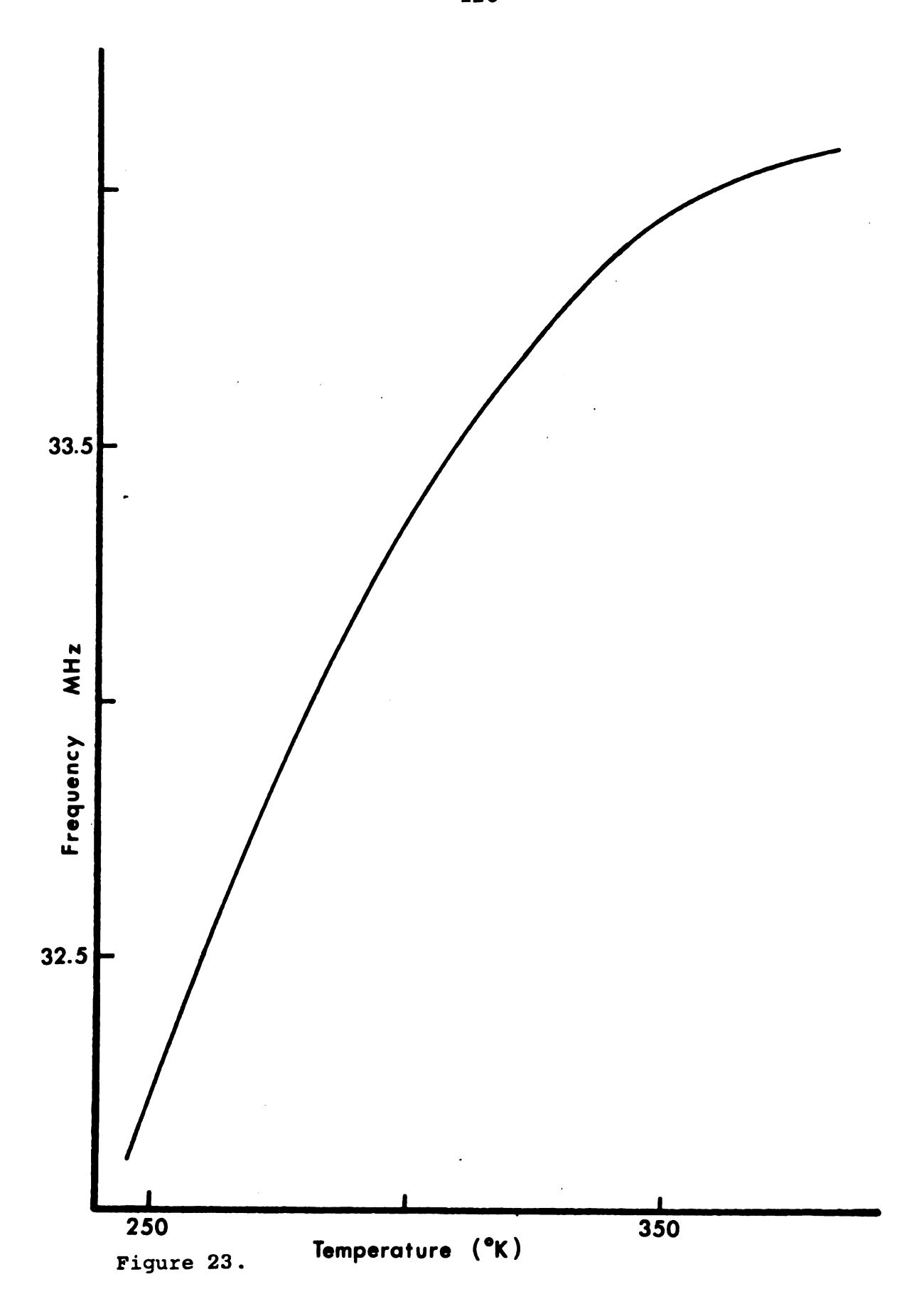
the Bayer term, $(\frac{\partial \nu}{\partial T})$. Torsional modes with this type of behavior are called soft librational modes and are usually observed on the high-temperature side of phase transitions. In cases where symmetry restrictions prohibit direct observation of such a mode by Raman or infrared spectroscopy the NQR results can give previously unobtainable vibrational data. In the case of NH₄ReO₄ the librational mode is vibrationally active and since the infrared and Raman results show that the torsional mode in NH₄ReO₄ behaves normally, this mechanism is also not operable here. The magnitude of the temperature coefficients normally observed in cases where these two mechanisms are applicable preclude applying them to the NH₄ReO₄ data, but detailed discussion of this point will be deferred until after the experimental results are presented.

The experimental rhenium quadrupole resonance frequencies measured at various temperatures are given in Table 17, with the results displayed graphically in Figure 23. The ^{185}Re resonance is not shown since the isotopic ratio $^{185}\text{Re}/^{187}\text{Re}$ does not vary over the temperature range. It has been shown previously (11) that η = 0 over the range 257°K to 300°K and therefore only the $(\pm 5/2 \iff \pm 3/2)$ transition was followed. The disappearance of the NQR signal at 245°K is not abrupt; the resonance gradually broadens and loses intensity as the temperature is decreased. If an instrument of greater sensitivity were used the resonance definitely could be followed to lower temperatures.

Table 17. Experimental frequencies observed at various temperatures for the $(\pm 5/2 \iff \pm 3/2)$ transition of the 187 Re pure quadrupole resonance spectrum.

Temperature (OK)	Frequency (MHz)	Temperature (°K)	Frequency (MHz)
245.4	32.0953	324.7	33.6283
246.4	32.1098	334.1	33.7560
248.4	32.1941	334.5	33.8153
250.9	32.2711	338.4	33.8274
256.2	32.4290	344.5	33.8905
262.0	32.5339	352.5	33.9648
265.7	32.6470	361.1	33.9937
273.9	32.8750	365.9	34.0160
274.6	32.8909	367.1	34.0428
278.7	32.9447	367.6	34.0294
283.3	33.0250	372.6	34.0574
294.2	33.2393	375.8	34.0699
296.8	33.2972	377.8	34.0758
308.2	33.4533	383.0	34.0837
313.6	33.5280		

Figure 23. Experimental temperature dependence of the $(\pm 5/2 \iff \pm 3/2)^{-187}$ Re transition in NH₄ReO₄.



In attempting to explain the experimentally observed behavior in NH4ReO4, the effect of the substitution of the ammonium ion for the simple cations should be considered, since in other respects the perrhenates with the Scheelite structure are quite similar. The strong temperature dependence of the field gradient at the rhenium nucleus suggests that changes in the ammonium ion motion may be responsible. Before going into detail regarding the mechanism of this effect, a somewhat analogous case will be presented. As previously mentioned the temperature behavior of ^{127}I in NH₄I₃ (85) is anomalous, although the rubidium and cesium salts having the same crystal structure show completely normal behavior. Kubo et al. (85) postulate that this behavior may be caused by the onset of ammonium group rotation after which the rotating ammonium group simulates a simple alkali metal cation. No detailed model of the modulation of the NQR frequency by the change in ammonium motion was given. The NH4I3 results, particularly the magnitude of the temperature coefficient, will be compared to ammonium perrhenate below.

The crystal structure of NH₄ReO₄ is unfortunately not very reliable with regard to the oxygen positions since it was carried out quite a long time ago (87). However, recent redeterminations of the crystal structures of KReO₄ (88) and NaIO₄ (89) have been carried out and some of the conclusions from these results are applicable to NH₄ReO₄. The question of main interest is the orientation of the

NH4 tetrahedron in the lattice since the hydrogen positions are not available from the crystal structure. The recent structure refinement of NaIO₄ by Cruickshank (89) shows that the sodium atom has two tetrahedra of oxygen atoms enclosing it, four at a distance of 2.54A and the other four at 2.60A. The same type of arrangement is present in KReO₄, the corresponding Re-O bond distances being 2.77Å and 2.88A. The earlier determination of the oxygen positions in NaIO₄ by Hazelwood (90) in 1938 gave Na-O separations of 2.573A and 2.577A and indicated a much less distorted IO4 tetrahedron than the work quoted above. The corresponding Re-O distances in NH₄ReO₄, using oxygen parameters from the old structure determination (87), are 2.84A and 2.87A indicating that the two sets of tetrahedrally arranged oxygens are not equivalent. Since a structure refinement could give as large a change as for NaIO4, the inequivalence and relative ordering of the two tetrahedra may be open to question. If the X-ray results are taken to be qualitatively correct, however, a definite preferred choice for the orientation of the ammonium ion hydrogens can be made.

The four H-atoms of the NH₄⁺ group are naturally arranged in the correct shape to line up pointing toward the four closest tetrahedrally-arranged oxygen atoms at a distance of 2.84Å. The ordered state existing at very low temperatures, and possibly at 770K, would have all the ammonium ions in this favored configuration, which will be

denoted as Orientation I. At somewhat higher temperatures a second configuration, corresponding to alignment of the four hydrogen atoms toward the second group of oxygen atoms (Orientation II), should become energetically allowable and a transition of the order-disorder type should occur. Transitions between the two configurations would be achieved by some of the ammonium ions possessing enough energy to be in the continuum above the bound energy levels of the librating group and, therefore, undergo free rotation for a short time before losing energy and again becoming a librating group in either Orientation I or II. Upon increasing the temperature a large number of the ammonium ions would tend to spend more time in the freely rotating state and the transition to a phase in which the ammonium ions are undergoing free rotation should be sharp. A model similar to this has been used to explain the phase transitions, NMR, and Raman and infrared results in the ammonium halides (68,69,91).

If the order-disorder transition occurred between 77°K and room temperature it should have been observable in the Raman results, but no changes in selection rules or large shifts of the ReO₄ fundamentals from the other salts with the Scheelite structure were observed. Therefore, the behavior of the ammonium fundamentals, and disappearance of the NH₄ ion librational mode upon warming, tend to indicate a first-order transition (92) from bound to free rotation. This conclusion is consistent with the NQR results

independent of the exact mechanism which modifies the field gradient at the rhenium nucleus.

In NH4ReO4 there are apparently four closest oxygen atoms arranged tetrahedrally around the ammonium ion and a second group of four oxygens slightly further away. In each of the ReO₄ tetrahedra two of the oxygens are coordinated with hydrogens in Orientation I while the remaining two are coordinated in Orientation II. Regardless of the mechanism, when the ammonium ion is aligned with the hydrogens in Orientation I the resulting field gradient at the rhenium is different than when the ammonium ion is in Orientation II. Therefore, if a field gradient exists in the lowest-temperature, completely ordered state it probably has a large asymmetry parameter. Above the orderdisorder transition the rapidly (on the NQR time scale) reorienting ammonium ions, from Orientation I to a mixed configuration of Orientations I and II, will cause a rapidly fluctuating field gradient at the rhenium nucleus, effectively making the resonance unobservable. If a second transition to freely rotating ammonium ions occurs as the temperature is increased the rate of rotation will increase until, on the NQR time scale, an increasing number of ammonium ions begin to resemble alkali metal ions to the rhenium nuclei. The rhenium nuclei in the ReO₄ tetrahedra no longer having ammonium ions aligned toward their oxygen atoms produce an observable NQR signal which then increases in intensity as a greater fraction of the rotating ammonium ions resemble alkali metal cations.

The exact mechanism causing the observed positive temperature shift is probably a mixture of contributions from the change in covalent bonding of the Re-O bonds as the weak 0 · · · H hydrogen bond breaks, and an electrostatic effect from the effective positive charge of the H⁺ atom being replaced by a NH₄ ion with the positive charge about 1A further away. This effective charge displacement would tend to decrease the positive contribution to the total field gradient from the ammonium ions in the lattice. Since the total field gradient is apparently negative (11), the above mechanism leads to an increasing field gradient with increasing temperature, as observed, and would have a much stronger effect on the field gradient than the mechanisms discussed previously. This can be seen by a comparison of their NOR temperature coefficients. Table 18 lists a number of the larger positive temperature coefficients observed in other compounds for comparison with results for NH4ReO4. Note that the coefficients for two compounds, NH_ReO_ and NH_I3, are an order of magnitude larger than those for the others. Because of the similarity between the temperature coefficients in NH4ReO4 and NH4I3 it is doubtful that the mechanism involved in modulating the field gradient in ammonium triiodide is direct hydrogen bonding, since no such possibility exists for ammonium perrhenate. However, if the N-H···I hydrogen bond is weak the effect on the field gradient might be about the same as in NH4ReO4.

Table 18. Positive temperature coefficients of NQR frequencies observed in NH_4ReO_4 and several other compounds.

Compound	$\frac{1}{\nu}(\frac{d\nu}{dT}) \times 10^3 {}^{0}K^{-1}$	Reference
NH ₄ ReO ₄	1.0	This work
NH ₄ I ₃	1.29	85
${\tt K_2ReCl}_6$	0.0094	93
K ₂ ReBr ₆	0.022	93
$(NH_4)_2$ ReBr ₆	0.0047	93
$(\mathrm{NH_4})_2\mathrm{ReI}_6$	0.022	93
WCl ₆	0.195	81
WBr ₆	0.180	28
CsNbCl ₆	0.130 0.107	28
CsWCl ₆	0.080	28
Cs ₂ WCl ₆	0.030	28

The NQR and Raman results are consistent with a model of NH₄ReO₄ in which the crystal is an ordered arrangement of librating ammonium ions at low temperatures and undergoes an order-disorder transition, apparently below 77°K, to a disordered state consisting of librating ammonium ions in dynamic equilibrium between two different orientations. At some higher temperature (below 245°K) the ammonium ions begin rotating freely and, as the frequency of rotation for an appreciable fraction of the total number becomes greater

than $\sim 10^6$ Hz, an NQR signal becomes observable, although the frequency shifts strongly with temperature as the rate of rotation of the ammonium ion increases. Near $380^\circ K$ the rate has increased to the point that the ammonium ions begin to resemble simple cations and the temperature variation of the field gradient becomes normal. This model predicts an NQR signal with an appreciable asymmetry parameter should be observable at liquid helium temperature if the librational motion of the ammonium ion does not perturb the field gradient at the rhenium nucleus too strongly.

C. Electric Field Gradient Calculations

1. Method of Calculation

The attempts to calculate field gradients from X-ray diffraction data in this study were based on two relationships. The field gradient is related to the electron density (Equation (24)), which in turn can be expressed as an infinite Fourier series with the expansion coefficients related to the intensity of X-ray diffraction maxima (94, 97,98),

$$\rho(x,y,z) = \frac{1}{V} \sum_{h,k,l}^{\infty} F(hkl) \exp\{-2\pi i (hx + ky + lz)\}, (60)$$

where V is the unit cell volume, F(hkl) is the structure factor, and $\rho(x,y,z)$ is the electron density at some point in the crystal. The intensity of an X-ray diffraction maximum of order hkl is proportional to $\left|F(hkl)\right|^2$ so, in

principle, electron distributions in crystals may be calculated by obtaining |F(hkl)| from experiment. In practice, however, there are numerous problems associated with carrying out such a calculation, many of which are discussed elsewhere (94,97,98). The problems directly related to the field gradient calculation and its accuracy will be covered in the next section.

The choice of a suitable crystal structure for use in calculating the field gradient was limited by two requirements -- the structure determination had to be recent enough so that confidence could be placed in the observed structure factors and the compound had to be one for which experimental quadrupole resonance data were available. Additionally, it was hoped that the crystal structure would be a simple ionic-type lattice with few atoms per unit cell. Unfortunately, these requirements severely limit the number of choices, since structure determinations for most simple inorganic salts were carried out too long ago to be useful. The only compound for which field gradient calculations were actually carried out in this investigation was β -ICl; at room temperature there are two modifications of iodine monochloride, β-ICl is the metastable one. Electron density maps were also calculated for several other compounds but because of the unsatisfactory nature of the maps for field gradient calculations further work on these compounds was discontinued for reasons outlined below.

 β -ICl is monoclinic, crystallizing in the space group with eight molecules per crystallographic unit cell (95). The NQR results (106) show two inequivalent iodine atoms and two inequivalent chlorine atoms per unit cell, in agreement with the X-ray results. In the following discussion the two types of atoms are denoted as I(a), I(b), Cl(a), and Cl(b). The first step in the calculation of the field gradient tensors for 6-ICl was to calculate the electron density map using the observed structure factors from the crystal structure determination (95). The program used in evaluation of the Fourier sum was a general type (96) suitable for many different space groups. The program evaluates the sum in Equation (60) at a grid of points in the unit cell, then provides the electron density values in a matrix of numbers corresponding to slices in the unit cell. Options in the program allow evaluation of $\rho(x,y,z)$ at either 30, 60, or 120 points along each axis leading to $(30)^3$, $(60)^3$, or $(120)^3$ points in the unit cell where the density would be evaluated. The fineness of the grid chosen was dictated both by the amount of computer time available and, more importantly, by the experimental resolution; dividing the cell into 120 parts along a particular axid usually exceeded the theoretical resolution for a particular X-ray source and unit cell size. Because of symmetry considerations, the grid points in only one-quarter of the unit cell needed to be evaluated using Equation (60), the remaining points being related by translations.

By drawing contour lines, corresponding to various fixed values of electron density, the center or maximum of electron density could be located for each atom. At various distances away from each atomic position the electron density values dropped to the background level and the electron density of the atom was assumed to truncate at this point. Then, assuming that the nucleus was located at the maximum of electron density the field gradient from the surrounding atoms was calculated. The calculation was carried out using a modified point-charge method with each non-zero grid point representing a fractional electronic charge. The values of the electron density at the grid points around each atomic position were scaled such that the total charge on the iodine and chlorine atoms agreed with the degree of ionic character obtained from a Townes-Dailey treatment of the experimental quadrupole coupling constants of iodine and chlorine in ICl (19). Then, a point-charge-type field-gradient summation using these grid points was carried out using a modified version (LAT2U), of a program developed by Ryan (47) from the method of DeWette and Schacher (15,16). Input for this program was supplied by another computer program that calculated the additional grid points necessary to complete the unit cell, adjusted the fractional charges to give the correct ionic charges on the atoms, and punched the input deck for the lattice summation program.

The first problem encountered was the choice of atomic positions to use in the calculation. In β -ICl, as in most structure determinations, the atomic positions, based on the maxima in electron density (denoted in the following as the map origin), are not usually the final atomic positions; these are instead calculated using a least-squares procedure to minimize the difference between observed and calculated structure factors (referred to as the least-squares origin). As detailed below, the field gradient in β -ICl was extremely sensitive to the choice of origin.

2. Results and Problems Encountered

The calculation for β-ICl involved a point-charge summation with over 1000 points of fractional charge, resulting in an extremely lengthy calculation on the CDC 6500 computer (about one hour per run). The magnitude of the field gradient computed at I(a) was very large due to an artifact in the calculation. When the least-squares origin was employed, the origin was located asymmetrically between the grid points resulting in abnormally large contributions to the field gradient from the adjacent grid points. This problem was compensated for by removing the twelve grid points directly adjacent to the origin. When the map origin was used slight variations in the coordinates of the origin produced large changes in the field gradients. The field gradients calculated using the map origin and using the least-squares origin were found to differ. Numerical

results for various choices of origin and various calculation conditions are given in Table 19.

One of the most serious deficiencies in the ICl calculation is the unreliability in the field gradient introduced by not having the grid of points at which the electron density is calculated spaced such that the atomic position of I(a) is coincident with a grid point. However, the program used for calculating the density map in this work employs standard formulas (99) for $\rho(x,y,z)$ for which the allowable values of x,y,z are n/30, n/60, or n/120of a unit cell side. Shifting the unit cell origin in order to make a grid point coincident with a particular atomic position invalidates the standard formulas for electron density, since the formula for a specific space group has been simplified by using symmetry relations of that particular space group. There is a possibility that transforming the unit cell to the triclinic system would allow any choice of origin but this was not attempted.

Aside from these computational difficulties, there are some serious theoretical objections to expecting accurate results from this type of calculation, especially in the case of ICl. This calculation is based primarily on the equality between $\rho(x,y,z)$ and the infinite Fourier summation of Equation (60). Since the highest-order reflection observable experimentally is usually less than h,k, or l = 15 (12,0,0 for β -ICl), series truncation errors leading to inaccurate electron distributions occur. The results of

Table 19. Calculated electric field gradients in $\beta\text{-ICl}$. (in A^{-3})

Calculation Conditions	Field Gradient (eq)	Asymmetry Parameter (η)
Field Gradient at I(a)b		
<pre>Experimental^a</pre>	-115.2	
Point Charge Model	-0.043	0.21
Least-squares Origin	-81106	0.033
Least-squares-12 points	-380	0.34
Least-squares-all I(a)	-22	0.22
Map Origin (.500,.118,.261) ^C	-206	0.25
(.515, .118, .261)	-971	• • •
(.500, .128, .261)	-20634	
(.500, .118, .251)	-206	0.25
Field Gradients at other Nuclei		
Cl(a) ^b : Least-squares Origin	-10784	0.044
Cl(b) ^b : Least-squares Origin	-2795	0.497

aReference 106.

bAtomic positions from Reference 95: I(a)-(.5028, .1182, .2629), I(b)-(.8135, .0321, .1250), Cl(a)-(.2547, .2898, .3695), Cl(b)-(.8876, .3002, .1069).

^CFourier map position from Reference 95.

such truncation errors are clearly visible in the Fourier maps, manifested as a background electron density of appreciable magnitude. To partially eliminate the truncation errors the field gradients were calculated using the actual Fourier map rather than directly substituting the Fourier summation from Equation (60) into the integral in Equation (24).

The second objection to this type of calculation concerns the thermal anisotropies. The contours of electron density drawn for the iodine and chlorine atoms in ICl show definite asymmetries, but these are almost certainly due to anisotropic thermal motion, rather than any effect attributable to chemical bonding. The contributions of the valence electrons to the density map are difficult to observe for several reasons. The outer valence electron shells contribute almost nothing to the total atomic scattering factor except for very low values of $\sin \theta/\lambda$. In addition, competing effects from thermal motion must therefore be completely removed before the difference electron density maps will show an accurate picture of chemical bonding. In ICl both the iodine and chlorine electron densities represent almost entirely K and L shell electrons which are essentially spherically symmetrical and should yield an electric field gradient not greatly different from the contribution given by the point-charge model due to the neighboring nuclei. The anisotropic thermal motions would, however, lead to an additional contribution

to the field gradient at a given nucleus from the remaining atoms of the crystal. In the case of AlPO₄, the additional polarization introduced by the anisotropic thermal motions was found (100) to be small. There is also a contribution to the field gradient at a given nucleus from the inner shell electrons of that atom. This would be essentially zero unless the anisotropic thermal motions in the crystal introduced a field gradient but this is unlikely since the electrons should follow the nuclei (Born-Oppenheimer approximation). In the calculations of Table 16, however, the largest contribution to the field gradient at the iodine nucleus appeared to arise from the electron distribution around that same nucleus.

There are, then, three principal deficiencies in the calculations as presently carried out: (1) The contribution of the valence electrons to the electric field gradient at the nuclei of a given molecule is not evaluated accurately since these electrons are ineffective in scattering the X-radiation and are not located precisely on the electron density maps. (2) The contribution of the inner shell electrons to the field gradient at the nucleus of an atom is very important but difficult to evaluate accurately since these electrons are smeared out anisotropically in the electron density maps as a result of the anisotropic thermal motion of the atom. (3) The uncertainties in the field gradient resulting from having the grid points placed asymmetrically around the atomic positions in the electron

density map. As a result of these factors, the results for ICl are not reliable.

Some other compounds, which might be less sensitive to these factors, were also tried. Cyanuric acid, C3N3H3O3, appeared to be the best choice available at present for correctly evaluating the effects of valence electrons since an extremely accurate X-ray structure determination has been carried out (101,102). Great care was taken in this X-ray investigation to obtain accurate structure factors and evidence of chemical bonding was obtained. Because of the low atomic numbers present the electron densities should reflect bonding character and field gradients calculated for this compound were expected to be more theoretically satisfying. Unfortunately, the electron density map which was calculated was quite complex and the number of grid points required to carry out a calculation was so large that the lattice sum would have taken too much computer time to properly evaluate. Other simple, or low atomic weight, compounds considered were Al₂O₃ and CrCl₂. In both the structure determination of CrCl₂ (103) and the structure refienment of Al₂O₃ (104), however, only a few structure factors outside the hkO plane were reported and the resulting maps are effectively two-dimensional projections in the ab plane.

In summary the calculation of field gradients using electron densities from X-ray diffraction data might be possible if suitable X-ray data were available for a

favorable case. Such an ideal system would be a compound with component atoms of low atomic weight with a relatively simple structure. The X-ray determination should be carried out at, or near, 40K to reduce thermal smearing and accompanied by a complimentary neutron diffraction study to obtain information about nuclear thermal motion. If the quadrupolar nuclei were located at symmetry points, or if the entire problem were transformed to the triclinic system, the difficulties in the computation arising from choice of origin might be eliminated. Further research along these lines should be informative.



LIST OF REFERENCES

- 1. H. B. G. Casimir, "On the Interaction Between Atomic Nuclei and Electrons," <u>Teyler's Tweede Genootschap</u>, E. F. Bohn, Haarlem (1936).
- 2. N. F. Ramsey, "Nuclear Moments," New York: John Wiley and Sons, Inc., 1953.
- 3. H. Kopfermann, "Nuclear Moments," New York: Academic Press, 1956. English translation by E. E. Schneider.
- 4. M. H. Cohen and F. Reif, Solid State Phys., 5, 321 (1957).
- 5. C. P. Slichter, "Principles of Magnetic Resonance, New York: Harper and Row, 1963.
- 6. J. R. Reitz and F. J. Milford, "Foundations of Electromagnetic Theory," Reading: Addison-Wesley, 2nd Ed. 1967.
- 7. The quadrupole term is non-vanishing for I ≥ 1. A good discussion of the spin restrictions is given by Ramsey (2), page 24.
- 8. T. Das and E. Hahn, "Nuclear Quadrupole Resonance Spectrocopy Solid State Phys.," Suppl. I, New York: Academic Press, Inc., 1958.
- 9. R. Bersohn, <u>J. Chem. Phys.</u>, <u>20</u>, 1505 (1962).
- 10. R. Livingston and H. Zeldes, "Tables of Eigenvalues for Pure Quadrupole Spectra, Spin 5/2," Oak Ridge National Laboratory Report ORNL-1913 (1955).
- 11. M. T. Rogers and K. V. S. Rama Rao, J. Chem. Phys., 49, 1229 (1968); Abstracts, 156th American Chemical Society Meeting, (1968).
- 12. R. Bersohn, <u>J. Chem. Phys.</u>, 29, 326 (1958).

- 13. R. R. Sharma and T. P. Das, <u>J. Chem. Phys.</u>, <u>41</u>, 3581 (1964).
- 14. C. K. Coogan, Aust. J. Chem., 17, 1 (1964).
- 15. F. W. DeWette, Phys. Rev., 123, 103 (1961).
- 16. F. W. DeWette and G. E. Schacher, Phys. Rev., 137, A92 (1965).
- 17. B. R. A. Nÿboer and F. W. DeWette, Physica, $\underset{\sim}{24}$, 422 (1958).
- 18. R. M. Sternheimer, Phys. Rev., 159, 266 (1967) and references given therein.
- 19. C. H. Townes and B. P. Dailey, <u>J. Chem. Phys.</u>, <u>17</u>, 782 (1949).
- 20. C. H. Townes and B. P. Dailey, <u>J. Chem. Phys.</u>, <u>20</u>, 35 (1952).
- 21. E. Scrocco in "Molecular Biophysics," New York: Academic Press, 1965.
- 22. H. Bayer, Z. Physik, 130, 227 (1951).
- 23. T. Kushida, G. Benedek, and N. Bloembergen, Phys. Rev., 104, 1364 (1956).
- 24. C. Kittel, "Introduction to Solid State Physics," New York: John Wiley and Sons, Inc., 3rd Edition, 1967, Chap. 2 and 5.
- 25. J. M. Ziman, "Principles of the Theory of Solids,"
 London: Cambridge University Press, 1964, Chap. 1 and 2.
- 26. T. E. Haas and E. P. Marram, J. Chem. Phys., 43, 3985 (1965).
- 27. R. Ikeda, D. Nakamura, and M. Kubo, <u>J. Phys. Chem.</u>, 69, 2101 (1965).
- 28. T. L. Brown and L. G. Kent, <u>J. Phys. Chem.</u>, <u>74</u>, 3572 (1970).
- 29. R. L. Armstrong and G. L. Baker, Can. J. Phys., 48, 2411 (1970) and references contained therein.
- 30. J. R. Partington and R. K. Bahl, <u>J. Chem. Soc.</u>, 1934, 1086 (1934).

- 31. M. Stedman and D. J. McCauley, Chem. Ind. (London) 1966, 1883 (1966).
- 32. L. Kirkpatrick and R. G. Dickinson, J. Am. Chem. Soc., 48, 2328 (1926).
- 33. A. E. H. Tutton, "Crystallography and Practical Crystal Measurement," London: MacMillan and Co., 1922, 2nd Ed., Vol. I, p. 202.
- 34. N. H. Hartshorne and A. Stuart, "Crystals and the Polarizing Microscope," London: Edward Arnold and Co., 1950, 2nd ed.
- 35. R. G. Brown, J. Denning, A. Hallett, and S. D. Ross, Spectrochim. Acta, 26A, 963 (1970).
- 36. R. E. Miller, K. L. Treuil, R. R. Getty, and G. E. Leroi, Tech. Rept. No. 4(29), D.D.C. Accession No. 669797, May 1968.
- 37. D. A. Hatzenbuhler, Ph.D. Thesis, Michigan State University, 1970.
- 38. R. E. Rondeau, J. Chem. Eng. Data, 11, 124 (1966).
- 39. A. C. Rose-Innes, "Low Temperature Techniques," London: Van Nostrand Co., Inc., 1964.
- 40. C. A. Swenson and E. H. Stahl, <u>Rev. Sci. Instrum.</u>, 25, 608 (1954).
- 41. G. K. White, "Experimental Techniques in Low Temperature Physics," London: Oxford, 1968, 2nd Ed.
- 42. R. B. Scott, "Cryogenic Engineering," Princeton: Van Nostrand, 1959.
- 43. C. M. Herzfeld, Ed., "Temperature: Its Measurement and Control in Science and Industry," New York: Reinhold, 1962, Vol. 3, Pt. 2.
- 44. W. F. Giauque, R. M. Buffington, and W. A. Schulze, J. Amer. Chem. Soc., 49, 2343 (1927).
- 45. Order No. AC-5014, Thermoelectric Co., Inc., Saddle Brook, New Jersey. Professor F. Horne kindly provided the wire used in this study.
- 46. R. L. Powell, L. P. Caywood and M. D. Brown, <u>Cryogenics</u>, 1, 139 (1961).
- 47. J. A. Ryan, Ph.D. Thesis, Michigan State University, 1967.

- 48. R. G. Brown, J. Denning, A. Hallet, and S. D. Ross, Spectrochim. Acta, 26A, 963 (1970).
- 49. D. A. Hatzenbuhler and R. A. Johnson, 25th Ohio State Symp. on Molec. Struct. and Spect., Sept. 1970.
- 50. A. Müller, Z. Naturforsch., A21, 433 (1966).
- 51. A. Müller and B. Krebs, Z. Naturforsch., B21, 3 (1966).
- 52. K. Ulbricht and H. Kriegsmann, Z. Anorg. Allg. Chem., 358, 193 (1968).
- 53. R. S. Halford, <u>J. Chem. Phys.</u>, <u>14</u>, 8 (1946).
- 54. H. Winston and R. S. Halford, <u>J. Chem. Phys.</u>, <u>17</u>, 607 (1949).
- 55. D. F. Hornig, <u>J. Chem. Phys.</u>, <u>16</u>, <u>1063</u> (1948).
- 56. S. Bhagavantam, Proc. Ind. Acad. Sci., A13, 543 (1941)
- 57. W. G. Fateley, N. T. McDevitt, and F. Bentley, Appl. Spectrosc., 25, 155 (1971).
- 58, G. Herzberg, "Molecular Spectra and Molecular Structure II. Infrared and Raman Spectra of Polyatomic Molecules," New York: Van Nostrand Company, Inc., 1945.
- 59. B. D. Saksena, Proc. Ind. Acad. Sci., A11, 229 (1940).
- 60. T. Damen, S. Porto and B. Tell, Phys. Rev., 142, 570 (1965).
- 61. R. Fonteyne, Naturwetensch. Tydschr., 20, 20 (1938).
- 62. D. Clutter and W. Thompson, <u>J. Chem. Phys.</u>, <u>51</u>, 153 (1969).
- 63. C. J. H. Schutte and A. M. Heyns, <u>J. Chem. Phys.</u>, <u>52</u>, 864 (1970).
- 64. J. R. Durig and D. J. Antion, <u>J. Chem. Phys.</u>, <u>51</u>, 3639 (1969).
- 65. T. C. Waddington, J. Chem. Soc., 1958, 4340 (1958).
- 66. D. A. Dows, E. Whittle and G. C. Pimentel, <u>J. Chem. Phys.</u>, <u>23</u>, 1475 (1955).

- 67. R. C. Plumb and D. F. Hornig, <u>J. Chem. Phys.</u>, 23, 947 (1955).
- 68. E. L. Wagner and D. F. Hornig, <u>J. Chem. Phys.</u>, <u>18</u>, <u>305</u> (1950).
- 69. E. L. Wagner and D. F. Hornig, <u>J. Chem. Phys.</u>, <u>18</u>, 296 (1950).
- 70. C. J. H. Schutte, Chem. Phys. Lett, 1, 585 (1968).
- 71. Some representative KBB treatments are: (a) Ref. 23, (b) C. Dean and E. Lindstrand, J. Chem. Phys., 24, 1114 (1956), (c) H. S. Gutowsky and G. A. Williams, Phys. Rev., 105, 464 (1957), (d) Reference 29.
- 72. R. J. C. Brown, <u>J. Chem. Phys.</u>, 32, 116 (1960).
- 73. R. R. Hewitt, Phys. Rev., 121, 45 (1961).
- 74. H. S. Gutowsky and G. A. Williams, <u>Phys. Rev.</u>, 105, 464 (1957).
- 75. E. Schempp, G. E. Peterson, and J. R. Carruthers, <u>J. Chem.</u>, Phys., 53, 306 (1970).
- 76. R. F. Tipsword, J. T. Allender, E. A. Stahl, Jr., and C. D. Williams, J. Chem. Phys., 49, 2464 (1968).
- 77. D. B. Utton, <u>J. Chem. Phys.</u>, <u>47</u>, 371 (1967).
- 78. R. F. Tipsword and W. G. Moulton, <u>J. Chem. Phys.</u>, $\widetilde{39}$, 2730 (1963).
- 79. W. D. Partlow and W. G. Moulton, <u>J. Chem. Phys.</u>, 39, 2381 (1963).
- 80. V. Nicely and J. L. Dye (unpublished results).
- 81. R. P. Hamlen and W. S. Koski, <u>J. Chem. Phys.</u>, <u>25</u>, 360 (1956).
- 82. R. G. Barnes and R. D. Engardt, <u>J. Chem. Phys.</u>, 29, 248 (1958).
- 83. A. H. Reddoch, J. Chem. Phys., 35, 1085 (1961).
- 84. A. Sasane, D. Nakamura, and M. Kubo, <u>J. Mag. Res.</u>, <u>3</u>, 76 (1970), and references contained therein to extensive earlier work.
- 85. A. Sasane, D. Nakamura, and M. Kubo, <u>J. Phys. Chem.</u>, <u>71</u>, 3249 (1967).

- 86. G. P. O'Leary, Phys. Rev. Lett., 23, 782 (1969).
- 87. J. Beintema, Z. Krist., 97A, 300 (1937), results quoted in R. W. G. Wyckoff, "Crystal Structures,"

 New York: Interscience, 1965, 2nd. Edition, Vol. 3.
- 88. J. C. Morrow, Acta. Cryst. 13, 443 (1960).
- 89. A. Kalman and D. W. J. Cruickshank, Acta Cryst., B26, 1782 (1970).
- 90. E. A. Hazelwood, Z. Krist., A98, 439 (1938).
- 91. J. Itoh and Y. Yamagata, <u>J. Phys. Soc.</u>, <u>Jap</u>., <u>17</u>, 481 (1962).
- 92. L. D. Landau and E. M. Lifshitz, "Statistical Physics," Reading: Addison Wesley Pub. Co., Inc., 1958, Chapter 14.
- 93. R. Ikeda, D. Nakamura, and M. Kubo, <u>J. Phys. Chem.</u>, 70, 2926 (1966).
- 94. R. Brill, Solid State Phys., 20, 1 (1967).
- 95. G. B. Carpenter and S. M. Richards, Acta Cryst., 15, 360 (1962).
- 96. Program No. B-149 from Professor Tulinsky's X-ray structure group at Michigan State University.
- 97. G. A. Jeffrey and D. W. J. Cruickshank, Quart. Rev. (London), 7, 335 (1953).
- 98. G. E. Bacon, "X-Ray and Neutron Diffraction," London: Pergammon Press, 1966.
- 99. "International Tables of X-Ray Crystallography," Birmingham: Kynoch Press, 1952, Volume I.
- 100. D. Schwarzenbach, Z. Krist., 123, 422 (1966).
- 101. G. C. Verschoor, Doctoral Thesis, State University, Groningen, The Netherlands, 1967.
- 102. G. C. Verschoor and E. Keulen, Acta Cryst., B27, 134 (1971).
- 103. J. W. Tracy, et al., Acta Cryst., 14, 927 (1961).
- 104. R. E. Newnham and Y. M. deHaan, Z. Krist., 117, 235 (1962).

- 105. W. E. Wentworth, <u>J. Chem. Educ.</u>, <u>42</u>, 96 (1965).
- 106. S. Kojimia, et al., J. Chem. Phys., 23, 1963 (1955).

